INVESTIGATING THE ROLES OF LACTATE DEHYDROGENASES IN THE RICE BLAST FUNGUS *MAGNAPORTHE ORYZAE*

A Thesis Submitted to the College of

Graduate Studies and Research

In Partial Fulfillment of the Requirements

For the Degree of Doctor of Philosophy

In the Department of Biology

University of Saskatchewan

By

TENGSHENG ZHOU

PERMISSION TO USE

In presenting this thesis/dissertation in partial fulfillment of the requirements for a postgraduate degree from the University of Saskatchewan, I agree that the Libraries of this University may make it freely available for inspection. I further agree that permission for copying of this thesis/dissertation in any manner, in whole or in part, for scholarly purposes may be granted by the professor or professors who supervised my thesis/dissertation work or, in their absence, by the Head of the Department or the Dean of the College in which my thesis work was done. It is understood that any copying, publication, or use of this thesis/dissertation parts thereof for financial gain shall not be allowed without my written permission. It is also understood that due recognition shall be given to me and to the University of Saskatchewan in any scholarly use which may be made of any material in my thesis/dissertation.

Requests for permission to copy or to make other use of material in this thesis in whole or part should be addressed to:

Head of the Department of Biology

University of Saskatchewan

112 Science Place

Saskatoon, Saskatchewan S7N 5E2

ABSTRACT

Magnaporthe oryzae is a filamentous ascomycete fungus that causes rice blast, the most destructive disease of rice worldwide. Upon attachment of pathogen spores to the plant surface, a specialized cell called an appressorium differentiates from the germ tubes to facilitate fungal entry into plant tissues using mechanical force. The appressorium development is fuelled by nutrient reserves carried in spores mainly in the form of lipids and glycogen. Previous studies suggest that breakdown of lipids and glycogen, primarily restricted to the peroxisomes and the cytosol respectively, culminates in production of pyruvate. However, downstream metabolism of pyruvate and its coordination with mitochondrial activities remain elusive. In this study, we showed that D-lactate, interconvertible with pyruvate by activities of lactate dehydrogenases, is a central metabolite utilized during spore germination and appressorium development. Genome-wide analysis of five lactate dehydrogenase genes in *M. oryzae* demonstrated that a D-lactate dehydrogenase, namely MoDLD1, located on the mitochondrial inner membrane, is responsible for conversion of D-lactate to pyruvate. Targeted replacement of *MoDLD1* resulted in failure of efficient appressorium formation, which was associated with inability to utilize lipids and glycogen in fungal spores, and consequently the loss of fungal pathogenicity. In summary, our findings reveal a novel metabolic pathway operated by MoDLD1 that bridges metabolite flow to the mitochondria, and contributes to the fungal development and virulence of *M. oryzae*.

ACKNOWLEGMENTS

Firstly, I would like to thank my supervisor Dr. Yangdou Wei for all his supervision, advice and patience during this research. I am very grateful that he offered me this opportunity to pursue this project in his lab. Secondly, I would also like to thank the members of my advisory committee, Dr. Jitao Zou, Dr. Susan Kaminskyj, Dr. Randy Kutcher and Dr. David Greenshields for their advice and guidance. Thanks also go to Dr. Guosheng Liu and Dr. Zhuqing Zhou for their help in the microscopic techniques. Many thanks to everyone in Dr. Wei's lab during past and presence, in particular Li Qin, Dr. Tao Song, Dr. Long Yang and Jiangying Tu for their help in experimental techniques and discussion. This project is funded by Natural Science and Engineering Research Council (NSERC) Discovery Grant awarded to Dr. Wei. I am also financially supported by Biology Graduate Scholarship and Graduate Teaching Fellowship from Department of Biology, University of Saskatchewan.

Finally, endless gratitude goes to my parents for their every effort to raise me up, educate and encourage me to make this happen.

TABLE OF CONTENTS

LIST OF TABLES

LIST OF FIGURES

LIST OF ABBREVIATIONS

ABBREVIATION	FULL NAME
AGT	Alanine: glyoxylate aminotransferase
AOA	Aminooxyacetic acid
ATGs	Autophagy-related genes
ATP	Adenosine triphosphate
cAMP	Cyclic adenosine 3′, 5′-monophosphate
CFEM	Extracellular membrane-spanning domain
CINN	a-cyano-4-hydroxycinnamate
CM	Complete medium
DAG	Diacylglycerol
DIC	Differential interference contrast
DLD	D-lactate dehydrogenase
dpi	Day post inoculation
EchA	Enoyl-CoA hydratase
eGFP	Enhanced Green fluorescent protein
GPCRs	G protein coupled receptors
hph	Hygromycin-B phosphotrasferase gene
hpi	Hours post inoculation
HR	Hypertensive Response
HSL	Hormone-sensitive lipase
ICL	Isocitrate lyase
LLD	L-lactate dehydrogenase
MAG	Monoacylglycerol
MAPK	Mitogen-activated protein kinase
MCT	Monocarboxylate transporter
MDH	Malate dehydrogenase

MFPs	Multifunctional proteins
MM	Minimal medium
MPCs	Mitochondrial pyruvate carrier complex
MS	Malate synthase
MTS	Mitochondrial targeting signal
NADH	Nicotinamide adenine dinucleotide
NADPH	Nicotinamide adenine dinucleotide phosphate
neo	Neomycin resistant gene
NHEJ	Non-homologous end joining pathway
ORF	Open reading frame
OXA	Oxamic acid
PCR	Polymerase chain reaction
PDA	Potato dextrose agar
PDE	Phosphodiesterase
PI	Propidium iodide
PKA	Protein kinase A
ROS	Reactive oxygen species
SEM	Scanning electron microscope
T6P	Trehalose 6-phosphate
TAG	Triacylglycerol
TCA	Citric acid cycle
TEM	Transmission electron microscope
TM	Transmembrane domain
TPS1	Trehalose-6-phosphate synthase
WT	Wild type

CHAPTER 1 INTRODUCTION

1.1 Rice blast disease

Rice blast is the most devastating rice disease worldwide. Over 90% of rice production is consumed by humans and nearly half of the global population relies on rice as the major source of calories; rice blast poses a constant threat to global food security (Goff, 1999). The causal agent of rice blast is a filamentous ascomycete fungus called *Magnaporthe oryzae*, which is one of four major species in the *Magnaporthe* genus that originated as a grass-adapted complex and branched phylogenetically following host shifts (Ainsworth, 2008; Couch et al., 2005). The origin of *M. oryzae* was suggested to coincide with the early domestication of rice from its wild ancestor, *Oryza rufipogon*, in the middle of the Yangtze valley, China, around 7000 years ago (Couch et al., 2005). Blast symptoms in rice occur first on leaves, where ellipsoid lesions enlarge and the pathogen sucks nutrients from plant tissues. After the heading stage of rice, fungal spores are transferred to the panicle, causing neck blast symptoms and resulting in direct yield losses (Kobayashi et al., 2001). In recent years, outbreaks of blast epidemics have led to severe economic losses globally. For instance, over 6 million hectares of rice were destroyed in 2005 in Heilongjiang province, China (Xiaohong et al., 2013). Severe epidemics sometimes result in total losses of rice production, which has occurred on occasion in Korea, Japan, Vietnam and the United States. In general, the annual yield loss due to rice blast is estimated to range between 10% to 30% across the globe (Talbot, 2003). In addition to rice, other host crops are also susceptible to *M. oryzae*, resulting in severe yield losses. Wheat blast disease has emerged as the major problem of wheat production in Brazil, mainly causing spike infection resulting in up to 100% yield loss in susceptible fields (Kohli et al., 2011). Blast disease caused by *M. oryzae* has been identified as the main constraint for finger millet production in eastern African countries where finger millet plays an important role in nutrient supply to farming communities (Takan, 2004). Other agriculturally important crops including oats, barley, rye and maize are also susceptible to infection by *M. oryzae* (Ou, 1985).

The successful control of rice blast disease involves the combination of various management strategies including cultural strategies, breeding of genetically resistant cultivars, biological control, and use of chemical fungicides. Genetic resistance has been regarded as the most practical and economic approaches for blast disease control. However, its efficiency is time-limited, since disease resistance is usually overcome after 2-3 growing seasons due to the high genetic variation of *M. oryzae* strains due to high rates of mutation (Ou, 1985). To extend the effective lifetime of resistant cultivars, different race-specific resistant genes are introduced into the same cultivar, conferring quantitative resistance. Growing genetically diverse cultivars within a field is a highly efficient approach to suppress rice blast disease. Cultivar mixtures of glutinous and blast-resistant hybrid varieties in the same cropping system resulted in nearly a 90% yield increase of the glutinous variety, which is highly susceptible to blast but has a greater market value (Zhu et al., 2000). Another approach to combat blast disease is the use of fungicides, either as seed treatments to prevent the infection of seedlings after germination or applied on the foliage to prohibit the spread of the pathogen to panicles when they are initiated from the shoots (TeBeest et al., 2007). The use of fungicides is associated with potential environmental and food security risks. Therefore, a better understanding of the molecular mechanisms underlining fungal development and pathogenesis is necessary to more efficiently mitigate losses caused by rice blast.

In addition to its economic importance, developmental similarities between *M. oryzae* and other important cereal pathogens in infection structures, such as appressorium formation and invasive hyphal extension in host cells, make it a model phytopathogen (Ebbole, 2007). This allows pathogenicity determinants identified in *M. oryzae* to be conceptualized for broad-spectrum protection against various crop diseases. Sequencing of the *M. oryzae* genome and the experimental tractability of this fungus opens up the possibility of investigating the genetic and molecular basis of pathogenesis of *M. oryzae*.

1.2 The disease cycle of *M. oryzae*

M. oryzae reproduces sexually and asexually. Two mating types, *MAT1* and *MAT2*, are present; mating between opposite types was observed under laboratory conditions. Sexual fruiting bodies called perithecia are formed after pairing isolates of opposite mating types on an appropriate sporulation medium at 21℃ for three weeks (Valent et al., 1991). Ascospores resulting from meiosis were liberated by dissecting the asci in perithecia. The infection cycle of *M. oryzae* only involves the asexual development; the ascospores play no role in the infection.

Foliar attack of *M. oryzae* on host plants commences with the attachment of a three-celled conidium on leaves, where leaf surface hydrophobicity is required to induce the secretion of adhesives from the apical compartment at the spore tip (Hamer et al., 1988). Following attachment, the apical cell of the conidium produces a single polarized germ tube, which swells into a hook-like structure at the end, followed by development of a dome-shaped infection structure called an appressorium upon the perception of environmental cues such as hydrophobicity, nutrient deprivation and hardness of the plant surface (Choi and Dean, 1997) (Fig 1.1). Appressorium development is cell cycle-regulated, depending on checkpoints that modulate the appressorium initiation and maturation, respectively. The nucleus in the apex cell of the conidium migrates into the polarized germ tube during the onset of germination and divides into two daughter nuclei. One daughter nucleus moves to the incipient appressorium with increasing diameter, providing genetic information for the infection, while the other returns to the original conidium. Coinciding with appressorium development, three nuclei remaining in the coinidium are degraded by autophagy machinery, through which nutrient reserves in the conidium are recycled to the appressorium (Saunders et al., 2010; Veneault-Fourrey et al., 2006). As the appressorium matures, increasing amounts of compatible solutes such as glycerol (de Jong et al., 1997), start to accumulate. The appressorium forms a cell wall within which chitin and a layer of melanin are deposited. The melanin acts as a physical barrier to prevent the efflux of glycerol while permitting water inflow to the appressorium, which helps to generate huge hydrostatic turgor pressure outward (Chumley and

Valent, 1990). Turgor pressure is then transformed into mechanical force, directed down to the penetration peg at the base of the appressorium, breeching the plant cuticle and cell wall (Fig 1.1).

Early invasive hypha growth in the first infected cells occurs by the extension of bulbous primary hyphae, invaginating the host plasma membrane, which is termed as biotrophic infection (Mosquera et al., 2009). Primary hyphae function as specialized feeding structures drawing nutrients from living host cells to support fungal growth without causing host tissue damage. Between 36-48 hpi a physiological transition occurs, referred to as the hemibiotrophic switch, which is hallmarked by the cell-to-cell movement of invasive hyphae through plasmodesmata, leading to the full occupation of adjacent cells by secondary hyphae (Khang et al., 2010). The hemibiotrophic switch is associated with secretion of effector proteins to the plant apoplastic space and cytosol to induce host cell death, resulting in leakage of nutrients at infection sites. Nutrients acquired from broken host tissues enable the continuous ramification of secondary hyphae, accompanying the occurrence of expanding necrosis on the plant surface. After 72-96 hours post inoculation, typical blast lesions are produced on plant leaves, where profuse conidia are formed under highly humid conditions, spreading rapidly to land on neighboring plants by wind and dew drop splash (Ebbole, 2007) (Fig 1.1).

In addition to leaf infection, *M. oryzae* is also able to invade roots through root-specialized infection structures that are typical of root pathogens. After spreading through vascular tissues from the roots to aerial parts of the plant, *M. oryzae* causes classical disease symptoms on foliage (Sesma and Osbourn, 2004). In contrast, biotrophic growth is only restricted in the first infected cell at leaf infection; *M. orzyae* prefers a prolonged asymptomatic growth phase in roots during the invasive growth from rhizodermal to vascular tissues (Marcel et al., 2010).

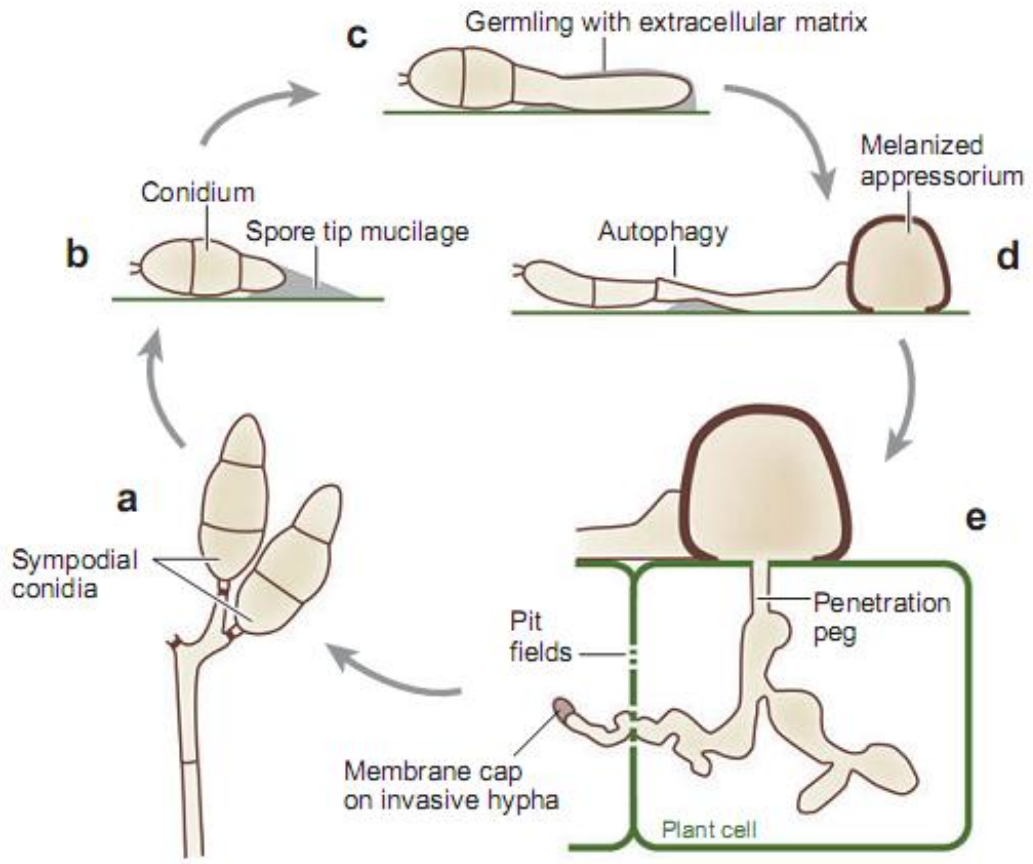

Figure 1.1 Disease cycle of *M. oryzae.*

(a) Conidia grow in a sympodial manner on the conidiophore. (b) The conidium attaches to the plant surface by secreted mucilage at the spore tip. (c) The conidium develops a filamentous germ tube from the apical cell. (d) The melanized appressorium is differentiated from the swelling hook of the germ tube. (e) A penetration peg driven by turgor pressure penetrates the plant cuticle and cell wall, followed by the appearance of bulbous primary hyphae in first infected plant cells and cell-to-cell movement of invasive hyphae to adjacent cells through plasmodesmata by secondary hyphase. (Ebbole, 2007).

1.3 Cellular signaling for infection-related development by *M. oryzae*

1.3.1 Recognition of physical and chemical signals of plant surfaces

During the interaction between phytopathogenic fungi and host plants, the initiation of infection-related development involves the recognition of environmental cues associated with physical and chemical properties of the plant surface (Tucker and Talbot, 2001). Hardness and

hydrophobicity of the plant surface as well as chemicals, such as primary alcohols of epicuticular waxes and cutin monomers, are well-known surface signals recognized by *M. oryzae*. These signals are transmitted to the nucleus via signal transduction pathways, leading to the expression of genes related to morphological changes, thereby triggering the differentiation of infectious structures such as spore attachment, conidial germination, appressorium initiation and maturation (Liu et al., 2011). Transmembrane-localized receptor proteins that bind to extracellular ligands detect environmental clues on the plant surface and transmit signals to the cell interior by activating downstream targets.

A large group of extracellular membrane-spanning domain (CFEM domain)-containing proteins called G protein coupled receptors (GPCRs) has been identified in the *M. oryzae* genome (Dean et al., 2005). One of GPCRs in *M. oryzae*, Pth11, was found to be transcriptionally induced in the appressorium stage, and was required for fungal pathogenicity since its existence was necessary for the response to environmental stimuli to induce appressorium formation (DeZwaan et al., 1999). GPCRs respond to extracellular stimuli, leading to conformational change and consequently activation of associated heterotrimeric (αβγ) guanine nucleotide binding proteins (G-proteins). These act as intrinsic molecular switches to turn on downstream effectors. The activated GPCRs function as guanine nucleotide exchange factors (GEFs) to promote the switch from GDP to GTP binding in the cognate Gα subunit. This switch triggers its dissociation from the Gβγ subunits and renders it active to target downstream effectors (Dohlman and Thorner, 2001). In addition, Gβγ moieties are able to propagate different downstream signaling cascades (Liu and Dean, 1997). In *M. oryzae* three G protein α subunit genes: *magA*, *magB* and *magC*, have been cloned and functionally characterized. Disruptions of either *magA* or *magC* had no effects on infection-related development but affected the sexual development. However, targeted replacement of *magB* resulted in significant reduction of vegetative growth, conidiation and appressorium formation, and therefore subsequent loss of pathogenicity. These results indicated that members of G protein α subunits act in unique signal transduction pathways to regulate different aspects of

growth, development, and pathogenicity in *M. oryzae* (Liu and Dean, 1997). The role of the Gβ subunit in fungal development and pathogenicity of *M. oryzae* was characterized. Disruption of the Gβ subunit coding gene (*MGB1*) completely inhibited appressorium formation and pathogenicity, indicating that the Gβ subunit is specifically involved in the signaling pathway for the regulation of appressorium formation in *M. oryzae* (Nishimura et al., 2003).

Signals perceived by transmembrane receptors are transmitted to multiple intracellular effectors by the mediation of G proteins, resulting in signal propagation and diversification. The most well defined signaling pathways that function in regulating fungal development and pathogenicity of *M. oryzae* upon recognition of environmental cues are the cyclic AMP (cAMP) signaling pathway and mitogen-activated protein kinase (MAPK) signaling pathways (Fig 1.2). In addition to signal recognition by transmembrane-localized GPCRs on the plant surface, sensor proteins bound to the plasma membrane are deployed to detect extracellular stimuli in *M. oryzae*. For example, two recently identified membrane sensor proteins, MoMsb2 and MoSho1, were indicated to act as upstream sensors to activate the Pmk1 MAPK pathway for appressorium formation. MoMsb2 was suggested to be essential for sensing plant surface hydrophobicity and cutin monomers, while MoSho1 has an important role in recognizing leaf waxes (Liu et al., 2011). Although the downstream effectors for MoMsb2 and MoSho1 signal transduction are unknown, a small GTPase Cdc42 responsible for polarity establishment was shown to interact with Msb2 in yeast (Pitoniak et al., 2009).

1.3.2 The cyclic AMP signaling pathway

Cyclic adenosine 3′, 5′-monophosphate (cAMP) is the first identified secondary messenger molecule that triggers physiological changes in response to extracellular stimulations by primary messengers. cAMP has been shown to be an important regulator of fungal development. In *M. oryzae*, studies have indicated that cAMP has a central role in regulating the appressorium formation. Appressorium formation is typically aborted if conidial germination occurs on a non-inductive surface, however this is rescued by extracellular

application of cAMP (Lee and Dean, 1993). The relationship between the cAMP signaling pathway and molecule-switch G proteins was established through demonstration that the intracellular cAMP level in the *ΔmagB* mutant was reduced and that the defect in appressorium formation in the *ΔmagB* mutant can be restored after the conidia are treated with exogenous cAMP during germination (Nishimura et al., 2003) (Fig 1.2).

The intracellular level of cAMP is subjected to regulation by two types of enzymes, the adenylyl cyclase (AC) for synthesis and the cyclic nucleotide phosphodiesterase (PDE) for hydrolysis (Fimia and Sassone-Corsi, 2001). Deletion of the adenylyl cyclase-coding gene *MAC1* in *M. oryzae* caused defects in sexual development, vegetative growth, conidiation and appressorium formation, consequently losing the ability to infect host plants. However, appressorium development and pathogenicity of *⊿mac1* mutants were remediated by adding exogenous cAMP to germinating spores (Choi and Dean, 1997). These results indicated that the cyclic AMP (cAMP) response pathway was involved in the regulation of appressorium morphogenesis. Moreover, cAMP generated by adenylyl cyclase binds to the regulatory subunit of cAMP-dependent protein kinase A (PKA), allowing its dissociation from the PKA catalytic subunit CpkA, and thus rendering it the catalytic activity. Loss of the PKA regulatory subunit Sum1 led to constitutive activation of CpkA, overriding the requirement of cAMP stimulation for appressorium development, as deletion of *sum1* in the background of *⊿mac1* mutants restored the appressorium formation in *M. oryzae* (Adachi and Hamer, 1998). However, mutants with targeted replacement of *CpkA* can produce deformed appressoria that showed failed penetration on plant surface, resulting in a loss of pathogenicity. While deformed appressoria of *cpkA* mutants were able to elaborate invasive hyphae and induce blast symptoms on surface-abraded plants, suggesting that the cAMP-dependent activation of protein kinase PKA was specifically required for production of functional appressoria in *M. oryzae* (Xu et al., 1997). Given the deletion of the adenylyl cyclase gene *MAC1* has pleiotropic effects rather than on appressorium development, different effectors including PKA may locate at the downstream response to cAMP for specific regulation of different aspects of fungal development and

pathogenicity in *M. oryzae* [Fig 1.2].

1.3.3 MAPK signaling pathways

In eukaryotic organisms, each mitogen-activated protein kinase (MAPK) signaling pathway, which is involved in transduction of wide varieties of extracellular signals to modulate the cellular growth and differentiation, consists of three regulatory levels, controlled by MAPK kinase kinase (MEKK), MAPK kinase (MEK) and MAP kinase (MAPK), respectively [Ludwig et al, 2005]. In *M. oryzae*, three MEKKs and three MEKs together with three MAPKs have been identified and assigned to three different signal cascades, which are responsible for various aspects of cellular development in response to environmental cues (Dixon et al., 1999; Xu and Hamer, 1996; Xu et al., 1998) (Fig 1.2).

The Pmk1 MAPK pathway is the first identified pathway that is mediated by MAP kinase Pmk1 to regulate appressorium formation and penetration in *M. oryzae* (Xu and Hamer, 1996). Pmk1 is homologous to yeast Map kinases FUS3/KSS1 that control filamentous growth and mating pheromone response (Elion et al., 1991). Loss of *Pmk1* in *M. oryzae* led to defects in appressorium formation on plant surface and invasive growth inside plant cells, rendering the mutant completely non-pathogenic. However, the ⊿*Pmk1* mutant was normal with respect to vegetative growth in mediums, as well as asexual and sexual reproduction, indicating that the Pmk1-meidated signal cascade was uniquely required for appressorium formation in *M. oryzae* (Xu and Hamer, 1996). The upstream kinases of Pmk1 in the cascade have been identified and characterized in *M. oryzae* as well, and include Mst7 and Mst11, which are functionally homologous to yeast MEK Ste7 and MEKK Ste11, respectively. Individual deletion mutants of either *MST7* or *MST11* failed to initiate appressoria on plant surface and were unable to cause blast symptoms on rice. The expression of a constitutively active form of *MST7* in the ⊿*mst11* mutant restored its appressorium formation on hydrophobic surface, suggesting that Mst11 kinase activates Mst7 in the cascade. In wild type, the unique role of Pmk1 in the regulation of appressorium formation was further confirmed when Pmk1 was shown phosphorylated only

during the appressorium stage. Pmk1, however, was phosphorylated and activated during all stages in transformants that expressed the constitutively active form of *MST7*. These results indicate that Mst11-Mst7-Pmk1 likely acts as a signal cascade was likely (Xu and Hamer, 1996). Although no direct physical interaction was detected between members within this cascade, a scaffold protein Mst50 homologous to yeast Ste50 for Mst11-Mst7-Pmk1 was identified and characterized in *M. oryzae. MST50* was highly induced in appressoria, and its gene product was shown to physically interact with Mst7 and Mst11 during appressorium stage in co-immunoprecipitation assays. Mutants with disrupted *MST50* failed to form appressoria and induce disease on plants. Therefore, Mst50 may function as an adaptor, which recruits Ste11 and Ste7 in proximity for signal transduction upon the targeted phosphorylation (Park et al., 2006) (Fig 1.2).

MPS1 is the second MAP kinase gene identified in *M. oryzae*, which is the functional homolog of yeast *SLT2* that is involved in maintaining the cell wall integrity (Torres et al., 1991). The *MPS1* null mutant of *M. oryzae* was still able to form appressoria but failed to penetrate the plant surface and caused disease on rice seedlings; however, circumvention of appressorium penetration by wounding the plant leaf surface enabled invasive growth of the ⊿*mps1* mutant inside host cells, resulting in visible symptoms on the plant surface. Moreover, the ⊿*mps1* mutant showed progressive autolysis during colony growth on CM medium and was found to be hypersensitive to cell wall degrading enzymes, pointing out that loss of cell wall integrity could be the cause of the lack of penetration by appressoria in these mutants. The ⊿*mps1* mutant was also unable to efficiently reproduce asexually, which was likely due to the improper regulation of cell wall biogenesis in aerial hyphae (Xu et al., 1998). The gene replacement of a MEKK *MCK1* in *M. oryzae*, which was functionally related to yeast *BCK1* that functions as an upstream kinase of SLT2, displayed comparable phenotypes to the ⊿*mps1* mutant in appressorium penetration, invasive growth, cell wall integrity and conidiation (Jeon et al., 2008). In contrast to that the Pmk1 MAPK signal pathway regulating appressorium formation, the Mps1-mediated signal cascade is likely responsible for appressorium penetration

through the control of cell wall biogenesis to modulate the generation of turgor pressure prior the penetration in *M. oryzae* (Fig 1.2).

A third MAPK encoding gene, *OSM1,* appears to regulate in response to osmotic stress in *M. oryzae*. *OSM1* is a functional homolog of the yeast MAPK HIGH-OSMOLARITY GLYCEROL1 (*HOG1*), which is involved in regulation of cellular turgor in yeast. In fungi, the production of compatible solutes owing to hyperosmotic stress can prevent the efflux of water and regulate the cellular turgor. Large amounts of glycerol accumulate in mature appresoria of *M. oryzae* during turgor generation, which is required for the successful penetration through the plant cuticle and cell wall (de Jong et al., 1997). The inactivation of *OSM1* gene by targeted gene replacement in *M. oryzae* resulted in sensitivity to osmotic stress and morphological defects during growth under hyperosmotic conditions but remained unaltered in appressorium morphology and turgor pressure (Dixon et al., 1999). These results suggest that independent signal pathways rather than OSM1 MAPK are responsible for turgor pressure regulation to enable appressorium penetration in *M. oryzae*.

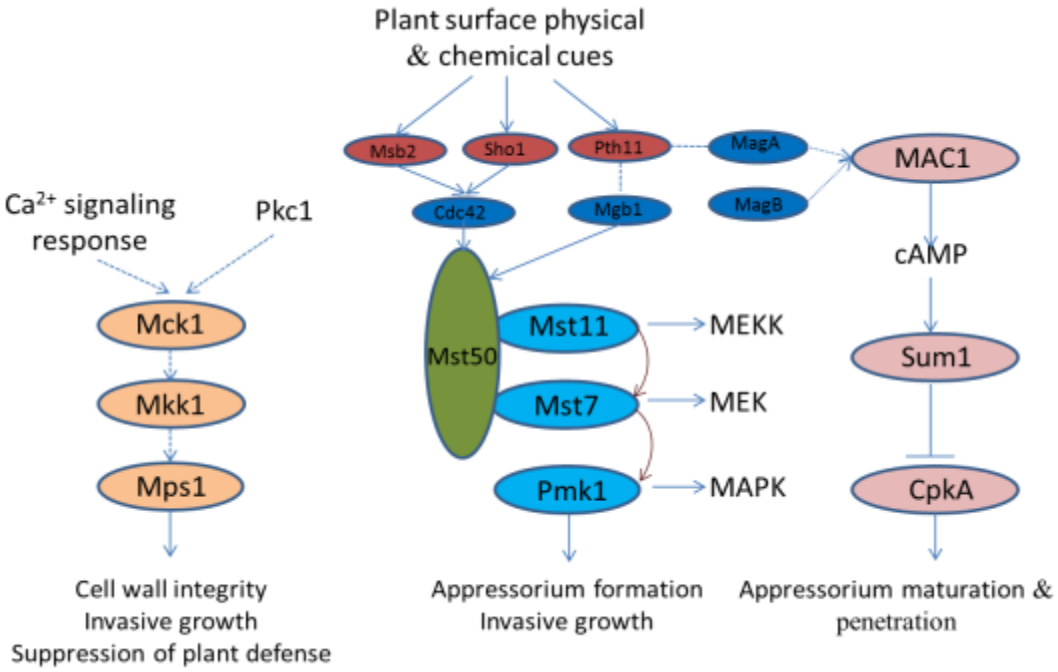

Figure 1.2 Signal transduction pathways required for infection-related development by *M. oryzae*.

The Pmk1 MAPK linkage is tethered by the scaffold protein Mst50, and relies on consecutive phosphorylation that culminates in entry of phosphorylated Pmk1 to the nucleus and activates transcription factors to induce morphological changes. Activation of the Pmk1 pathway involves beta-subunit of G protein Mgb1 and CPCR Pth11 upon the perception of surface hydrophobicity and hardness. Membrane sensor proteins Msb2 and Sho1 are also responsible for detecting surface hydrophobicity, cutin monomers and primary alcohols for activation of the Pmk1 pathway through a small GTPase Cdc42. cAMP generated by MAC1 binds to the PKA regulatory subunit Sum1, allowing its dissociation from the PKA catalytic subunit CpkA and subsequently liberating the activity of CpkA. The cAMP response pathway is possibly targeted by Gα-subunit protein MagA and MagB, which may rely on activation by Pth11. The Mps1 pathway is required for appressorium penetration and plant tissue colonization. Activation of Mps1 occurs through the upstream MEK Mkk1 and MEKK Mck1. The Mps1 pathway is responding to calcium channel proteins and protein kinase C in other organisms. Physical or genetic interactions supported by experimental evidence between proteins are denoted in solid lines, while dotted lines indicate putative interactions that need further experimental demonstration.

1.4 Physiology of *M. oryzae* during the plant infection

Appressorium development is coupled with rapid metabolic changes to bring about energy production and synthesis of biomass. The generation of glycerol, in such amounts that create enormous turgor pressure estimated to be as high as eight Mpa, involves the mobilization of nutrient reserves from conidia and de novo synthesis in appressoria, since appressorium formation on the plant surface does not require exogenous nutrients. It was shown that glycogen, trehalose and lipid bodies as prominent storage reserves are mobilized from the conidium to the appressorium prior to turgor generation in *M. oryzae*. The molecular mechanism underlining this process is likely related to the Pmk1 MAP kinase pathway, through which the authophagy machinery is activated to conduct nutrient and organelle turnover in the conidium in advance of appressorium development (Thines et al., 2000).

1.4.1 Role of autophagy in appressorium development of *M. oryzae*

Autophagy (also termed macroautophagy) is an intracellular process responsible for bulk degradation of cytoplasmic constitutes under starvation stress conditions. In addition to maintaining the nutrient homeostasis, autophagy is also necessary for many aspects of development such as cell cycle progress, cellular differentiation and cell death in multicellular organisms. Autophagy is a multiple-step process, with each key step mediated by sets of autophagy-related genes (*ATG*s) from induction to autophagosome formation and degradation. The initiation of autophagy is usually related to nutrient starvation, which is followed by the formation of a functionally specialized double-membrane organelle called an autophagosome that is developed from the surrounding and engulfing of cytoplasmic components by a single membrane structure, a phagophore (Mizushima, 2007). In fungal cells, the autophagosome is further fused with the lytic compartments, such as the vacuole, to sequester its contents for the degradation by hydrolases (Mizushima, 2007). Through hydrolytic degradation, macromolecules are broken down into monomeric units that are exported to the cytosol for reuse (Mizushima, 2007). Besides macroautophagy, there are several other forms of autophagy

that rely on selectivity, including organelle-specific autophagy pathways (pexophagy, mitophagy and reticulophagy) and the cytoplasm to vacuole targeting (Cvt) pathway (Yu et al., 2008).

To date, *ATG* genes that encode proteins necessary for the autophagy process have been identified in the yeast *S. scerevisiae* (Cao et al., 2008). In *M. oryzae*, 24 *ATG* genes homologous to yeast genes have been identified, some of which are up-regulated during the appressorium maturation stage. By referring to the established findings in yeast, those *ATG* genes in *M. oryzae* can be separated into different subgroups based on their putative roles in governing the autophagy process. The initiation of autophagy involves *MoATG1, MoATG13* and *MoATG17*. While *MoATG3, MoATG4, MoATG5, MoATG7, MoATG8, MoATG10, MoATG12, and MoATG16* are genes that participate in phagophore and autophagosome expansion. *MoATG2, MoATG9, MoATG15*, and *MoATG18* are required for nutrient and organelle recycling. The further genome-wide functional characterization indicates that nonselective macroautophagy is an important pathway for turgor pressure generation of the appressorium in *M. oryzae* (Kershaw and Talbot, 2009). The pathogenicity of *M. oryzae* was totally abolished when any of 16 nonselective *ATG* genes was knocked out, as gene disruption mutants were unable to penetrate the plant due to lack of turgor pressure. Conidial collapse was not observed in *ATG* gene mutant strains, indicating that the recycling of nutrient reserves was prevented during appressorium development. In contrast, deletion of any individual selective autophagy genes specifically associated with pexophagy or mitophagy does not affect fungal virulence in *M. oryzae* (Kershaw and Talbot, 2009).

1.4.2 Trehalose metabolism in pathogenicity of *M. oryzae*

1.4.2.1 Trehalose synthesis and degradation

Trehalose is a non-reducing disaccharide with two glucose molecules, found in a wide range of organisms from bacteria, fungi, and plants to mammals. Trehalose is well known for its

metabolic and mechanic role in the protection of cells against environmental injuries and nutrient limitation (Argüelles, 2000; Müller et al., 2001). The biosynthetic pathway to produce trehalose involves two sequential biochemical steps. Firstly, trehalose-6-phosphate (T6P) is produced as an intermediate from glucose-6-phosphate (G6P) and UDP-glucose by trehalose-6-phosphate synthase (T6PS). Subsequently, the phosphate group is removed from T6P by trehalose phosphate phosphatase (TPP) to yield trehalose. Until now, many details regarding the trehalose metabolism were revealed based on studies in *S. cerevisiae*, within which two regulatory subunits of trehalose 6-phosphate synthase/phosphatase complex, TPS3 and TSL, are also required for trehalose synthesis (Argüelles, 2000). Trehalose degradation involves activity of trehalase, hydrolyzing one trehalose into two glucoses that are further metabolized through glycolysis.

1.4.2.2 Regulatory function of trehalose metabolism via trehalose-6-phophate synthase (TPS1)

Besides acting as a nutrient, trehalose metabolism plays a regulatory role in diverse cellular processes in eukaryotic organisms, such as growth and development in plants, and primary metabolism in yeast (Eastmond et al., 2002; Silva‐Udawatta et al., 2001). Trehalose was found to be present in trace amounts in plants, suggesting that it played other roles rather than serving as a storage compound. Deletion of trehalose-6-phophate (T6P) synthase homolog gene *TPS1* in *Arabidopsis thaliana* embryos resulted in a series of defects associated with development including reduced cell division rate, delay in seed development, and alteration of cell wall deposition (Gómez et al., 2006). The role of the T6P intermediate as a signal molecule in the regulation of primary metabolism was implicated by multiple evidences showing that *⊿Tps1* mutants in *A. thaliana* embryos accumulated increased amounts of sucrose and starch due to the repression of genes responsible for their degradation (Schluepmann et al., 2003). In *S. cerevisiae*, T6P is able to regulate the carbon influx into glycolysis over the control of hexokinase activity. Loss of T6P in yeast *⊿Tps1* mutants caused disordered input of glucose

into glycolysis, resulting in accumulation of phosphorylated glycolytic intermediates and consequently depletion of cellular ATP (Thevelein and Hohmann, 1995).

It was observed that trehalose was quickly mobilized from the conidium to the appressorium during appressorium formation in *M. oryzae.* Deletion of *Tps1* in *M. oryzae* resulted in the inability to utilize nitrate, but not nitrite and amino acids as nitrogen source for vegetative growth on minimal medium (Wilson et al., 2007). ⊿*Tps1* mutants formed normal appressoria on the hydrophobic surface or plant surface, which however cannot penetrate the plant cell wall due to reduced turgor generation (Foster et al., 2003). While, deletion of the trehalase encoding gene *TRE1* in *M. oryzae,* which was responsible for trehalose degradation, had no effects on appressorium formation and penetration, but caused delay of proliferation of invasive hyphae during plant infection (Foster et al., 2003). These results indicated that during infection-related development in *M. oryzae*, T6PS-operated trehalose metabolism may have a role to integrate carbon and nitrogen metabolism, leading to the control over disparate cellular processes rather than serving as a storage compound (Fernandez and Wilson, 2011). Further provided evidence demonstrated that TPS1 also acted as sensor and regulator of intracellular G6PDH activity and NADPH level in response to nitrate as nitrogen source, raising a possible link between trehalose metabolism and intracellular NADPH/$NADP^+$ ratio control (Wilson et al., 2007).

It was further found that disruption of any of NADP-dependent transcriptional corepressor Nmr-encoding genes (*Nmr1*, *Nmr2*, and *Nmr3*) in the ⊿*Tps1* mutant can partially rescued its pathogenicity. This suggested that, via modulation of intracellular NADPH/$NADP^+$ ratio, switching on/off transcriptional corepressors including Nmr1, Nmr2, and Nmr3 related to control the expression of virulence-associated genes were subjected to the regulation of TPS1-mediated trehalose metabolism (Wilson et al., 2010). Taken together, it can be concluded that TPS1 acts as a molecular sensor to maintain the dynamic equilibrium of NADPH/$NADP^+$ ratio in response to nutrient and redox changes during appressorium development in *M. oryzae*, through which the bulk of virulence-associated genes are activated via the depression of

transcriptional repressors in a NADP-deprive manner (Fernandez and Wilson, 2011).

1.4.3 Glycogen metabolism in pathogenicity of *M. oryzae*

1.4.3.1 Mobilization and degradation of glycogen during appressorium development

Infection-related development is highlighted by sequential morphological alterations including conidial adhesion, germination, appressorium formation and penetration, and invasive growth inside plant cells, which occur in a nutrient-free environment. Therefore, the pathogen should utilize storage nutrients in the conidium to provide energy and metabolite requirement for plant infection. Glycogen, a polymer of glucose, is one of the main nutrients available in the conidium, and its metabolism is tightly coupled with appressorium development in *M. oryzae*. During germination and appressorium initiation (2-4 h on hydrophobic surface), glycogen is gradually broken down in the conidium. Glycogen starts to accumulate in the incipient appressorium as its emergence post 6 h induction on hydrophobic surface, but is degraded quickly during appressorium maturation. When the appressorium is fully melanized, small amounts of glycogen are visible, suggesting that glycogen acts as the major carbohydrate source for appressorium maturation including cell wall melanization and establishment of turgor pressure (Thines et al., 2000).

1.4.3.2 Roles of glycogen synthesis and degradation in fungal pathogenicity

Glycogen consists of chains of glucose linked by α-1, 4-glycosidic bonds, with chains branching off by α-1, 6-glycosidic bonds at every 8-12 glucose residues. Degradation of glycogen involves the combined action of two enzymes, the de-branching enzyme amyloglucosidase and the phosphorylase that finally releases glucose. Amyloglucosidase hydrolyses α-1, 6-glycosidic bonds to de-branch chains of glucose, while phosphorulyase liberates glucose by acting on α-1, 4-glycosidic bonds of the non-reducing ends in the form of glucose-1-phosphate (Cox and Nelson, 2004). Homologs of amyloglucosidase exist in

prokaryotic and eukaryotic kingdoms, and have been purified from several organisms such as bacteria, yeast and mammals (Chen et al., 1987; TABATA and HIZUKURI, 1992). In the yeast *S. cerevisiae*, *Gdb1* was found to encode the cytosolic amyloglucosidase responsible for glycogen degradation. Deletion of *Gdb1* totally prevented glycogen degradation, while the expression of *Gdb1* was induced in response to stress conditions that caused glycogen accumulation in yeast (Teste et al., 2000).

A putative amyloglucosidase-encoding gene *AGLl* was identified in the *M. oryzae* genome. The amino acid sequence of AGLl showed 47% identity to yeast glycogen de-branching enzyme Gdb1. Deletion of *AGLl* in *M. oryzae* prevented mobilization of glycogen stores during appressorium development because of loss of amyloglucosidase activity. However, the appressorium formation and penetration were not affected due to deletion of *AGLl*. The invasive hyphal growth of ⊿*AGLl* was impaired during infection on host rice and barley, which was less bulbous and branched than the wild type, resulting in significantly reduced ability to cause blast disease (Badaruddin et al., 2013). A putative cytosolic glycogen phosphorylase GPH1 was also identified in the *M. oryzae* genome, which displayed a high degree of sequence similarity with members of glycogen phosphorylase across fungal kingdom. Deletion of *GPH1* led to both losses of amyloglucosidase and glycogen phosphorylase activities, suggesting that glycogen degradation was an orchestrated manner, within which the glucose chain points can only be cleaved when they were made accessible by phosphorylase. Phenotypes caused by deletion of *GPH1* were identical to those due to loss of *AGLl*, including delay on glycogen mobilization, growth defects on glycogen-containing medium and dramatic reduction of virulence (Badaruddin et al., 2013).

Given the important role of glycogen mobilization and degradation in fungal virulence, the role of glycogen synthesis was also investigated in *M. oryzae*. Glycogen synthesis is a multiple-step process that requires combined activities of three proteins including glycogenin, a seft-glucosylating initiator protein, glycogen synthase that transfers glucose residues into polymeric glucose chain through the synthesis of α-1, 4 linkages, and the branching enzyme,

making glycogen a branched polymer by forming α-1, 6 linkages between glucose chains (Farkas et al., 1991; Rowen et al., 1992). In yeast, the accumulation of glycogen is correlated with emergence of nutrient limitation or other environmental stresses such as heat, osmotic, or saline stress (Parrou et al., 1997). Genes encoding glycogenin, glycogen synthase and the branching enzymes were identified and shown to participate in glycogen synthesis through functional characterization in eukaryotic organisms. Yeast cells contained two isoforms of glycogen synthase, GSY1p and GSY2p. Deletion of *GYS2* resulted in approximately 90% reduction of glycogen stores in yeast cells, suggesting that GSY2p was the main isoform of glycogen synthase for glycogen synthesis (Farkas et al., 1991). Moreover, induction of *GYS2* in yeast cells required the cAMP-dependent protein kinase pathway that was shown to regulate the glycogen mobilization and degradation during appressorium development in *M. oryzae* (Hardy et al., 1994). BLASTX algorithm search using yeast *GYS1* and *GYS2* in the *M. oryzae* genome led to the identification of a putative glycogen synthase gene *GSN1*. Deletion of the *GSN1* gene resulted in significant reduction on glycogen deposits in conidia and appressoria of *M .oryzae* compared to the wild type strain. However, ⊿*GSN1* mutants were still able to cause rice blast disease symptoms identical to that induced by the wild type strain on rice seedlings, which could be taken as evidence to conclude that synthesis of glycogen as a stored compound was not required for pathogenicity in *M. oryzae* (Badaruddin et al., 2013).

Interestingly, both ⊿*agl1* and ⊿*gph1* mutants showed reduced intracellular levels of trehalose, indicating that enzymatic activities of AGL1 and GPH1 or the glycogen degradation was related to the synthesis of a trehalose precursor. Expression of *Tps1* and *Tps3*, encoding the regulatory subunits of the trehalose-6-phosphate synthase/phosphatase complex, were reduced in the background associating with either loss of *AGL1* or *GPH1* compared to that in the Guy11 wild type strain. Moreover, deletion of the transcriptional inhibitor gene *NMR3*, which partially restored pathogenic phenotype of ⊿*tps1* mutants, also complemented the virulence deficiency of ⊿*agl1*⊿*gph1* double knock-out mutants (Badaruddin et al., 2013). Thus, based on these data, it was concluded that glycogen degradation may carry out an unexpected regulatory role

through the connection with the NADPH-dependent TPS1 genetic switch, but does not present a direct requirement to fuel appressorium development by providing energy and biosynthetic precursors in *M. oryzae*.

1.4.4 Lipids metabolism in pathogenicity of *M. oryzae*

1.4.4.1 Biological functions of lipids

The continuous providence of metabolic energy is necessary for the maintenance of living systems. Compared to carbohydrates, lipids that contain many reduced hydrocarbons store more energy in average grams, and thus are referred as the long-term storage source of energy for many organisms (Thiam et al., 2013). In addition, lipids provide building blocks for the synthesis of cellular membranes, within which the lipid bilayers act as a physical barrier to insulate the cell from the environment. Lipids are also signal molecules mainly in forms of steroid hormones that carry messages to intracellular receptors, resulting in the alteration of gene expression (Walther and Farese Jr, 2012). Lipids are involved in protein modification by attaching lipophilic groups to specific amino acids, which help to increase protein's affinity to cellular membranes and confer them distinct properties (Resh, 2013). Lipogenesis, consisting of two sequential steps of fatty acid synthesis and triglyceride synthesis, is the process that synthesizes lipids inside cells and requires the participation of several groups of enzymes including multiple enzymatic complex fatty acid synthase and triacylglycerol synthesis enzymes. The degradation of lipids, conversely, involves the hydrolysis of triglycerides into glycerol and free fatty acids. The relationship between lipid metabolism and carbohydrate metabolism is closely connected through the common intermediate acetyl-CoA and is tightly regulated in gene transcriptional levels in response to changes of nutrient intake (Kersten, 2001).

1.4.4.2 Hydrolysis of triglycerides into glycerol and fatty acids

Through activities of triacylglycerol (TAG) lipases, lipid bodies are broken down into fatty acids and glycerol. In detail, the hydrolysis of TAG is accomplished by specific lipases in a sequential order and liberates fatty acids at each step together with the production of DAG (diacylglycerol), MAG (monoacylglycerol), and glycerol. HSL (hormone-sensitive lipase) that exerts function on glycerides among broad substrates has been extensively studied and shown to control the hydrolysis of TAG. The actions of HSL including cellular localization, enzyme activity, and substrate specificity are under the regulation of stress-activated protein kinase pathways (Kraemer and Shen, 2002). Lipid bodies in the conidium were shown to mobilize through the germ tube to the incipient appressorium during germination and appressorium initiation under the regulation of Pmk1 MAPK-dependent pathway in *M. oryzae*. While further degradation of lipid bodies or lipolysis that occurred in the appressorium vacuoles relayed on the regulation of cAMP-dependent protein kinase pathway (Thines et al., 2000). To investigate the role of TAG lipase in infection-related development of *M. oryzae*, TAG lipase activity was determined within the developing appressoria. The enzyme assay showed that TAG lipase rapidly accumulated at the onset of appressorium formation and remained highly active during the maturation and turgor generation (Thines et al., 2000). In the *M. oryzae* genome, eight putative lipase-encoding genes were identified. Determination of transcriptional levels by RNA gel blots revealed different genes were specifically induced in response to different substrates, suggesting that *M. oryzae* contained a set of lipases targeting on various substrates in processing lipids (Wang et al., 2007). However, deletion of any of eight putative TAG lipase-encoding genes was unable to prevent the fungal infection; furthermore, deficiencies on nutrient utilization with lipids as substrates were not observed on each individual gene deletion mutant. These results indicated that intracellular lipolysis associated with the appressorium maturation involved cooperative action of a set of TAG lipases in *M. oryzae* (Wang et al., 2007).

1.4.4.3 The β-oxidation of lipid bodies during appressorium development

Intracellular level of lipids is maintained in a homeostatic state with constant flux, as the lipid content is determined by the balance between lipid uptake rate, lipolysis and further oxidation (Thiam et al., 2013). The subsequent metabolism of fatty acids freed due to activity of TAG lipase is required. The cellular degradation of fatty acids occurs primarily through the β-oxidation pathway found in the peroxisomes or mitochondria in all eukaryotes. During β-oxidation, fatty acid chains, categorized as short-chain fatty acids, medium-chain fatty acids, long-chain fatty acids and very long-chain fatty acids by length, are continuously shortened by oxidative removal of two-carbon units in the form of acetyl-CoA from the carboxyl end of the chains. After several cycles of oxidation, fatty acid chains are converted to groups of two-carbon acetyl-CoA molecules, which serve as sources of energy or biosynthetic precursors for other metabolic pathways. β-oxidation that degrades straight-chain-statured fatty acids consists of four basic steps catalyzed by the four activities of specific enzymes, namely acyl-CoA dehydrogenase, enoyl-CoA hydratase, *β*-hydroxyacyl-CoA dehydrogenase, and acyl-CoA acetyltransferase in both peroxisomes and mitochondria (Cox and Nelson, 2004; Hiltunen et al., 2003). In contrast, degradation of unsaturated fatty acid chains with carbon double bonds requires the additional participation of auxiliary enzymes such as Delta(3), Delta(2)-enoyl-CoA isomerase and 2,4-die-noyl-CoA reductase (Goepfert et al., 2005). In mammals, long chain fatty acids are processed by the β-oxidation in the peroxisomes, while oxidation of medium and short chain fatty acids occurs in the mitochondria (Hynes et al., 2006). In *S. cerevisiae* yeast, the β-oxidation of fatty acids was shown to solely occur in the peroxisomes to provide a major proportion of acetyl-CoA for subsequent utilization as carbon and energy sources (Smith et al., 2000). A group of proteins in eukaryotes and prokaryotes, referred as multifunctional proteins (MFPs) characteristic of the β-oxidation system, were demonstrated to have activities of enoyl-CoA hydratase and *β*-hydroxyacyl-CoA dehydrogenase, catalyzing the second and third steps of the β-oxidation (Hiltunen et al., 1992). Sequence analysis on a *S. cerevisiae* MFP named FOX2p showed that, beyond the N-terminal

dehydratase domain, it had two dehydrogenase domains, rendering its specific preferences on different substrates (Hiltunen et al., 2003). Research also suggested that the mitochondrial β-oxidation exists in the filamentous fungus *Aspergillus nidulans*. The gene encoding a mitochondrial enoyl-CoA hydratase (EchA) was identified in *A. nidulans.* Deletion of *echA* caused dramatic reduction of 2-butenoyl-CoA hydratase activity in isolated mitochondria and prevented fungal growth on short-chain and long-chain fatty acids (Maggio‐Hall and Keller, 2004).

To investigate the role of the β-oxidation in infection-related development of phytopathogenic fungi, the gene encoding the multifunctional protein (MFP1), whose homolog in yeast showed to localize in the peroxisome and having a vital role to mediate the β-oxidation, was identified and characterized in *M. oryzae*. Deletion of *MFP1* caused the delay of lipid mobilization during germination and appressorium formation, resulting in a dysfunctional appressorium that was unable to penetrate the plant cell surface, and consequently non-pathogenic on host plants (Wang et al., 2007). The mitochondrial enoyl-CoA hydratase Ech1 was also identified in *M. oryzae* and was shown to be required for utilization of short and medium-chain fatty acids for fungal growth. Disruption of *ech1* however did not prevent the appressorium development, but led to impaired invasive growth due to the failure of suppressing the oxidative burst response of host cells during infection (Patkar et al., 2012). Taken together, the peroxisomal β-oxidation of fatty acids is essential for appressoria maturation and host penetration in *M. oryzae*, while the mitochondrial β-oxidation acts as a machinery to detoxify the oxidative burst encountered at the post-penetration stage to facilitate fungal growth inside host cells.

1.4.4.4 The glyoxylate cycle and fungal virulence

The oxidation of fatty acids leads to the production of acetyl CoA that as a vital carbon intermediate, has different metabolic fates, one of which is assimilation into the glyoxylate cycle. The glyoxylate cycle, modified from the citric acid cycle (TCA) with the leak of two

decarboxylation steps, is an anaerobic pathway involved in utilization of non-fermentable carbon sources and fatty acids for biosynthesis of macromolecules. Five enzymes were uncovered to constitute the glyoxylate cycle, three of which shared with TCA cycle are citrate synthase, aconitase and malate dehydrogenase, while the other two enzymes, namely isocitrate lyase (ICL) and malate synthase (MS), are unique to the glyoxylate cycle (Cox and Nelson, 2004) . Studies in the human fungal pathogen *Candida albicans* showed that both ICL and MS localized in the peroxisomes and were required for the proper functioning of the glyoxylate cycle (Piekarska et al., 2008). Deletion of *ICL* in *C. albicans* impeded fungal growth on non-fermentable carbons including acetate, ethanol and glycerol, as well as resulted in remarkably reduced virulence in mouse model compared to the wild type strain (Lorenz and Fink, 2001). This result was consistent with the important role of the ICL-operated glyoxylate cycle in the metabolism of fatty acids and virulence of infecting immune-competent mouse in the human bacterial pathogen *Mycobacterium tuberculosis* (McKinney et al., 2000).

Besides occurring in the peroxisomes, part of the glyoxylate cycle also takes place in the cytosol. In *S. cerevisiae*, aconitases distribute distinctly in two subcellular compartments, mitochondria and the cytosol to participate in the TCA cycle and the glyoxylate cycle, respectively (Regev-Rudzki et al., 2005). In spite of the native peroxisomal localization of ICL and MS in *C. albicans*, re-targeting both of them to the cytosol through disruption of the peroxisomal importing machinery did not affect the functioning of the glyoxylate cycle, moreover, rescued the growth deficiency of the ⊿*fox2* mutant strain on non-fermentable carbon source (Piekarska et al., 2008). In *M. oryzae*, the expression of *ICL1* was induced during appressorium formation and penetration stages. Targeted replacement of *M. oryzae ICL1* led to the growth deficiency on acetate and olive oil, and caused delayed germination, appressorium formation and cuticle penetration, resulting in reduced virulence (Wang et al., 2003). These results indicate that the β-oxidation and the glyoxylate cycle are coordinated in a sequential order to regulate the lipid catabolism during infection-related development in *M. oryzae*.

1.4.4.5 Production of pyruvate in the peroxisomes via the alanine: glyoxylate aminotransferase (AGT1)

The net result of the glyoxylate cycle is the production of succinate through the absorption of two molecules of acetyl CoA, resulting from the degradation of fatty acids, as well as production of other four-carbon intermediates of the TCA cycle. Succinate is then transported to the mitochondria where it is converted to malate, and eventually to oxaloacetate as a precursor for the gluconeogenesis in the cytosol (Cox and Nelson, 2004) . Therefore, the enzymatic transformations of dicarboxylic and tricarboxylic acids through the glyoxylate cycle, the TCA cycle and gluconeogenesis in three subcellular compartments peroxisomes, mitochondria and the cytosol bring about the production of glucose from two-carbon acetyl CoA in plants and fungi. In *M. oryzae*, the gluconeogenesis could further provide biosynthetic precursors for generation of chitin and glucan essential for appressorium development (Wang et al., 2003).

In addition, intermediates of the glyoxylate cycle could feed various biosynthetic pathways, one of which is for the synthesis of amino acids that have critical roles in cellular metabolism. As a key intermediate of the glyoxylate cycle, the importance of glyoxylate in the biosynthesis of amino acids has been described (Igarashi et al., 2006; Sinha and Cossins, 1965). Through activities of glyoxylate aminotransferases, an amino group from the donor amino acid is exchanged with the keto group in the glyoxylate to produce glycine and the corresponding α-keto acid. In plants, peroxisomal glyoxylate aminotransferases are involved in the photorespiratory pathway, a process that requires the participation of various biochemical reactions and metabolite exchange between chloroplasts, peroxisomes and mitochondria (Liepman and Olsen, 2001). In *S. cerevisiae*, the gene *AGX1* was shown to code for the alanine glyoxylate aminotransferase that was in charge of one of three metabolic pathways in the production of glycine (Schlösser et al., 2004). The alanine glyoxylate aminotransferases (AGTs) have more profound roles in mammal systems, of which species exerting AGT activity in mitochondria as well as peroxisomes have been described (Danpure et al., 1990). In humans,

miss-localization of AGT, which is targeted to the peroxisomes in humans, is associated with the hereditary disease primary hyperoxaluria type 1 (PH1) (Motley et al., 1995). In *M, oryzae*, the homology of AGT was functionally analyzed, showing that AGT localizes to the peroxisomes and is indispensable for the mobilization and degradation of lipid bodies during appressorium formation and maturation. The defect in utilization of lipid bodies resulted in non-functional appressoria that were unable to penetrate the plant surface, and consequent loss of pathogenicity (Bhadauria et al., 2012). When considering together with other metabolic pathways for oxidation of fatty acids in the peroxisome in *M. oryzae*, this result indicated that the alanine: glyoxylate aminotransferase held a critical role in coordination with the β-oxidation and the glyoxylate cycle for degradation of lipid bodies during infection-related development.

1.5 Channeling of reducing equivalents via the metabolite shuttles

1.5.1 Generation of reducing equivalents coupled with the fatty acid oxidation

In mitochondria and peroxisomes, one consequence of β-oxidation is the accumulation of reducing equivalents NADH and FADH2 in cellular compartments. The machinery employed to transport reducing equivalents and harness the associated reducing power varies accordingly in different organelles. Electrons in reducing equivalents are removed by an oxidoreductase-rich transmembrane structure to the respiratory chain in the inner mitochondrial membrane, accompanied by ATP production. The process that oxidoreductases transfer electrons from reducing equivalents to O_2 is accomplished by combined effects of four distinct complexes, embedded in the inner mitochondrial membrane, including complex 1 of NADH: ubiquinol oxidoreductase, complex II of succinate dehydrogenases, complex III of ubiquinol: ferricytochrome c oxidoreductase and complex IV of ferrocytochrome c: O_2 oxidoreductase (Walker, 1992; Weiss et al., 1992). While production of NADH and $FADH_2$ due to the β-oxidation in the peroxisomes is not coupled with cellular respiration immediately. Given that cellular membranes are impermeable to reducing equivalents, instead the intra-organelle redox

shuttle is utilized to export reducing equivalents from the peroxisomes to the cytosol and eventually to the mitochondria for oxidation by O_2. The redox shuttle is described as a cycle through which substrates are interconverted by dehydrogenase activities and then traverse across cellular membranes, so as to translocate reducing equivalents between cellular compartments and maintain the redox balance (Van Roermund et al., 1995).

1.5.2 The malate/aspartate shuttle and the glycerol-3-phosphate (G-3-P) shuttle

The most active redox shuttle is the malate/aspartate shuttle, which has received extensive studies in mammal systems (Bremer and Davis, 1975; Mettler and Beevers, 1980). In the cytosol, reducing equivalents of NADH are transferred to oxaloacetate by malate dehydrogenase to yield malate. The malate formed is transported through the mitochondrial inner membrane by the action of a malate-α-ketoglutarate transporter to the mitochondrial matrix, within which the reducing equivalents stored in malate are passed to NAD^+ by the activity of malate dehydrogenase with the production of oxaloacetate and NADH. Electrons in the thus formed NADH are directly passed to the respiratory chain in the mitochondrion (Cox and Nelson, 2004) . The primary role of the malate/aspartate shuttle in translocating reducing equivalents between cellular compartments was implicated by multiple lines of evidences in which functional interference of the shuttle resulted in the disorder of intercellular redox state and impairments of mitochondrial energetics and nutrient metabolism (Cheeseman and Clark, 1988; Lane and Gardner, 2005). The malate/aspartate shuttle mainly involves redox adjustment in higher eukaryotes and appears to be umimportant in fungal organisms (de Vries and Marres, 1987).

A different redox shuttle, namely the glycerol-3-phosphate (G-3-P) shuttle, is designated to channel cytosolic reducing equivalents to the mitochondria for cellular respiration. The G-3-P shuttle has been widely identified operating in all eukaryotic model organisms from animals and fungi to plants. Combined action of two G-3-P dehydrogenases with different substrate preferences, including a cytosolic NAD^+ dependent G-3-P dehydrogenase (GPDH)

and a mitochondrial FAD-dependent G-3-P dehydrogenase, necessitates the functioning of the G-3-P shuttle (Cox and Nelson, 2004) . In the cytosol, GPDH passes reducing equivalents in NADH to dihydroxyacetone phosphate (DHAP) with the production of G-3-P. The thus resulting G-3-P is translocated into the mitochondrial intermembrane space, where it is reoxidized into DHAP by mitochondrial inner membrane-located FAD-dependent GPDH with the concomitant production of $FADH_2$ that further donates electrons to the mitochondrial ubiquinone pool. Studies in *Arabidopsis* have indicated that the G-3-P shuttle has a critical role in the maintenance of steady state NADH/NAD^+ ratio, redox homeostasis and mitochondrial respiration rate (Quettier et al., 2008; Shen et al., 2006). In yeast, G-3-P dehydrogenases that operate the G-3-P shuttle were identified, as they are the NAD-dependent GPDH GPD1 in the cytosol and the FAD-dependent GUT2 in the mitochondrial inner membrane (Albertyn et al., 1994; Rønnow and Kielland‐Brandt, 1993). The G-3-P shuttle activity was activated under aerobic conditions when yeast strains were grown in the non-fermentable substrates such as ethanol, and to maintain the cytoplasmic redox balance; however it was also suggested that alternative systems using external NADH dehydrogenase are involved in maintaining cytosolic redox balance in yeast (Larsson et al., 1998).

1.5.3 The lactate shuttle hypothesis

1.5.3.1 Lactate dehydrogenases in different cellular compartments

As a glycolytic product, lactate accumulates under hypoxic conditions in contracting muscle and is continuously utilized for energy production until the aerobic condition is recovered. In this regard, lactate provides a direct linkage between glycolytic and oxidative metabolism (Brooks, 2007). In mammals, the role of lactate is also emphasized as a regulator of cellular redox state through its movement between intracellular compartments and then exchange with its more oxidized analogue, pyruvate, by activity of lactate dehydrogenases. When lactate is translocated between intracellular compartments or distal tissues and organs,

the redox state of both the removal and delivering destinations are usually affected (Brooks, 2002). It is likely that there is a redox shuttle operated by lactate dehydrogenase, functionally analogous to the malate-aspartate and G-3-P shuttles, which exists intracellularly to transport metabolic reducing equivalents across cellular membranes and regulate the redox state. The presence of lactate dehydrogenases has been suggested in the peroxisomes, mitochondria and the cytosol of various cell types in mammal systems. Immunolabeling detection using specific antibodies of different isoforms of lactate dehydrogenases in rat tissues indicated that distribution of different lactate dehydrogenases was unique to tissues and organelles. In particular, the mitochondria were shown very active in the oxidation of excess lactate due to the abundant presence of a lactate dehydrogenase isoform there (Brooks et al., 1999). In the peroxisomal matrix of rat hepatocytes, the presence of lactate dehydrogenase was implicated using the same technique of immunoelectron microscopy and was shown to be more abundant compared to the presence in the cytosol (Lu et al., 2011). Given that enzymes other than lactate dehydrogenase involved in the glycolytic pathway were not identified in the purified peroxisomes, it seemed that lactate dehydrogenases in the peroxisomes did not participate in the glycolysis. However, it is more likely that peroxisomal lactate dehydrogenases are involved in the reoxidation of NADH produced by the β-oxidation of fatty acids, as the elevation of lactate dehydrogenase activity in the peroxisomes is positively correlated with the induction of β-oxidation enzymes and a decreased amount of NADH (Baumgart et al., 1996).

1.5.3.2 Translocation of lactate or pyruvate via monocarboxylate transporters between cellular compartments

The other control point of a redox shuttle, the lactate-specific transporters facilitating the cross-membrane translocation, was also identified in cellular membranes of mammal cells (Poso, 2002). Two monocarboxylate transporter 1 (MCT1) and MCT2 were shown to be present in purified peroxisomal membranes by immunoblot detection in rat liver tissues. It was found that lactate was released from isolated peroxisome preparations when treated with exogenous

pyruvate, suggesting elevation of lactate dehydrogenase that converted pyruvate into lactate in the peroxisomes and efflux of lactate out of the peroxisomes by monocarboxylate transporters (McClelland et al., 2003). As a result, reducing equivalents generated through the β-oxidation pathway were attached to pyruvate coinciding with the production of lactate and NAD^+, which in return, was fed back into β-oxidation and led to its thus stimulation. However, the stimulation effect of pyruvate was partially inhibited by the addition of the MCT blocker a-cyano-4-hydroxycinnamate (CINN) (McClelland et al., 2003). These results indicated that monocarboxylate transporters in the peroxisomal membranes were specifically responsible for the export of intraperoxisomal lactate and were important for maintaining the functioning of the β-oxidation. Meanwhile, the treatment of CINN on the prepared mitochondria from rat tissues blocked the respiration with lactate or pyruvate as the substrate; however, the blockade effect was restored when the substrate was changed to succinate or glutamate (Brooks et al., 1999). Based on this result, it suggested that CINN inhibited the mitochondrial respiration though the upstream transport limitation of lactate or pyruvate, which was supposed to deliver to the mitochondrial intermembrane space to proceed with oxidation. It was further revealed that the cytosolic concentration of lactate was 10-fold higher than that of pyruvate. Therefore, in comparison with pyruvate, lactate should be the main monocarboxylate that enters the mitochondria for the oxidation by the mitochondrial lactate dehydrogenase (Brooks et al., 1999).

1.5.3.3 Potential roles of the lactate shuttle in nutrient metabolism and redox balance of *M. oryzae*

Therefore, the presence of the so-called lactate shuttle facilitates the export of reducing equivalents in peroxisomes to the cytosol and eventually to mitochondria. (Brooks, 2009; Brooks et al., 1999; McClelland et al., 2003). In detail, accompanying the reduction of pyruvate to lactate in the peroxisome, accumulated NADH is reoxidized to NAD^+, which is then absorbed into β-oxidation. Lactate is exported to the cytosol and/or to the mitochondrion, where

it is oxidized to pyruvate with the concomitant production of NADH/$FADH_2$, subsequently followed by the donation of electrons to the mitochondrial respiratory chain. To form a metabolic cycle, the peroxisome requires the continuous availability of pyruvate, which can be channeled back from the cytosol and/or mitochondria. The production of pyruvate could also result from the transamination of intermediates in the peroxisomal glyoxylate cycle by action of aminotransferases, such as the alanine glyoxylate aminotransferase (AGT) that catalyzes the exchange of the amino acid between alanine and glyoxylate to produce pyruvate and glycine. In *M. oryzae*, deletion of the peroxisomal *AGT* gene caused the inability to form the appressoium and mobilize lipid droplets on artificial inductive surfaces such as cover slips; however, appressorium formation and mobilization of lipid droplets were restored when supplementing the conidial suspension with NAD^+ plus pyruvate. This result suggested that the conversion of glyoxylate to pyruvate, which was supposed to be reduced to lactate with the production of NAD^+ required for the proper functioning of the β-oxidation, was an important consequence of the β-oxidation and the glyoxylate cycle pathway in *M. oryzae* (Bhadauria et al., 2012).

Taken together, based on previous uncovering on metabolic pathways associated with lipid body utilization in the peroxisomes, we postulate that a redox shuttle, operated by lactate dehydrogenases and monocarboxylate transporters in different cellular compartments, facilitates the transportation of reducing equivalents from the peroxisomes to mitochondria. This redox shuttle, named the lactate shuttle, is vital for the sustainability of lipid metabolism in peroxisomes during the disease process of *M. oryzae*. In this model, lactate for pyruvate exchange and translocation across cellular membranes has two functions: a regulator of cellular redox state and a mobile fuel to deliver reducing power in the peroxisomes to mitochondria. Firstly, NADH is reoxidized to NAD^+ along with the conversion of lactate from pyruvate as a product of the β-oxidation and the glyoxylate cycle in the peroxisome. Moreover, reducing power created due to the fatty acid oxidation in the peroxisome is stored in lactate and carried across cellular membranes to the mitochondrion. Oxidation of lactate to pyruvate is associated with the release of reducing power in forms of $FADH_2$ and NADH, followed by donation of

electrons to the respiratory chain for cellular respiration. The control points of this model are lactate dehydrogenases catalyzing the interconversion between lactate and pyruvate in different cellular compartments and monocarboxylate transporters for the translocation of lactate from the peroxisome to the cytosol and the mitochondrion.

1.6 Overview of research hypothesis and objective

To test the lactate shuttle hypothesis in *M. oryzae* and reveal its roles in fungal development and pathogenicity, this project will functionally analyze lactate dehydrogenases in different cellular compartments. Meanwhile, to conduct the functional comparison between roles of different redox shuttles in *M. oryzae*, I also aimed at characterizing the G-3-P shuttle, whose involvements in the oxidation of non-fermentable carbons and adjustment of redox balance have been shown in yeast. In particular, the project was divided into five aspects as described below:

1. Chemical inhibitions were used to investigate the effects of aminotransferase and lactate dehydrogenase in infection-related development of *M. oryzae* and *C. higginsianum.*
2. Identification of lactate dehydrogenase genes in the *M. oryzae* genome and transcriptional characterization of these genes during *in vitro* and *in planta* stages.
3. Targeted gene replacement of *M. oryzae* lactate dehydrogenase genes using a PCR based split-marker method.
4. Phenotypic analysis of gene replacement mutants to determine roles of lactate dehydrogenases in fungal development and pathogenicity of *M. oryzae*.
5. Functional comparison of the lactate shuttle with the G-3-P shuttle in regulating fungal development and pathogenicity of *M. oryzae*.

CHAPTER 2 MATERIALS & METHODS

2.1 Fungal strains and culture condition.

PDA medium (3.9% potato dextrose) and Complete medium (CM) (0.6% acid casein hydrolysate, 0.6% yeast extract, 1% sucrose) were used to culture fungi. Minimal medium (MM) is 6 g/l NaNO3, 0.52 g/l KCl, 0152 g/l MgSO4.7H2O, 1.52 g of KH2PO4, 0.001% thiamine, 0.1% trace elements supplemented with 1% glucose or alternative carbon sources with equivalent amount. V8 medium was made by adding 200 ml V8 juice and 200 g CaCO3 in 1 L sterile H_20. Oatmeal medium (3% oatmeal) was used to produce fungal asexual spores. For all solid medium, agar concentration was made at 15 g/l.

Magnaporthe oryzae wild type strains and derived mutants created in this study were maintained on oatmeal medium plates. For long term storage, conidia of isolates were collected from oatmeal medium plates in 10% glycerol before storing in -80℃ ultra freezer.

2.2 Plant materials

The barley cultivar CDC Silky and Dwarf Indica rice (Oryza sativa) cultivar CO39, both of which are highly susceptible to *M. oryzae*, were used in this study for fungal infection. Barley was grown in a growth chamber with a 16 hr photoperiod at 24℃ for 10 days before leaves were detached for drop-inoculation. Rice was grown in small pots with a 16 hr photoperiod at 24℃ for two weeks, followed by spray-inoculation of conidial suspension.

2.3 DNA and RNA manipulation

Most of DNA and RNA manipulations were conducted according to protocols in (Green and Sambrook, 2012). Isolation of fungal DNA for polymerase chain reaction (PCR) was performed following the protocol described in (Chi and Lee, 2009). For DNA extraction, small

pieces of mycelium were taken from a 3-day old PDA plate and mixed with 400 µl DNA extraction buffer (1% SDS, 1M KCl, 100 mM Tris-HCl, 10mM EDTA) in a 1.5-ml Eppendorf tube. Mycelia were ground in buffer to release DNA followed by centrifugation at 8000 rpm for 10 min, the supernatant was transferred to a new tube and mixed briefly by inversion with equal volume of isopropanol and centrifuged at 12000 rpm for 10 min. the supernatant was discarded and the DNA pellet was washed in 600 µl 70% alcohol twice. The final DNA product was dissolved in 40 µl sterile H_2O and stored at -20℃. DNA fragments were purified from agarose gels using Thermo Scientific GeneJET Gel Extraction Kit (Thermo Scientific, Ottawa, Ontario). Plasmid DNA was isolated using the alkaline lysis method described in (Green and Sambrook, 2012). DNA blot was conducted with DIG DNA Labeling and Detection Kit I (Roche Applied Science), following the manufacturer's instructions.

For RNA extraction, fungal materials collected were firstly ground into a fine powder in liquid nitrogen then mixed with 15 ml RNA extraction buffer (150 mM LiCl, 5 mM EDTA, 50 mM Tris-Cl pH 9.0, 5% SDS) in a 50 ml centrifuge tube, followed by the vigorous shaking and centrifugation at 2500 rpm for 20 min. The supernatant was transferred into a new 50 ml tube with 15 ml phenol-chloroform. After shaking vigorously, the tube was centrifuged at 1500 rpm for 20 min. Then, the top phase was taken and mixed with 1.5 ml NaAc (4 M, pH 5.3) and 12 ml cold isopropanol to precipitate the DNA/RNA mixture at -20℃ overnight. Centrifugation at 8000 rpm for 20 min to collect the precipitate, which was further re-dissolved in 6 ml H2O and 2 ml 8 M LiCl following cooling on ice for 2 hr. The tube was centrifuged again at 8000 rpm for 20 min. After discarding the supernatant, RNA precipitates were washed with 1 ml of 70% cold alcohol and transferred to a 1.5 ml centrifuge tube, following the centrifugation at 12000 rpm for 20 min. The final RNA products were dissolved in 100 µl H_2O and subjected to concentration determination by NanoDrop 2000 UV-Vis spectrophotometer.

2.4 Gene expression analysis

RT-PCR was used to determine the gene expression of lactate dehydrogenases and mitochondrial G-3-P dehydrogenase in mycelia, conidial and *in planta* stages. Total RNA was isolated from mycelia harvested from liquid complete medium shaken at 110 rpm for 3 days, conidia collected from 10-day-old oatmeal agar medium, infected plant leaves harvested after 2h, 4 h, 20 h, 48 h and 96 h inoculation, with phenol/chloroform extraction and LiCl precipitation. cDNA synthesis was prepared using Super ScriptII Reverse Transcriptase (Invitrogen, USA), and used as template for RT-PCR analysis. The actin gene *Mgg_03982* of *M. oryzae* was used as the endogenous control for standardization. Twenty-eight PCR cycles were used to amplified the actin gene, while 28-32 cycles were used to amplified other target genes.

2.5 Generation of gene replacement constructs

The gene replacement construct was created by overlap PCR (Yu et al., 2004). Approximately 1-kb upstream and downstream flanking sequences of the targeted gene were amplified with primers and ligated with each half end of the hygromycin-B phosphotrasferase gene (*hph)* cassette by ligation PCR (Fig 2.1). Both constructs shared about a 300 bp overlapping sequence, which were transformed into protoplasts of wild type *M. oryzae*.

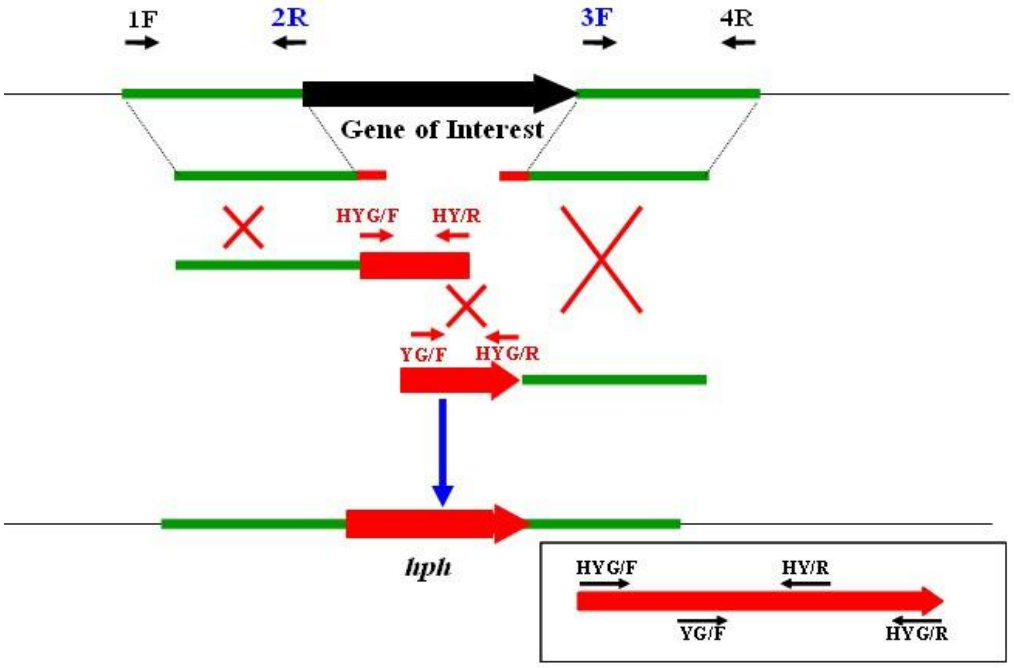

Figure 2.1 Schematic representation of a gene replacement cassette.
Primer 2R and 3F are chimeric primers of 45-50 bases with 25-30 bases overlapped by ends of selective marker. First round PCR: using the specific and chimeric primers to amplify 5' flanking fragment (1F-2R) and 3' flanking fragment (3F-4R) of ORF, and using (HYG/F-HY/R) and (YG/F-HYG/R) primers to amplify two split markers sharing 300 bp overlapped sequence. Second round PCR: without using any specific primers, the overhanging chimeric extensions function as primers and the first round PCR products serve as templates to assembe flanking fragments with split markers, respectively.

2.6 Generation of full ORF length and domain deletion eGFP-fusion constructs

The open reading frame (ORF) of genes of interest along with their native promoter sequence were amplified with primers and cloned into eGFP-tagged vector pKNTG with neomycin resistance marker using suitable enzyme digestion sites (Fig 2.2). The final eGFP fusion construct was transformed into protoplasts of recipient strains. The partial MoDLD1 sequence deleted of N-terminal mitochondrial targeting sequence plus transmembrane domain or transmembrane domain alone were cloned respectively with chimeric primers and fused with amplified PCR product of *MoDLD1* native promoter by ligation PCR as described above. The

ligation PCR products were digested and cloned into the eGFP-tagged vector pKNTG using suitable restriction sites. After confirmation by DNA sequencing analysis, the resulting eGFP fusion constructs were linearized with a restriction enzyme and transformed into protoplasts of ⊿*MoDLD1* mutants. The neomycin-resistant transformants from media were screened for eGFP expression by Confocal microscopy and confirmed by PCR.

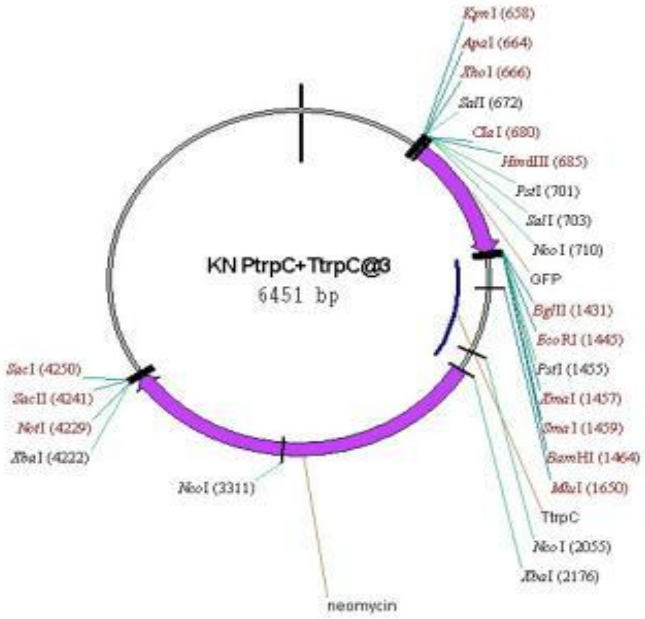

Figure 2.2 Schematic drawing of pKNTG plasmid for eGFP fusion.
The plasmid length is 6451 bp. It has ampicillin resistance to amplification in bacteria and resistance to neomycin (G418) in fungi. Unique digestion sites in red. Sequences of eGFP and neomycin resistance gene (*neo*) in purple color.

2.7 Fungal transformation

To make fungal protoplasts, *M. oryzae* mycelia from the surface of one 5-day-old PDA plate were transferred into 50 ml liquid CM medium in a 150 ml bottle. The culture was shaken for 2 days at 130 rpm at 26 ℃, and the mycelia collected and ground in a mortar. Ground mycelia were transferred into a new 150 ml bottle with fresh 50 ml liquid CM media. Mycelia were cultured with vigorous shaking for 18 hr at 180 rpm at 26 ℃ and then filtered through filter paper (VWR, Cat 28306-175). After washing twice with 50 ml sterile water and 1 M

sorbitol, the mycelia were gently shaken in 20 ml 1 M sorbitol containing 10 mg/ml Lysing Enzymes (Sigma, Cat L1412) for 3 hr at 30℃. Released protoplasts were checked under the microscope and harvested by filtering through 22-25 μm Miracloth (VWR, Cat 475855-1R) into a 50 ml tube which was centrifuged at 5000 rpm for 10 min to collect protoplasts. 15 ml of STC buffer (1 M sorbitol, 10 mM Tris pH=7.5, 50 mM $CaCl_2$) was used to re-suspend the pellet which was centrifuged again for collection. Protoplasts were re-suspended with 1 ml of STC buffer and transferred to a 1.5 ml micro centrifuge tube. The protoplast concentration was adjusted to 10^7/ml for transformation.

For transformation, 5 μg linearized plasmid or PCR product was gently mixed with 300 μl of protoplast suspension in a 50 ml tube which was kept on ice. After 20 min, 1.2 ml of freshly prepared PTC (40% PEG 3350 in PTC buffer) was added to the tube, followed by gentle shaking for few seconds and standing at room temperate for 20 min. Then, 30 ml melted TB_3 medium (3% yeast extract, 3% casamino acid, 20% sucrose, 1.5% agar) containing antibiotic (100 μg/ml hygromycin or 200μg /ml neomycin) was mixed with the protoplast suspension and poured into 15 cm diameter plate. After the medium was solidified, the plate was overlaid with 15 ml melted TB_3 medium containing antibiotic (300 μg/ml hygromycin or 400μg /ml neomycin). The plate was kept at 26 ℃ for 5-10 days until re-generated colonies grew up.

2.8 Treatment of aminotransferase and lactate dehydrogenase inhibitors on *M. oryzae* and *C. higginsianum*.

Wild type *M. oryzae* strain Guy11 and *C. higginsianum* strain IMI 349063 were used in this study. Conidia collected from 10-day-old oatmeal media were adjusted to $5*10^4$ spores/ml in sterile water for inoculation. Aminooxyacetic acid and oxamic acid were prepared in stock solution and added to conidial suspension to reach the final concentration, respectively. 20 μl of conidial suspensions treated with the inhibitor were placed on plastic cover slips to induce appressorium formation at room temperature. After 24 hr induction within the moisture chamber,

appressorium formation was observed and counted for statistical analysis. For the treatment test by pyruvate and AOA, sodium pyruvate stock solution was added to the conidial suspension containing 1 mM AOA to reach the concentration gradient of sodium pyruvate, and then 20 μl of conidial suspension was spotted on plastic cover slips for 24 h. For testing the effect of OXA on fungal virulence, 20 μl of conidial suspensions treated with different concentrations of OXA was inoculated on detached 10-day-old CDC silky barley leaves to allow the infection in the moisture chamber. Disease symptoms were monitored 5 dpi.

2.9 Expression of *MoDLD1* and *MoDLD1*$^{\Delta SP+TM}$ in the yeast *ScDLD1* mutant

To construct the vector for constitutive expression of *MoDLD1* and *MoDLD1*$^{\Delta SP+TM}$ in *S. cerevisiae*, the promoter of yeast Translation Elongation Factor 1 (TEF1) was amplified to replace the GAL1 promoter in pYES2 (Invitrogen, Cat.V825–20) using suitable enzyme restriction sites, resulting in a pTEF1 vector for constitutive expression of heterologous genes in yeast (Nevoigt et al., 2006). The *S. cerevisiae ScDLD1* mutant was created from *MATa* strain BY4741 (EUROSCARF). The coding sequence of *MoDLD1* ORF and *MoDLD1*$^{\Delta SP+TM}$ was amplified from the 1st strand cDNA of Guy11 and cloned into pTEF1 vector under the control of the TEF1 promoter. The resulting constructs pTEF1-*MoDLD1* and pTEF1-*MoDLD1*$^{\Delta SP+TM}$ were transformed into the *ScDLD1* mutant through the LiAc mediation method as described in (Gietz et al., 1995). Transformants were selected on SD-ura medium (0.17% yeast nitrogen base without amino acids and ammonium sulfate, 0.5% ammonium sulfate, 2% glucose, 0.077% -Ura DO Supplement, and 2% agar). For the growth assay on sodium D-lactate, the yeast transformants and BY4741 were cultured in liquid YPD medium (1% yeast extract, 2% peptone and 2% glucose) for 16 h at 28℃. Yeast cells were collected after centrifugation at 3000 rpm for 5 min, and then washed twice and re-suspended in sterile H_2O, followed by spotting 2.5μl of cell suspension, serially diluted to 10^6, 2×10^5, and 4×10^4 cells/ml, on agar plates containing sodium D-lactate or glucose as sole carbon source (0.17% yeast nitrogen base without amino acids and

ammonium sulfate, 0.5% ammonium sulfate, 2% carbon source, 0.077% -Ura DO Supplement, 0.01% Ura and 2% agar). Yeast strains were allowed to grow on media plates for 5 days at 28℃ before photos were taken.

2.10 Phenotypic analysis

To determine the vegetative growth rate, the diameter of mycelium colony grown on PDA or CM medium for 7 days was measured. The ability to produce conidia was quantified by counting the number of conidia collected from 10-day-old oatmeal agar plates. Five ml sterile H_2O was used to flood the plate to collect conidia, which were then counted using a hemacytometer under a microscope. To observe conidiophore and conidial formation, mycelium plugs in oatmeal were cultured on cover slides under constant light exposure for 36 hr and then were observed under the microscope as described in (Lau and Hamer, 1998). Conidia were observed microscopically for morphological change and conidial size was measured under a microscope.

For appressroium formation, 15 μl of conidia suspension adjusted to its concentration to approximately $5*10^4$ spores/ml, with or without desired compounds treatment, was dropped on plastic cover slips, onion epidermal cells or detached barley leaves in the moisture chamber at 24 ℃ for 16-24 h. For observation of infectious behavior by invasive hyphae, plant leaves challenged by conidia of *M. oryzae* strains for 48 h were collected. To observe the appressorium formation/penetration and invasive hyphae on plants clearly, fixation solution (60% methanol, 30% chloroform, 10% acetic acid) was used to remove the chlorophyll and fix samples. Appressorium formation/penetration and invasive hyphal development were examined with a bright field microscope.

2.11 Pathogenicity tests

For the infection assay, conidia collected from wild type and genetically manipulated strains on 10-day-old oatmeal plates were adjusted to 4×10^4 conidia/mL in sterile water. Two-week-old susceptible rice seedlings of Co39 cultivar were spray-inoculated with 10 ml conidial suspension containing 250 ppm Tween20. The inoculated plants were kept in a moisture chamber for 24 h in darkness and then moved to a highly humid growth chamber with 16 h photoperiod. Disease severity at 7 days post-inoculation was examined and photographed. For droplet inoculation, 20 µl conidial suspensions with adjusted concentrations from 4×10^4, 10^4 to 10^3 spores/ml were spotted on the leaf surface of 10-day-old detached susceptible barley cultivar CDC Silky. Environmental conditions for development of disease symptoms were identical to that for the spray inoculation on rice seedlings. Blast lesions on barley leaves were allowed to develop for 5 days before observation.

2.12 NAD^+/NADH treatment and cytological analysis

The NAD^+ and NADH were prepared in sterile water with stock concentration at 50 mM and were added to conidial suspensions of Ku70 and *⊿MoDLD1* at desired working concentrations. Conidial suspensions treated with NAD^+ or NADH were placed on plastic cover slips for 5 h in a moisture chamber to observe the effect. To assess conidial viability, water was removed from cover slips after NAD^+ or NADH treatment and prepared propidium iodide (PI) solution (15 µm) was added to indicate cell viability. Mobilization of lipid droplets during conidial germination and appressorium formation was visualized using Nile red staining. Fresh conidia harvested from Ku70 and *⊿MoDLD1* were inoculated on cover slips at room temperature. Cover slips upon induction at different time intervals were mounted with Nile red staining solution (Sigma, St. Louis, MO, USA) (2.5 µg/ml) to visualize movement of lipid droplets. Glycogen visualization was carried out by adding a solution containing 60 mg/ml KI and 10 mg/ml I_2 to cover slips inoculated with conidial suspension for varied time duration,

followed by observation under differential interference contrast (DIC) microscopy. For staining of cell walls and septa, fresh vegetative hyphae and conidia were stained by Calcofluor White (10 mg/ml, Sigma) for 5 min and washed twice with sterile water before observation.

2.13 Confocal and Fluorescence Microscopy

Confocal laser scanning microscopy was performed with a Zeiss Confocor2–LSM 510 META (Carl Zeiss, Jena, Germany). eGPF was excited with an Argon (488 nm) laser, Mito Tracker Red CMXRos, Nile red and PI were both excited with a HeNe1 (543 nm) laser. Fluorescence signals were captured through emission filters 505-530 nm for GFP, 600-650 nm for Mito Tracker Red CMXRos, Nile red and PI staining. Calcofluor White was excited with UV light from axioplan fluorescence microscope (Nikon).

2.14 Immunogold labeling electron microscopy and scanning electron microscopy

For immunogold labeling electron microscopy, procedures were modified from the description in (Sirerol-Piquer et al., 2012). Conidia of *MoDLD1-Com-eGFP-14* collected from a 10-day-old oatmeal plate were centrifuged in a 50 ml tube and then the conidial precipitate was transferred into a 1.5 ml tube, where it was re-suspended and fixed in 4% formaldehyde in 50 mM phosphate buffer for overnight at 4 ℃. After centrifugation, samples were dehydrated in 70%, 95% and 100% ethanol for 30 min at each concentration. The samples were incubated in mixture (1:1) of L. R. White and 100% ethanol overnight and transferred to pure L. R. White in three changes for 2 h each. Samples were kept in the last change of L.R. White overnight at room temperature. Finally, samples were placed in Gelatin capsule filled with L. R. White to the brim and incubated at 60 ℃overnight. Then, EM blocks were trimmed into 0.5 μm thick sections that were later cut into 70–90 nm sections and collected on formvar-carbon coated nickel grids. For primary antibody staining, grids were firstly incubated in 1% bovine serum

albumin for 1 h to block non-specific binding, and then were stained by anti-GFP antibody (abcam) in 1:50 dilution for 2 h at room temperature, followed by rinse in water for 3 times. The secondary anti-body Goat Anti–Mouse IgG (Invitrogen) was prepared in a 1:200 dilution and used to stain grids for another 2 h at room temperature. To contrast the staining, samples were further incubated in aqueous uranyl acetate for 15 min and lead citrate for 1-2 minutes at room temperature before observation. TEM images were taken by a Philips model CM10. In the control experiment, the primary antibody was omitted.

For scanning electron microscopy (SEM), *M. oryzae* strains were grown on oatmeal medium for 7 days under constant light exposure to induce conidiation. The sample preparation and operation for SEM were performed as described in (Bozzola and Russell, 1999; Samson et al., 1979). In detail, samples were sliced from the surface of oatmeal plates and fixed in 2.5% glutaraldehyde diluted by 50 mM phosphate buffer in 1.5 ml micro centrifuge tubes overnight. Samples were dehydrated in a graded ethanol series (30%, 50%, 75%, 95% and 100%) for 2 h at each concentration, and then were transferred to pure acetone for 2 h. Samples were dried by the critical-point method, and then were sputter-coated with gold. SEM images were taken by a phenom G2 Phenom G2 pro desktop SEM.

2.15 Data collection and statistical analysis

All data collected in the tests of mycelial growth rate, fungal conidiation, conidial germination, conidial size, conidial septum, appressorium formation with or without pharmacological treatment, appressorium penetration and invasive hyphal proliferation were subject to the statistical analysis. For the measurement of mycelial growth rate, three biological replicates with three independent experiments were carried out to produce data for statistical analysis. For fungal conidiation, at least three plates were calculated for conidiation for an individual strain in each biological replicate, and three biological replicates were conducted. For the measurement of conidial size and septa, 100 conidia were collected from a 10-day-old

oatmeal medium plate, and three independent replicates were performed in each test. For conidial germination assay, 100 conidia inoculated on plastic slips were counted for germtube formation, which was repeated three times for each biological replicate, and three biological replicates were required for this test. For appressorium formation assay, the experimental procedure was identical to the conidial germination test, except 100 conidia with germtubes were counted for appressorium formation. For appressorium penetration test, 50 appressoria induced on the plant surface were observed at one inoculation site, three inoculation sites were observed for each biological replicate, and three biological replicates were carried out. The mean values and standard deviations were calculated in Excel of Microsoft Office (Microsoft Company; Mississauga, CA). Analysis of variance (ANOVA) test with $P<0.05$ or $P<0.01$ was conducted to determine the difference among group means by SAS 8.0 software (SAS Institute Inc, NC, USA).

CHAPTER 3 RESULTS

3.1 Infection-related development I s prevented by either inhibitor of aminotransferase or lactate dehydrogenase in *M. oryzae* and *C. higginsianum*

Production of pyruvate/NAD^+ via the alanine glyoxylate aminotransferase (AGT) is an important consequence of peroxisomal lipid catabolism in *M. oryzae* (Bhadauria et al., 2012). To further investigate the role of aminotransferases in modulating germination and appressorium development, conidia of *M. oryzae* were germinated in aminooxyacetic acid (AOA), a well-recognized 4-aminobutyrate aminotransferase-specific inhibitor (Wallach, 1961). The germination and appressorium formation rates on an artificial hydrophobic surface were significantly affected in a dose-dependent manner, with 1mM AOA being completely inhibitory to appressorium initiation after 24 hr incubation (Fig 3.1A-B). However, co-incubation with a range of concentration gradients of pyruvate allowed appressorium formation on the artificial hydrophobic surface (Fig 3.1C-D), which confirmed the main role of aminotransferases is for production of pyruvate that appeared to be a central metabolite in coordinating lipid catabolism. Moreover, the pharmacological experimental data from the dicot fungal pathogen *Colletotrichum higginsianum* causing anthracnose disease on many foliar plants also supported the indispensable role of aminotransferase-mediated production of pyruvate in regulating development of infectious structures in phytopathogenic fungi (Huser et al., 2009). The germination and appressorium formation of *C. higginsianum* conidia were completely blocked after treatment with 1mM AOA for 24 hr, but gradually recovered by excess pyruvate with increment in concentrations (Fig 3.1E-F).

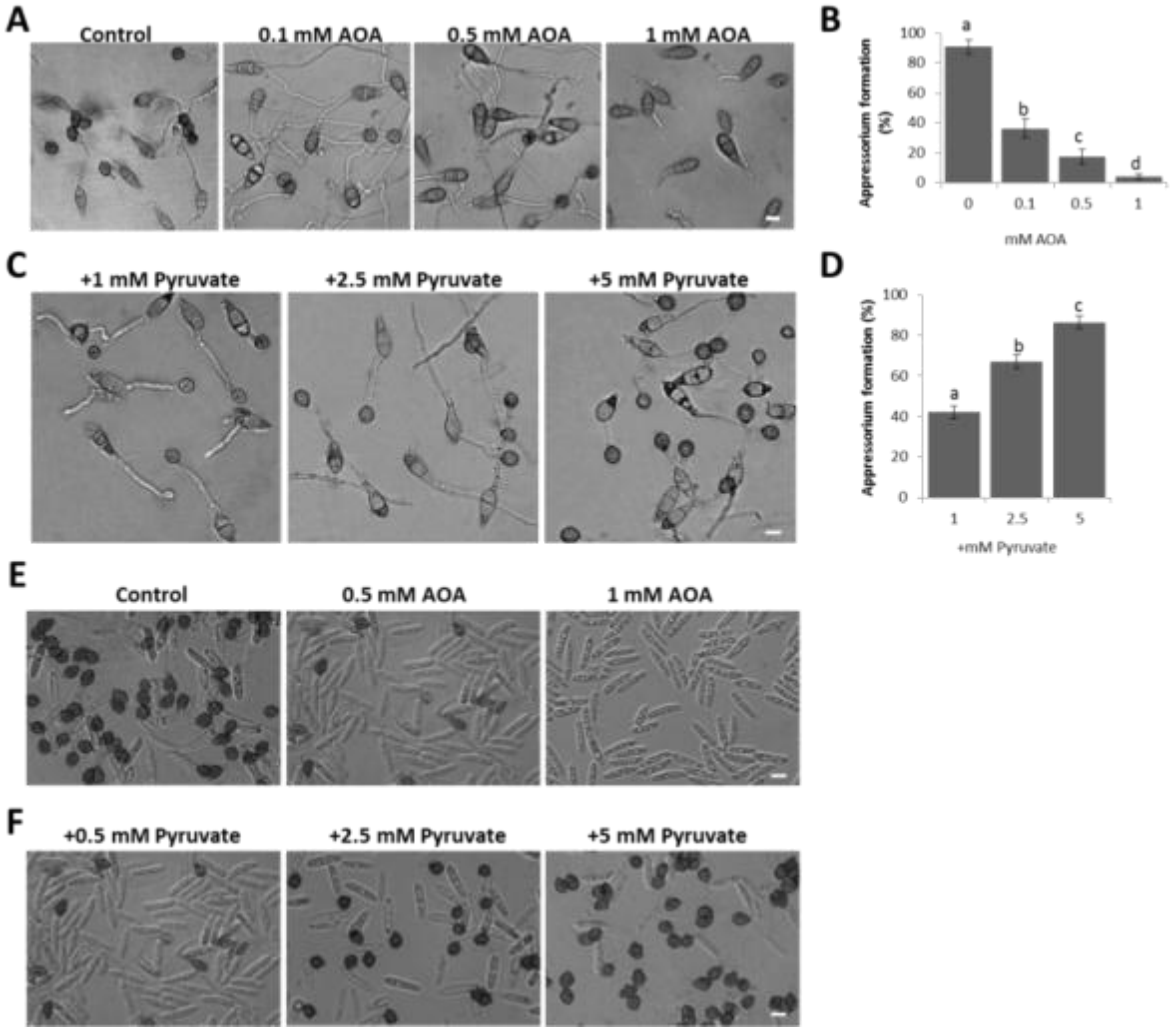

Figure 3.1 Exposure to aminotransferase inhibitor prevented infection-related development but restored by excess pyruvate in *M. oryzae* and *C. higginsianum*.

(A-B**)** Appressorium formation of *M. oryzae* was examined and measured statistically in the presence of 0.1, 0.5, and 1 mM aminooxyacetic acid (AOA) for 24 hr incubation on plastic cover slips. Bar=10 µm. Error bars represent standard deviations from three independent experiments with three replicates. Different letters in each data column indicate significant differences at P=0.01. (C-D) Excess 1, 2.5, and 5 mM pyruvate were added to a 1 mM AOA treatment in appressorium formation assay of *M. oryzae* for 24 hr incubation. Bar=10 µm. Error bars represent standard deviation from three biologic repetitions with three replicates and different letters in each data column indicate significant differences (P =0.01). (E) Appressorium formation of *C. higginsianum* was observed in the presence of 0.5 and 1 mM AOA for 24 hr incubation on plastic cover slips. Bar=10 µm. (F) Conidial suspension of *C. higginsianum* was allowed to form appressoria in 1 mM AOA plus 0.5, 2.5, and 5 mM pyruvate, respectively, for 24 hr on plastic cover slips. Bar=10 µm.

Furthermore, the role of lactate dehydrogenases in regulating infectious behavior of *M. oryzae* was assessed according to pharmacological intervention. Conidia were germinated in oxamic acid (OXA), which is routinely recognized as a lactate dehydrogenase-specific inhibitor (Novoa et al., 1959). On the artificial hydrophobic surface, appressorium formation was prevented in a dose-dependent manner, with 3 mM OXA completely inhibitory post 24 hr incubation (Fig 3.2A-B). Oxamic acid also abolished the virulence of *M. oryzae*. The addition of 1 mM oxamic acid resulted in smaller lesions compared to enlarging necrosis on barley leaves infected by the non-treatment strain. Disease development was almost non-existent in conidial suspension containing 5 mM OXA that had no observable effect on barley leaves (Fig 3.2C). The microscopic observation on infectious behaviors of OXA-treated wild type conidia on barley leaves post 48 h showed that appressorium formation was partially restored on the plant surface compared to the induction on nutrient-free plastic surface; however, the ramification of invasive hyphae was gradually prevented according to enhanced treatments of OXA (Fig 3.2D). The conidial suspension of *C. higginsianum* with the 1 mM OXA treatment for 24 hr resulted in differentiation of albino appressorium on an artificial hydrophobic surface, showing aberrant appressorium development. Moreover, the 3 mM OXA treatment in *C. higginsianum* conidia led to complete blockage of germination (Fig 3.2E).

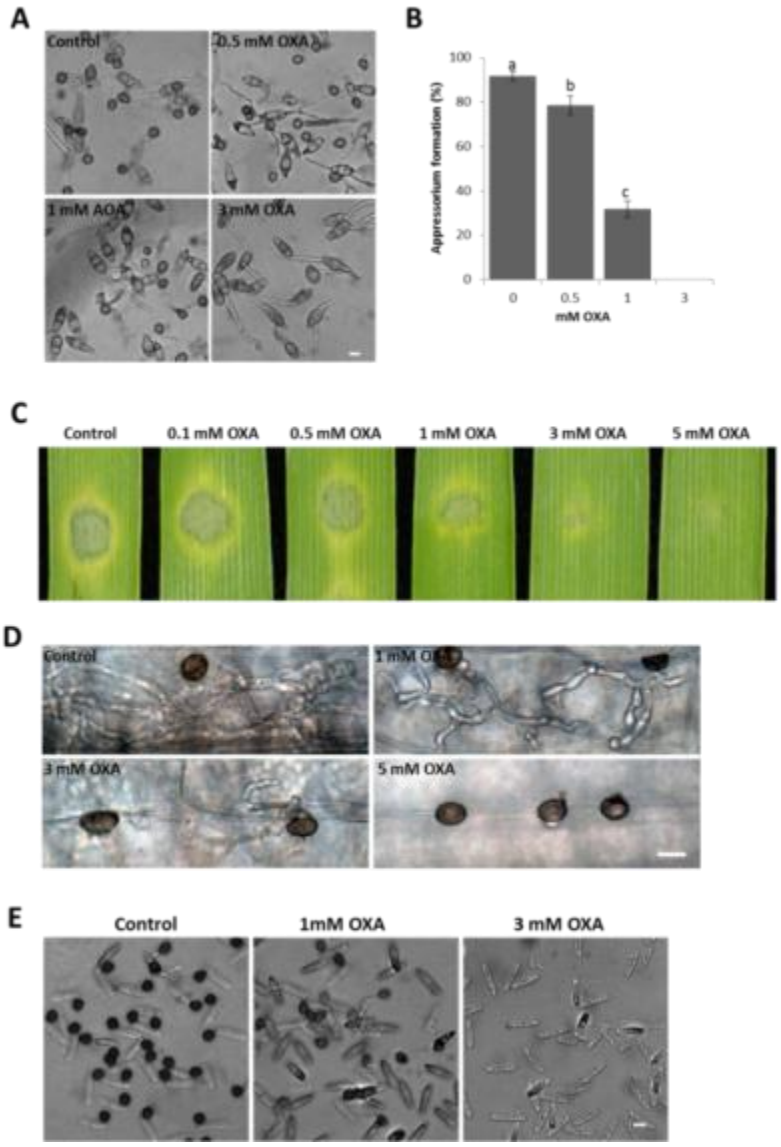

Figure 3.2 Exposure to lactate dehydrogenase inhibitor prevents infection-related development in *M. oryzae* and *C. higginsianum.*

(A-B) Appressorium formation of *M. oryzae* was examined and measured statistically in the presence of 0.5, 1, and 3 mM oxamic acid (OXA) for 24 hr incubation on hydrophobic surface. Bar=10 μm. Error bars represent standard deviations from three independent experiments with three replicates and different letters in each data column indicate significant differences (P =0.01). (C) Conidial suspensions of *M. oryzae* in differing concentrations of OXA were spotted on barley leaves. Disease progress was assessed 5 days after inoculation. (D) Appressorium formation and invasive growth of *M. oryzae* were observed under the microscope in the presence of 1, 3 and 5 mM oxamic acid (OXA) for 48 hr inoculation on barley leaves. (E) Appressorium formation of *C. higginsianum* was observed in the presence of 1 and 3 mM OXA for 24 hr incubation on hydrophobic surface. Bar=10 μm.

3.2 Identification and domain architecture analysis of putative lactate dehydrogenases in *M. oryzae*

Lactate dehydrogenases that catalyze the interconversion between lactate and pyruvate consist of two evolutionally unrelated enzymes: D-lactate dehydrogenases and L-lactate dehydrogenases (Cristescu et al., 2008). However, a possible evolutionary linkage was revealed between malate dehydrogenases and L-lactate dehydrogenases since they share the similar domain structures and are more closely related in amino acid sequence (Hall et al., 1992). In *S. cerevisiae*, there are four lactate dehydrogenases including three D-lactate dehydrogenases (ScDLD1, ScDLD2 and ScDLD3), and one L-lactate dehydrogenase CYB2 (Chelstowska et al., 1999; Lodi and Ferrero, 1993; Lodi and Guiard, 1991). Three malate dehydrogenases (ScMDH1, ScMDH2 and ScMDH3) have been identified in *S. cerevisiae* (McAlister-Henn and Thompson, 1987; Minard and McAlister-Henn, 1991; Steffan and McAlister-Henn, 1992). Amino acid sequences of D, L-lactate dehydrogenases and malate dehydrogenases in *S. cerevisiae* were used to search the *M. oryzae* genome database using blastP http://www.broadinstitute.org/annotation/genome/magnaporthe_grisea/MultiHome.html)(Dean et al., 2005), and yielded MoDLD1 (Mo_01202), MoDLD2 (Mo_12830) and MoDLD3 (Mo_12601) as putative D-lactate dehydrogenases, MoLLD1 (Mo_01723), MoLLD2 (Mo_00335), MoLLD3 (Mo_14264), and MoLLD4 (Mo_13441) as putative L-lactate dehydrogenases, and MoMDH1 (Mo_09367), MoMDH2 (Mo_08835) and MoMDH3 (Mo_10453) as putative malate dehydrogenases, respectively. In addition, using the domain search function in the *M. oryzae* genome database (Dean et al., 2005), the gene Mo_09872 was found to have the Malate/L-lactate dehydrogenase domain (Ldh_2), which was usually characteristic of bacterial and archaeal malate/L-lactate dehydrogenases (Honka et al., 1990; Jendrossek et al., 1993), and was therefore considered as a putative L-lactate dehydrogenase, namely MoLLD5.

Phylogenetic analysis was conducted to display similarities among amino acid sequences of D-lactate dehydrogenases in S. *cerevisiae* and *M. oryzae* using ClustalX1.83 (Fig

3.3A). Alignment of MoDLD1 with D-lactate dehydrogenase 1 (ScDLD1) in *S. cerevisiae* revealed 47% identity. Forty-nine percent identity is shared between MoDLD1 and MoDLD3, which was higher compared to identity with MoDLD2. MoDLD2 has 60% sequence similarity to D-lactate dehydrogenase 2 (ScDLD2) in *S. cerevisiae.* MoDLD3 also displayed higher sequence similarity to ScDLD1 than to ScDLD2 and ScDLD3, indicating absence of the yeast D-lactate dehydrogenase 3 (ScDLD3) homology in *M. oryzae*. Domain architecture analysis indicated that MoDLD1, MoDLD2, and MoDLD3 contained the FAD binding and FAD oxidase domains at their C-terminus and mitochondrial targeting sequences at the N-terminus, while both MoDLD1 and MoDLD3 also possessed an N-terminus transmembrane domain following the MTS sequences (Fig 3.3B). According to bioinformatic analysis of protein sequences of putative D-lactate dehydrogenases in *M. oryzae*, it was found that they are exclusively mitochondrial proteins (Finn et al., 2013).

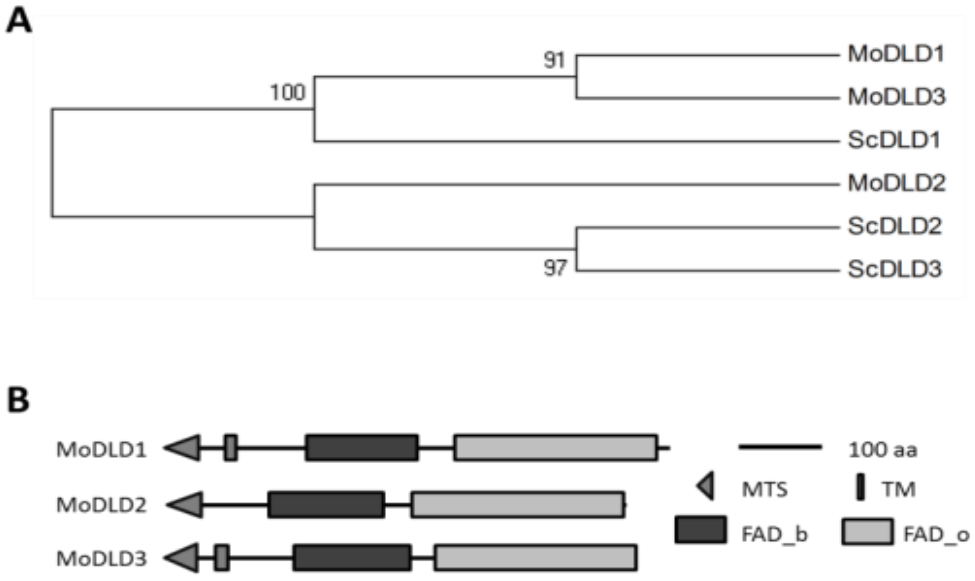

Figure 3.3 Phylogenetic analysis and domain architecture of D-lactate dehydrogenases in *M. oryzae*.

(A) Protein sequences of D-lactate dehydrogenases in *M. oryzae* and *S. cerevisiae* were aligned and the phylogenetic tree was generated using ClustalX1.83. ScDLD1, ScDLD2 and ScDLD3 are D-lactate dehydrogenases in *S. cerevisiae,* MoDLD1, MoDLD2 and MoDLD3 are D-lactate dehydrogenases in *M. oryzae.* (B) Schematic representation of protein domain architecture. MTS, mitochondrial targeting sequence; TM, transmembrane domain; FAD_b, FAD binding domain; FAD_o, FAD oxidase domain.

Similarities among homologs of L-lactate dehydrogenases and malate dehydrogenases in *M. oryzae* and *S. cerevisiae* were displayed according to phylogenetic analysis (Fig 3.4A). Through the alignment analysis, MoLLD1 displayed 52% identity to the L-lactate dehydrogenase ScCYB2 in *S. cerevisiae.* ScCYB2 also showed 36%, 37% and 38% sequence identity to MoLLD2, MoLLD3 and MoLLD4, respectively. MoLLD5 did not share sequence similarity with any member of the lactate dehydrogenases or the malate dehydrogenases in *M. oryzae* or *S. cerevisiae*, and displayed equal phylogenetic distance to malate dehydrogenases compared to L-lactate dehydrogenases. Putative L-lactate dehydrogenases including MoLLD1, MoLLD2, MoLLD3, and MoLLD4 contained N-terminus cytochrome b5-like Heme/Steroid binding domains and C-terminal FMN-dependent dehydrogenase domains (Fig 3.4B). Sequence analysis indicated that both MoLLD1 and MoLLD2 contained a predictable peroxisome-targeting signal I, suggesting the possible peroxisomal localization. MoLLD5 only had the Malate/L-lactate dehydrogenase domain and did not contain any possible organelle-targeting signal peptide, suggesting a possible cytosolic localization. Based on these results, it was realized that putative L-lactate dehydrogenases localized in the peroxisome and the cytosol.

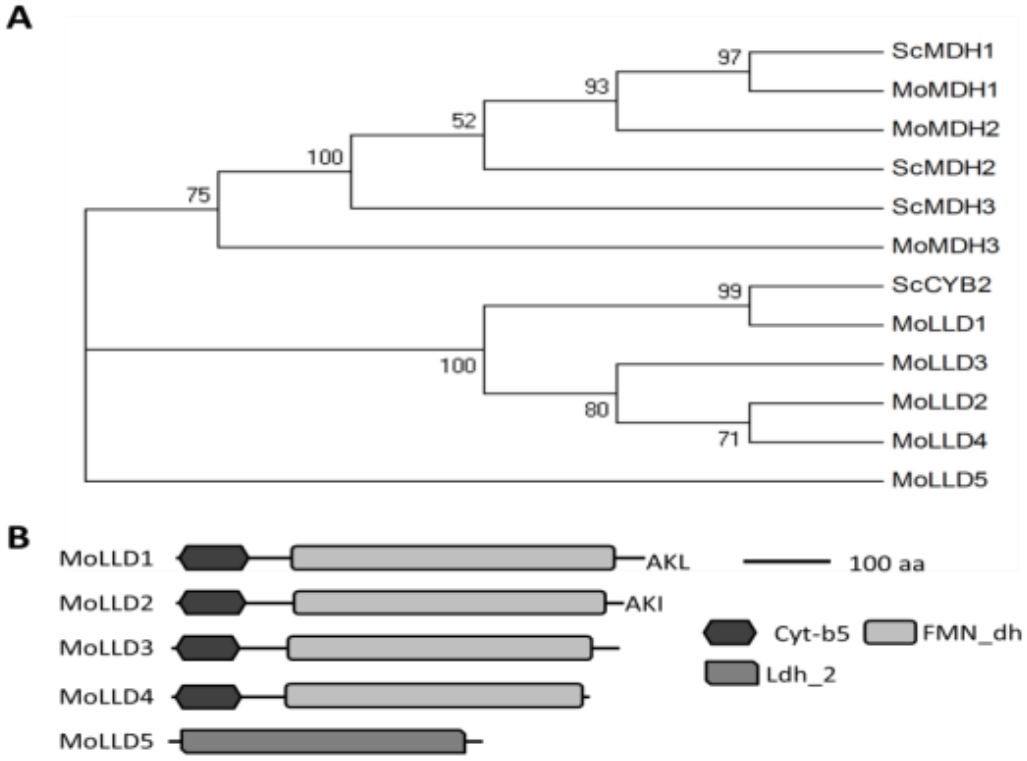

Figure 3.4 Phylogenetic analysis and domain architecture of L-lactate dehydrogenases in *M. oryzae*.

(A) Protein sequences of L-lactate dehydrogenases in *M. oryzae* and *S. cerevisiae* were aligned and a phylogenetic tree was generated using ClustalX1.83. ScCYB2 is the L-lactate dehydrogenase in *S. cerevisiae*, MoLLD1, MoLLD2, MoLLD3, MoLLD4 and MoLLD5 are L-lactate dehydrogenases in *M. oryzae.* (B) Schematic representation of protein domain architecture. Cyt-b5, cytochrome b5-like heme/steroid binding domain; FMN_dh, FMN-dependent dehydrogenase domain; Ldh-2, Malate/L-lactate dehydrogenase domain; AKL and AKI are the predicted peroxisome targeting signal I.

3.3 Transcriptional profiling of lactate dehydrogenase genes in *M. oryzae* during *in vitro* and *in planta* stages

To gain insight into possible functions of lactate dehydrogenases in the infection process of *M. oryzae*, transcriptional profiles of lactate dehydrogenase genes in stages of vegetative hyphae and conidia, 2, 4, 20, 48 and 96 hours post spore inoculation on plants (representing stages of attachment, germination, appressorium formation, primary hyphal and secondary

hyphal development) were examined by RT-PCR (Fig 3.5). The fungal actin gene (Mo_03982) was employed as the endogenous control. In comparison with the expression pattern in the mycelial stage, the *MoDLD1* gene was highly induced during early stages of infection-related development (2, 4, and 20 hai), in which the appressorium initiated and matured. In the conidial stage, the transcription level of the *MoDLD1* gene was induced compared to that in mycelial stage. This result suggested that MoDLD1 might have important roles in fungal conidiation and early infection-related development of *M. oryzae.* The *MoDLD2* gene displayed a relatively higher expression level in the mycelial stage compared to that in the conidial and late invasive growth stages. The *MoDLD3* gene did not vary at the transcriptional level during the mycelial, conidial, and early infection stages; however, it appeared that *MoDLD3* was induced rapidly at 48 h post inoculation, a stage that experienced the transition from biotrophic to necrotrophic infection. The transcriptional level of the *MoLLD1* gene was constitutive from in vivo to in planta stages when comparing to the fungal actin gene as a control. The *MoLLD2* gene displayed constitutive but minimal expression level during all stages tested. The *MoLLD5* gene had a lower level of expression during the conidial stage, followed by gradually induced transcription during infection-related development, suggesting that the function of MoLLD5 may be specific for the fungal infection of *M. oryzae*.

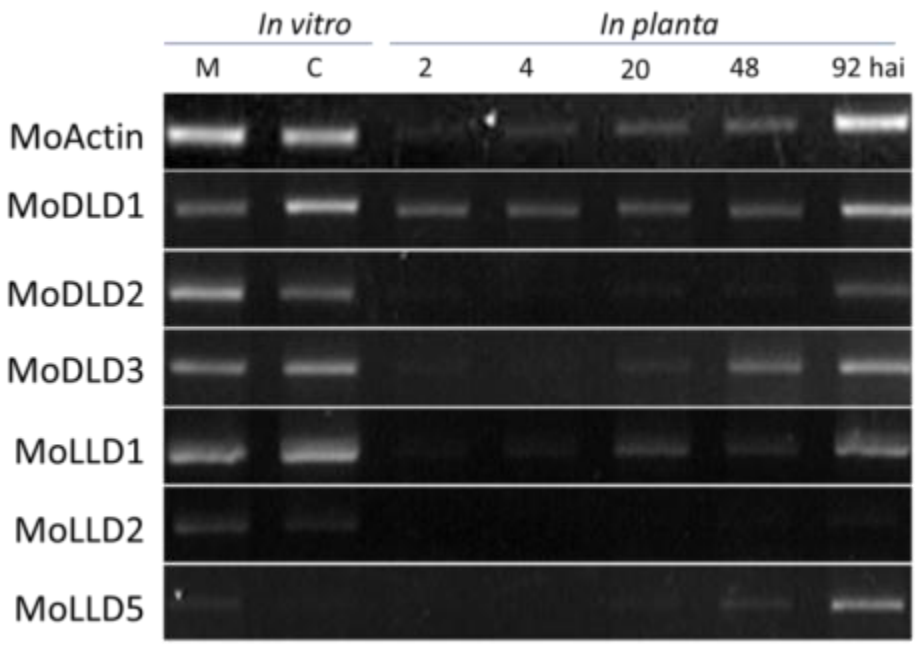

Figure 3.5 Transcript abundance dynamics of lactate dehydrogenase genes in *M. oryzae*. Expression profiling of transcripts encoding putative lactate dehydrogenases by semi-quantitative RT-PCR. M, mycelia; C, conidia; Hai, hours after inoculation on barley leaves.

3.4 Generation of gene deletion mutants of lactate dehydrogenase genes in *M. oryzae*

Based on our hypothesis of the lactate shuttle hypothesis in *M. oryzae*, lactate dehydrogenases in the peroxisomes and mitochondria would be the key point to operate this machinery. Therefore, members of putative peroxisomal and mitochondrial lactate dehydrogenases in *M. oryzae* were selected for further functional characterization. Despite putative cytosolic localization, the *in planta*-specific expression pattern of the *MoLLD5* gene and lack of homology among the *M. oryzae* genome (Dean et al., 2005), an implication of functional specification, led to the selection of *MoLLD5* in functional characterization as well. To determine the function of targeted genes, gene replacement was first performed using a PCR based split-marker method as described (Fig. 2.1). The gene replacement constructs containing the hygromycin phosphotransferase cassette as the selection marker were generated by overlap PCR and transformed into the protoplasts of the wild type *M. oryzae* strain though PEG

mediation. For each gene, at least two independent null mutant lines with identical phenotypes were generated. All of the gene deletion mutants were identified by PCR screening analysis (Fig 3.6). Two independent deletion mutant lines were obtained for *MoDLD1*, six obtained for *MoDLD2*, three obtained for *MoDLD3*, two obtained for *MoLLD1*, two obtained for *MoLLD2* and four obtained for *MoLLD5*. In this study, three wild type isolates (P131, Guy11 and Ku70) of *M. oryzae* were used to generate gene deletion mutants. P131 is a field isolate originally from Japan where japonica rice varieties are mainly cultivated (Peng and Shishiyama, 1988). Guy11 was isolated from the field in French Guyana, which has been widely used in laboratory-based research (Leung et al., 1988). The gene *MAT1* with two alleles *MAT1-1* and *MAT-2*, controls the mating type of *M. oryzae* strains (Kang et al., 1994). P131 has the MAT1-2 mating type, as opposed to the MAT1-1 mating type of Guy11. Ku70 is a genetically engineered strain from the field isolate Guy11, in which the non-homologous end joining pathway (NHEJ) is disrupted to enhance the frequency of gene targeting events (Kershaw and Talbot, 2009). Gene deletion mutants of *MoDLD1*, *MoDLD2*, *MoDLD3* and *MoLLD2* were generated in Ku70, while gene deletion mutants of *MoLLD1* and *MoLLD5* were created in wild type strains of Guy11 and P131, respectively.

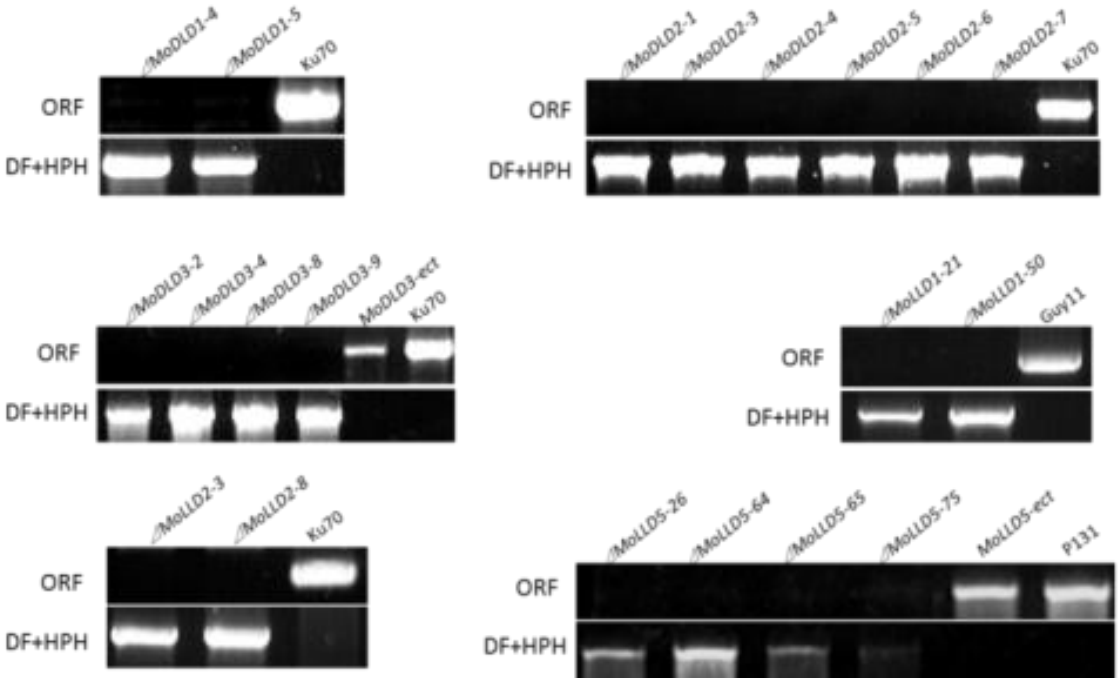

Figure 3.6 Generation and confirmation of lactate dehydrogenase gene deletion mutants. Total genomic DNA isolated from mycelia of control strains and lactate dehydrogenase gene deletion mutants were subjected to PCR analysis using gene-specific primers (ORF) and primers (DF+HPH) spanning the inserted hygromycin-resistance gene and the upstream flanking sequence of replaced fragments.

3.5 Functional analysis of putative D-lactate dehydrogenase 1 MoDLD1

3.5.1 Disruption of MoDLD1 results in dramatic defects in hyphal development, conidiogenesis and conidial morphology

⊿*MoDLD1* mutants dramatically reduced vegetative growth of *M. oryzae* on nutrient-rich PDA medium, as a nearly 75% reduction on growth rate was observed compared to that of Ku70 (Fig 3.7A); (Table 3.1). However, reintroduction of *MoDLD1* into the gene deletion mutant restored hyphal growth (Table 3.1). Frequent branching was observed at terminal mycelia of ⊿*MoDLD1* mutants. Microscopic observation of mycelia with cell wall staining by calcofluor white displayed normal septum formation, but much shorter intervals between septa in ⊿*MoDLD1* mutants (Fig 3.7B). The role of MoDLD1 on conidiogenesis was

examined. The microscopic observation showed that ⊿*MoDLD1* mutants failed to efficiently produce conidiophores and conidia compared to Ku70 strain, as only a few conidiophores were seen and rarely harbored asexual spores under constant light stimulation (Fig 3.7C). This result was consistent with observation by SEM, showing that few spores can be detected on the surface of ⊿*MoDLD1* mutants' culture (Fig 3.7D). Quantitative measurement of conidia confirmed the severe impairment in conidiogenesis of ⊿*MoDLD1* mutants (Table 3.1).

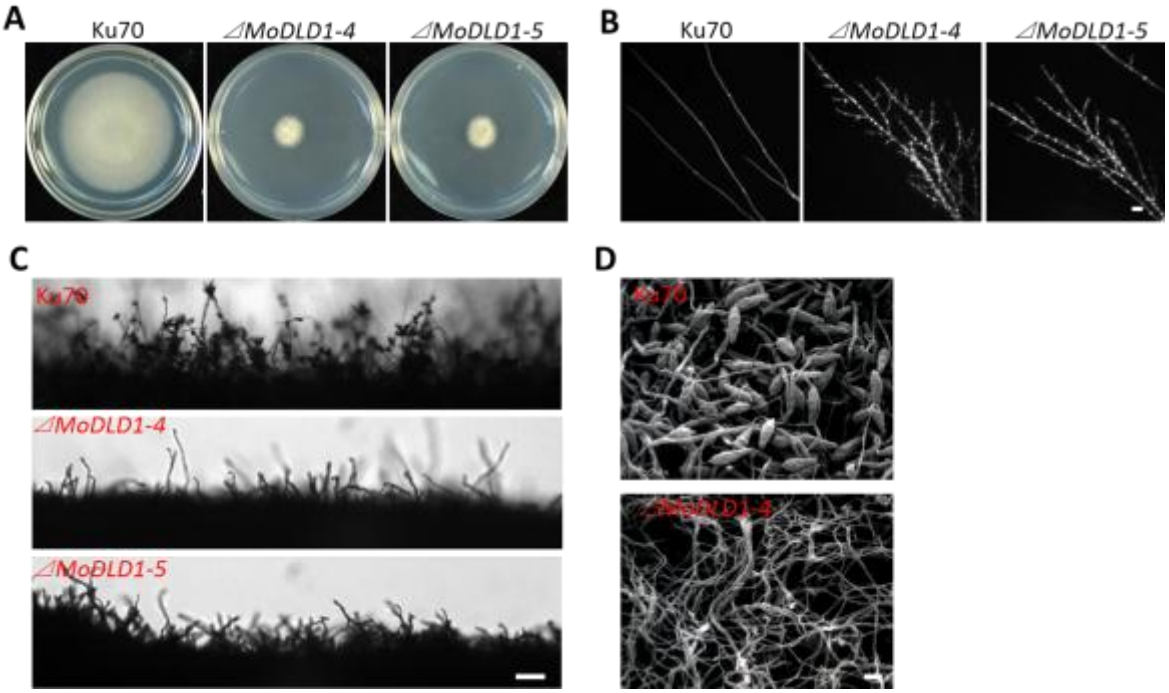

Figure 3.7 Effects of MoDLD1 on mycelia growth and conidiogenesis.

(A) Colonies of Ku70 strain, ⊿*MoDLD1-4* and ⊿*MoDLD1-5* formed on PDA medium. Photos were taken 5 days after inoculation. (B) Branching pattern of mycelia on PDA medium at day 3 after inoculation. Frequent branching occurred at terminal mycelia of ⊿*MoDLD1-4* and ⊿*MoDLD1-5* mutants. Staining by calcofluor white was used to visualize the distance between septa. Bar=20 μm. (C) Growth of conidia on conidiophores. Light microscopic observation was performed on aerial structure of strains grown on oat medium after 48 hr light exposure. Bar=50 μm. (D) Arial structure observation by scanned electron microscope. Bar=10 μm.

Table 3.1 Phenotypic analysis of *⊿MoDLD1* mutants.

Strains	Growth rate (mm/day)	Conidiation spore/cm^2 (10^3)	Appressorium formation (%)		IH movement to adjacent cells (%)[e]
			On hydrophobic cover slips	On onion epidermal cells	
Ku70	3.36±0.21 a	35.87±3.45 a	94.17±1.79 a	93.22±1.86 a	72.51±6.67 a
⊿MoDLD1-4	0.87±0.07 b	0.28±0.05 b	1.33±0.77 b	31.56±5.59 b	7.02±2.28 b
⊿MoDLD1-5	0.86±0.80 b	0.29±0.08 b	1.21±0.68 b	34.77±8.42 b	5.77±1.97 b
MoDLD1-Com-eGFP	3.32±0.22 a	34.99±3.08 a	96.34±2.58 a	92.10±2.21 a	76.51±3.24 a

Growth rate (daily extension in colony diameter) was measured on PDA or CM culture medium.

Number of conidia harvested from 10-day-old oatmeal agar plates at room temperature.

Percentage of appressorium formation over total number of conidia that form germ tubes 24 h post-inoculation on hydrophobic cover slips and epidermal cells.

IH movement to adjacent cells as observed at 48 hpi was observed from a total of 50 primary infected cells inoculated by each strain per replicate.

Data in all columns are means and standard deviations calculated with results from three independent experiments with three replicates. Different letters were used to mark statistically significant difference (P=0.01).

Accompanying asexual sporulation deficiency, conidial morphology was also altered by disruption of the *MoDLD1* gene. Most conidia produced by *⊿MoDLD1* mutants were remarkably shorter in length in comparison with those of Ku70 strain, although some conidia of *⊿MoDLD1* showed enhanced length (Fig 3.8A). Statistical analysis indicated that the average conidial length of *⊿MoDLD1* was approximately 18 μm compared to 23 μm for the Ku70 strain (Fig 3.8B). Calcofluor white staining revealed defects on septum formation in conidia of *⊿MoDLD1* mutants, as about 50% of the conidia harbored one septum and nearly 10% of the conidia had no septum (Fig 3.8C-D).

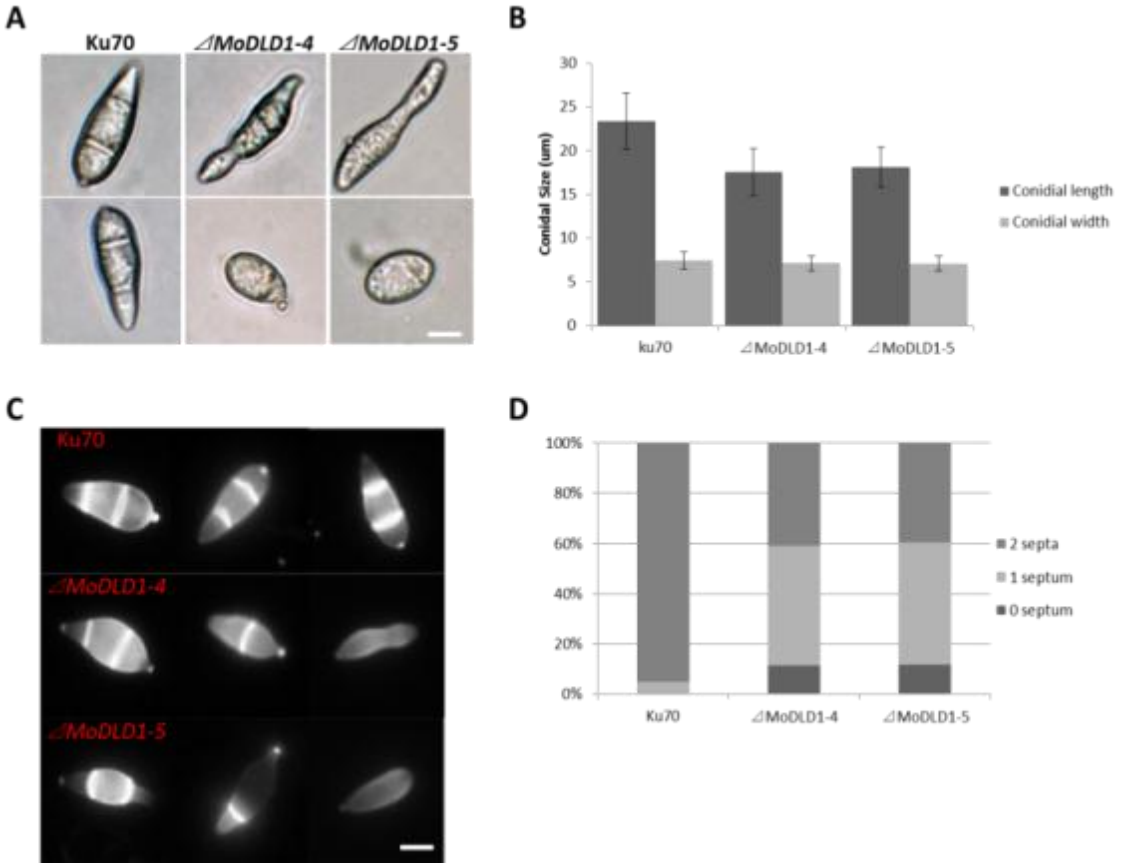

Figure 3.8 Deletion of *MoDLD1* leads to abnormal conidial morphology.

(A) Differential interference contrast (DIC) microscope of conidia collected from Ku70, *⊿MoDLD1-4* and *⊿MoDLD1-5*. Bar=10 μm. (B) Average conidial size of Ku70, *⊿MoDLD1-4* and *⊿MoDLD1-5* were calculated, based on 50 conidia of each strain from three independent replicates. Error bars are standard deviation. (C) Septum pattern of conidia from Ku70, *⊿MoDLD1-4* and *⊿MoDLD1-5* stained by calcofluor white. Bar=10 μm. (D) The percentage of conidia with 0, 1 and 2 septa in Ku70 strain and *⊿MoDLD1* mutants.

3.5.2 MoDLD1 encodes a D-lactate dehydrogenase

MoDLD1 shares 47% amino sequence similarity with yeast ScDLD1. The yeast ScDLD1 mutant was devoid of D-lactate dehydrogenase activity and was unable to grow on D-lactate (Lodi and Ferrero, 1993). To test whether *⊿MoDLD1* mutants can utilize external pyruvate and D-lactate as a sole carbon source, a growth test on minimal medium was carried out. The result showed that *⊿MoDLD1* was compromised in growth on D-lactate, but able to

use pyruvate (Fig 3.9A). Interestingly, neither Ku70 not ⊿*MoDLD1* can use L-lactate as a carbon source. To confirm the functional similarity of MoDLD1 with ScDLD1, the full coding sequence of MoDLD1 and a truncated coding sequence deleted for the N-terminal mitochondrial targeting sequence (MTS) and transmembrane domain (TM) were cloned into the yeast constitutive expression vector pTEF1 and transformed into the yeast ScDLD1 mutant. Only resulting transformants containing the full coding region of MoDLD1 pTEF1-*MoDLD1* and the wild type strain By4741 were able to grow on D-lactate as a sole carbon source, whereas expression of the truncated coding region pTEF1-*MoDLD1*$^{\Delta SP+TM}$ and the empty vector pTEF1 in yeast ⊿*ScDLD1* mutant cannot rescue growth on D-lactate (Fig 3.9B). This data indicated that MoDLD1 encoded a D-lactate dehydrogenase that may require proper localization to exert its activity.

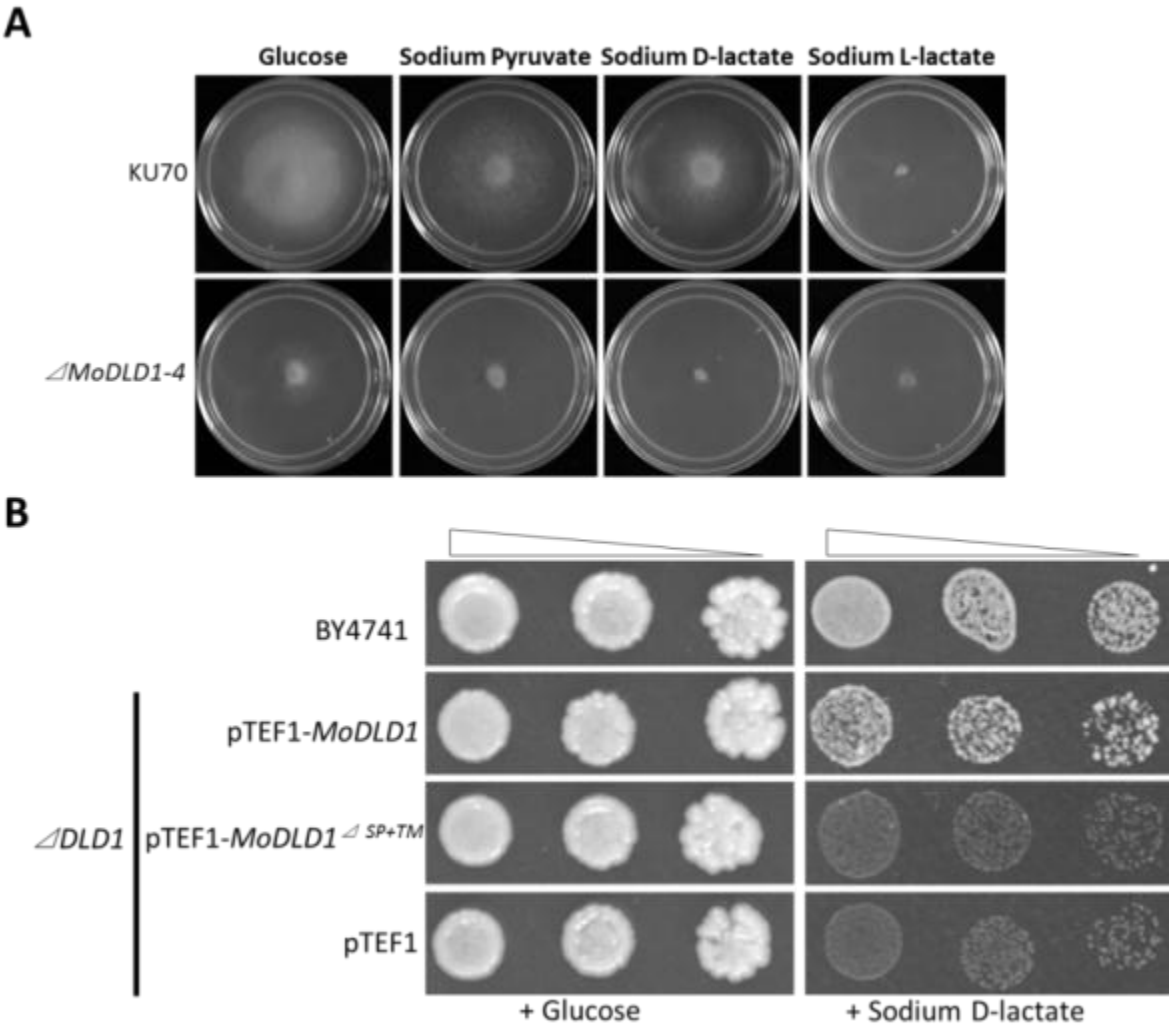

Figure 3.9 MoDLD1 is required for fungal growth on D-lactate and complements growth deficiency of the yeast ScDLD1 mutant on D-lactate.

(A) Ku70 and ⊿*MoDLD1* mutants were cultured on minimal medium with glucose, sodium pyruvate and sodium D-lactate as sole carbon sources. Plate cultures were grown for 7 days at 25 ℃. (B) Yeast cells with concentrations of 10^6, 2×10^5, and 4×10^4 cells/ml of BY4741 and transformants obtained from transformations of pTEF1-*MoDLD1*, pTEF1-*MoDLD1*$^{\Delta SP+TM}$ and the empty vector pTEF1 respectively into the ⊿*ScDLD1* mutant were assayed for growth on glucose and D-lactate.

3.5.3 The expression of *MoDLD1* and subcellular localization of its gene product

To determine the expression of *MoDLD1* and subcellular localization of its gene product, we generated a *MoDLD1-eGFP* fusion construct under the control of its native promoter. The

fusion construct was re-introduced into ⊿*MoDLD1* using protoplast transformation. In resulting transformants *MoDLD1-Com-eGFP*, defects of *MoDLD1* mutants on vegetative growth, conidiation, conidial morphology, appressorium development and pathogenicity were fully complemented to wild type phenotypes (Fig 3.10) (Table 3.1).

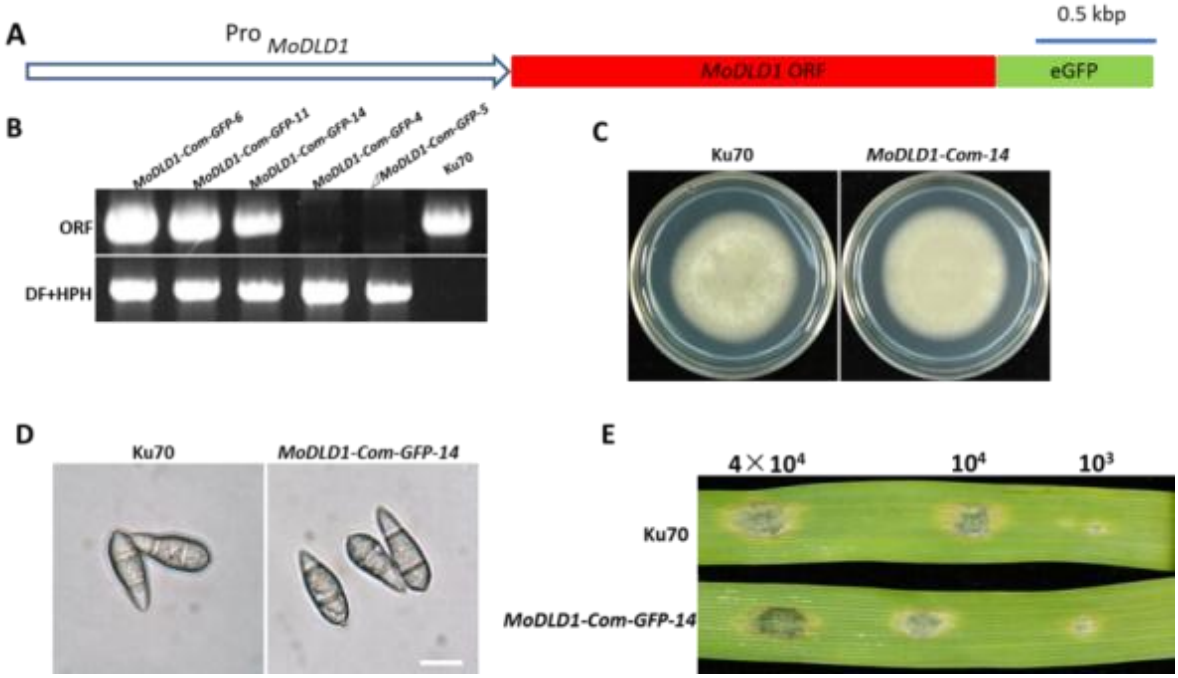

Figure 3.10 Morphology of Ku70 and the GFP strain *MoDLD1-Com-eGFP-14*.
(A) The schematic representation of complementation and cellular localization construct. (B) Total genomic DNA isolated from mycelia of Ku70 and *MoDLD1-eCom-GFP* transformants were subjected to PCR analysis using gene-specific primers (ORF) and hygromycin-resistant gene primers (DF+HPH). (C) Colonies of Ku70 and *MoDLD1-Com-eGFP-14* formed on PDA medium for 5 days. (D) Conidia from Ku70 and *MoDLD1-Com-eGFP-14* were collected and examined under the microscope. Bar=10 μm. (E) 10 day-old barley leaves were drop-inoculated by conidia of Ku70 and *MoDLD1-Com-eGFP-14* with different concentration. Typical leaves were photographed 5 dpi.

Confocal microscopy indicated that a higher level of *MoDLD1-eGFP* signal was observed in the conidial stage compared to that in the mycelial stage cultured in liquid complete medium (CM) (Fig 3.11A).To examine the induction of *MoDLD1* gene expression in response to lactate, the *MoDLD1-Com-eGFP-14* strain was cultured in CM medium, and then mycelia were recovered and transferred to minimal medium with either glucose or lactate as the sole

carbon source. Upon lactate induction, an intensified signal of GFP fluorescence was observed, which also appeared to be more aggregated as punctate structures compared to the growth on glucose as a sole carbon source (Fig 3.11A). Moreover, the expression of *MoDLD1* was highly induced during germination, appressorium development, and invasive growth stages when inoculated on an artificial hydrophobic surface or the plant cell surface (Fig 3.11B). These observed expression patterns are consistent with the RT-PCR analysis of *MoDLD1* expression during *in vitro* and *in planta* stages. Therefore, we conclude that the expression of *MoDLD1* is in response to the presence of lactate, and is highly induced associated with the differentiation of infectious structures during conidial, appressorium and invasive hyphae stages.

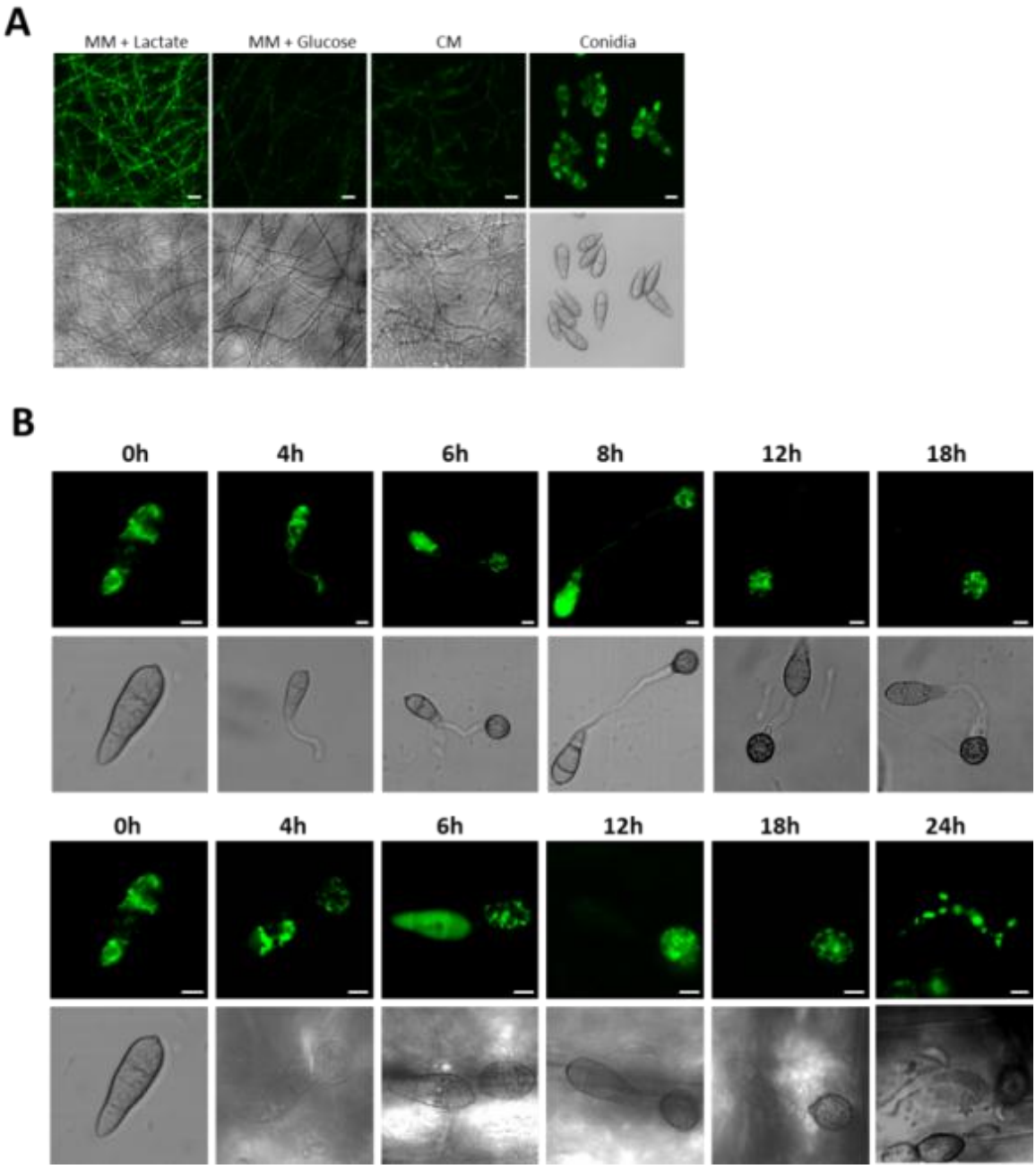

Figure 3.11 Confocal microscopy observations of the expression of *MoDLD1-Com-eGFP*. (A) Spatial analysis of expression in response to the presence of lactate. Bar=5 μm. (B) Expression of Mo*DLD1* during germination, appressorium development and invasive hyphae growth stages. Conidia of *MoDLD1-Com-eGFP-14* were inoculated on the surface of plastic cover slips (upper panels) and barley leaves (lower panels) to examine the expression pattern of *MoDLD1* associated with infection-related development of *M. oryzae*. Bar=5 μm. All photos were taken under the same conditions using confocal microscopy.

To examine the subcellular localization of MoDLD1, staining by a mitochondria-specific dye MitoTracker Red was used and displayed co-localization with *MoDLD1-eGFP* signals in vegetative hyphae grown in CM medium (Fig 3.12A). The mitochondrial localization of MoDLD1 was consistent during appressorium formation of *MoDLD1-Com-eGFP-14* on a hydrophobic surface (Fig 3.12B). Yeast ScDLD1 has a transmembrane domain in the N-terminus, which inserts the protein into the inner mitochondrial membrane, allowing the major hydrophilic part residing in the intermembrane space. To reveal the sub-mitochondrial localization of MoDLD1, immunogold labeling was conducted using an anti-GFP antibody in conidia of *MoDLD1-Com-eGFP-14.* The result showed that the antibody primarily labeled mitochondrial cristae and membrane structures (Fig 3.12C). These results indicated that, similar to ScDLD1, MoDLD1 has anchored to the inner mitochondrial membrane at the N-terminal, likely protruding into the intermembrane space for the catalytic domains.

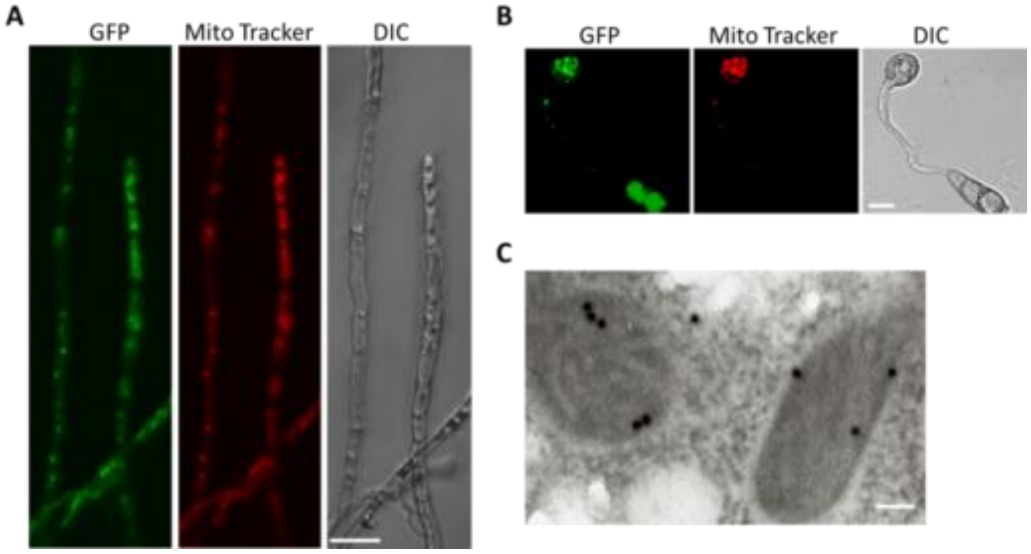

Figure 3.12 Subcellular localization of MoDLD1-eGFP protein.
(A-B) Confocal microscopy analysis of MoDLD1-Com-eGFP localization during vegetative and appressorium development in *M. oryzae.* The *MoDLD1-Com-eGFP-14* was stained with Mito-Tracker Red CMXRos to facilitate visualization of mitochondria at indicated stages. Bar=5 μm. (C) The immunogold electron micrograph of the conidial mitochondria in *MoDLD1-Com-eGFP-14*. Immunolocalization of anti-GFP antibodies is indicated by 10 nm gold particles. Bar=50 nm.

3.5.4 Appressorium formation on a nutrient-free hydrophobic surface requires MoDLD1

On the hydrophobic surface, ⊿*MoDLD1* mutants displayed normal conidial germination. However, germ tubes of ⊿*MoDLD1* usually failed to develop dome shaped appressoria at the ends, but kept elongating on artificial hydrophobic surface after 24 hr induction (Fig 3.13A). Under the same condition, 95% of conidia with germ tubes formed appressoria in Ku70 (Table 3.1). The appressoriun assay on host barley leaves indicated that a low proportion of conidia of ⊿*MoDLD1* mutants can form melanized appressoria at the end of germ tubes (Fig 3.13B). A similar result was also obtained through conidial inoculation on onion epidermal cells where approximately 30% of conidia of ⊿*MoDLD1* mutants were induced to form appressoria compared to over 90% Ku70 conidia that developed appressoria (Fig 3.13C) (Table 3.1). These results suggested that appressoium development by ⊿*MoDLD1* mutants was nutrient status–dependent. Nutrients associated with host and non-host plant surface could partially complement the appressorium formation deficiency caused by disruption of *MoDLD1*.

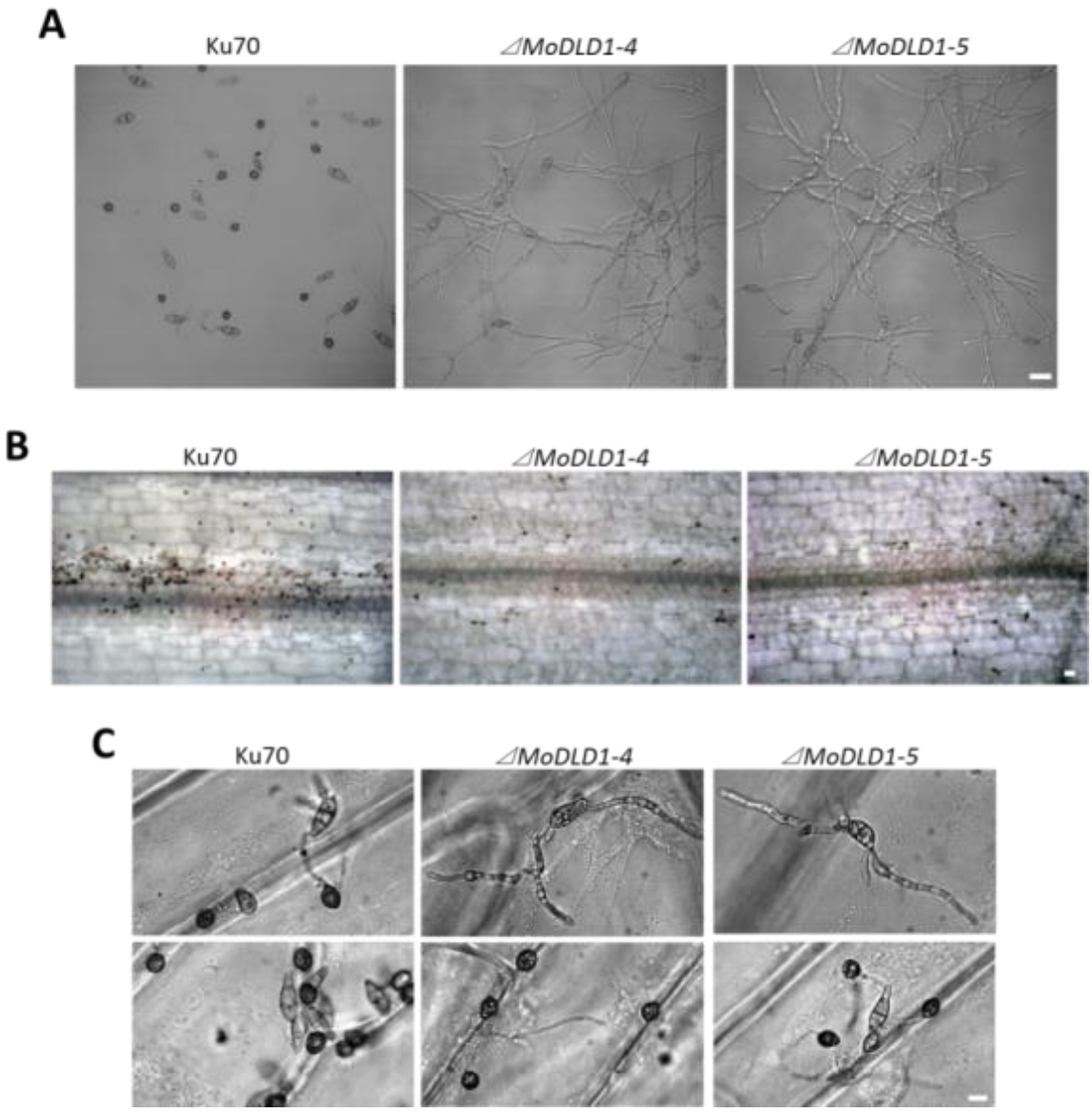

Figure 3.13 Appressorium formation assay on plastic cover slips and plant surface.
(A) Conidia from Ku70, ⊿*MoDLD1-4* and ⊿*MoDLD1-5* mutants were incubated on hydrophobic cover slips for 24 hr. Bar=20 μm. (B) Barley leaves inoculated with conidia of Ku70, ⊿*MoDLD1-4* and ⊿*MoDLD1-5* mutants. Melanized appressoria were induced 24 hpi. Bar=50 μm (C) The same set of strains was inoculated on onion epidermal cells to induce appressoria 24 hpi. Bar=10 μm.

3.5.5 MoDLD1 is involved in NADH/NAD^+ balance and utilization of conidial storage compounds during appressorium development on hydrophobic surface

To test if the appressorium deficiency of ⊿*MoDLD1* mutants on an artificial hydrophobic surface is associated with intracellular redox imbalance, conidia were incubated with excess NADH or NAD^+, respectively. Supplementing conidial suspension with 3 mM NAD^+ completely inhibited the germination of ⊿*MoDLD1* mutants on plastic cover slips during the early germination for 5 hr, whereas the germination of Ku70 conidia were not affected under the same conditions (Fig 3.14A-B). Staining by the nucleic acid dye propidium iodide, commonly used to detect the cell viability due to its impermeability to plasma membrane of living cells (Mather and Donahue, 1998), showed that treatment of 3 mM NAD^+ on ⊿*MoDLD1* mutants caused the collapse of cellular structures in more than 90% of conidia, while most of the non-NAD^+ treated conidia kept cell viability, indicated by a lack of PI staining (Fig 3.14A). However, conidia either from Ku70 or ⊿*MoDLD1* mutants treated with 3 mM NADH displayed no developmental alteration during induction on plastic cover slips compared to the non-treated control (Fig 3.14A). The hyper-sensitivity of ⊿*MoDLD1* mutants to extra NAD^+ treatment suggested that disruption of *MoDLD1* resulted in the accumulation of NAD^+ pool in cellular compartments, which was toxic to the mutants' conidia and caused the cell death.

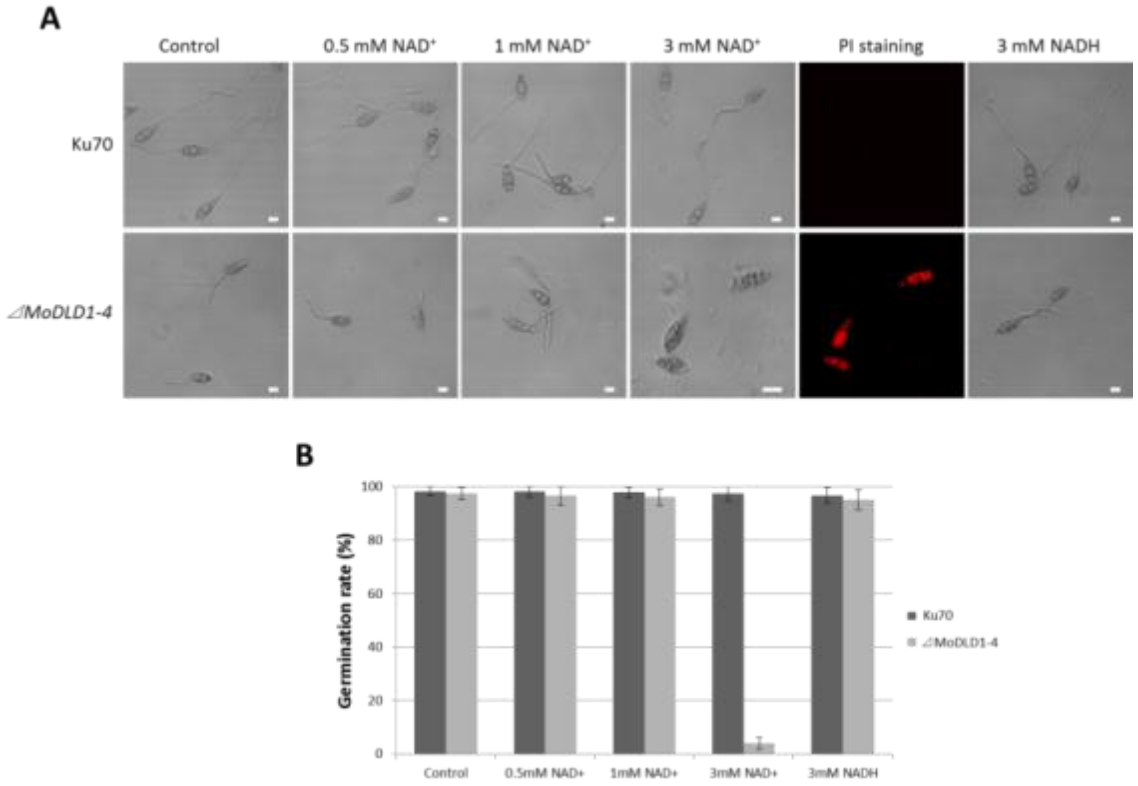

Figure 3.14 NADH and NAD$^+$ treatments during germination.

(A) Conidial suspension of Ku70 and *⊿MoDLD1-4* supplemented with 0.5 mM, 1 mM, 3 mM NAD$^+$ and 3 mM NADH were incubated on plastic cover slips for 5 hr. Conidia treated with 3 mM NAD$^+$ were later stained by propidium iodide (PI) as an indicator of cell viability. Bar=10 μm. (B) The bar chart showed percentage of conidia germination after incubation with 0.5 mM, 1 mM and 3 mM NAD$^+$ and 3 mM NADH on plastic cover slips for 5 hr. Error bars represent standard deviations from three experiments with three replicates.

To investigate the role of MoDLD1 in translocation and degradation of storage compounds during appressorium development, cellular distribution of lipid bodies and glycogen in *⊿MoDLD1* mutants were examined during conidial germination and appressorium formation. The spatial and temporal movement of lipid bodies and glycogen were visualized microscopically using the specific dyes Nile red and KI/I_2 solution, respectively. As shown in (Fig 3.15A), an abundance of lipid droplets was observed in conidia of Ku70 and *⊿MoDLD1* harvested from fresh culture plates. Six hours after inoculation on a hydrophobic

surface, lipid bodies began to enlarge in the nascent appressorium of Ku70 through germ tube transportation. Large amounts of lipid droplets were accumulated in the appressorium of the Ku70 strain 16 hours post inoculation, followed by coalescence and vacuolar uptake. lipid degradation was soon observed during appressorium maturation and melanization, and increasing amounts of appressoria formed 24 to 48 hr post inoculation were devoid of lipid droplets in Ku70. However, lipid droplets that were translocated into germ tubes of ⊿*MoDLD1* upon induction on artificial hydrophobic surface cannot be utilized, and thus associated with the failure to differentiate appressoria. Lipid droplets remained in conidia and germ tubes of *MoDLD1* even 48 hr after germination (Fig 3.15A). Staining by KI/I_2 solution showed abundant glycogen was present in the conidia of Ku70 and ⊿*MoDLD1*. In Ku70, glycogen was rapidly transported from conidia to the incipient appressoria during early induction on the hydrophobic surface (4 hr post inoculation), and then glycogen was largely accumulated in the cytoplasm of incipient appressoria 6 hr after inoculation. However, the degradation of glycogen deposits quickly occurred at the onset of appressorium maturation from 12 to 16 hr post inoculation, corresponding to the role of carbohydrate in appressorium development. In ⊿*MoDLD1*, however, the distribution of glycogen was retarded in conidia and germ tubes even after 24 hr of incubation on the hydrophobic surface (Fig 3.15B). These results suggested that redox state disorder caused by disruption of *MoDLD1* could lead to dysfunctionality of metabolic pathways required to utilize nutrient reserves in conidia to fuel appressorium development in *M. oryzae*.

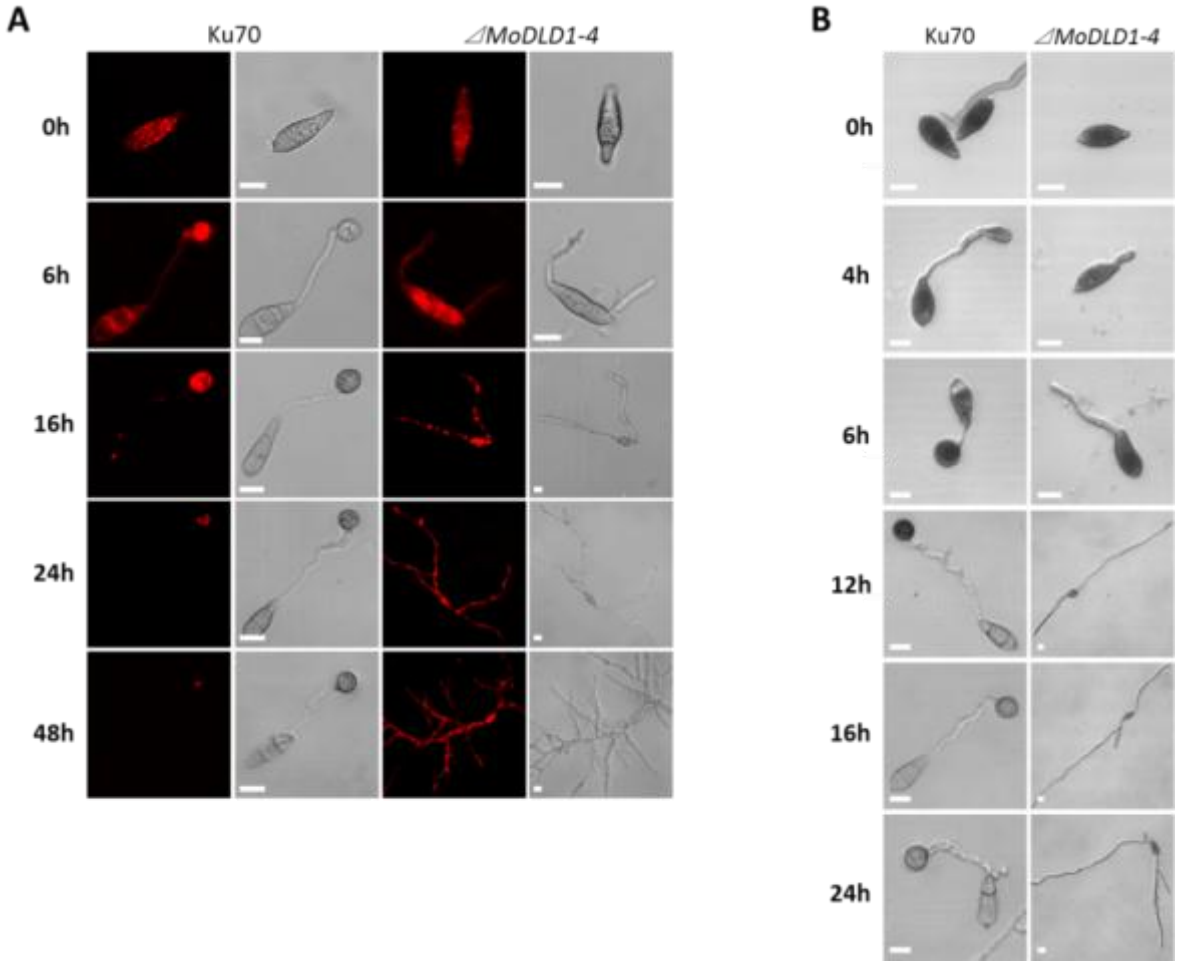

Figure 3.15 Cellular distributions of lipid droplets and glycogen during appressorium development in *M. oryzae*.

(A) Conidial suspension of Ku70 and *⊿MoDLD1-4* were allowed to form appressoria on plastic cover slips. Water was removed at intervals during a 48-hr period (0, 6, 16, 24 and 48hr after inoculation) and was stained with Nile red to visualize triacylglycerol by confocal microscopy (left panel) and DIC microscopy (right panel). Bar=10 μm. (B) Solution containing 60 mg /ml KI and 10 mg/ml I_2 was used to stain the same set of strains for visualization of glycogen during a 24-hr period (0, 4, 6, 12, 16 and 24 hr after inoculation) by DIC microscopy. Bar=10 μm.

3.5.6 MoDLD1 is required for full virulence of *M. oryzae*

To determine the effect of the *MoDLD1* mutation on fungal pathogenicity, spores of *⊿ MoDLD1* mutants and Ku70 were sprayed on a susceptible rice cultivar CO-39 to induce rice

blast symptoms. Numerous blast lesions were caused on leaves inoculated by Ku70 at 7 dpi, whereas only tiny visible restricted necrosis was detected on *⊿MoDLD1* mutant-infected leaves under the same conditions (Fig. 3.16A). To further confirm that MoDLD1 is indispensable for full virulence of *M. oryzae*, the susceptible CDC barley cultivar leaves were also drop-inoculated with conidial suspension of Ku70 and *⊿MoDLD1* at different concentrations. In comparison to extensive necrotrophic symptoms caused by Ku70 at each concentration at 5 dpi, restricted diffusion of necrosis was observed on barley leaves inoculated with spores of *⊿MoDLD1* at concentrations of 4×10^4/ml and 10^4/ml respectively (Fig. 3.16B). Moreover, spores from *⊿MoDLD1* at the concentration of 10^3/ml failed to elaborate any visible symptoms on barley leaves (Fig. 3.16B). *⊿MoDLD1* as described previously, was able to form appressoria on the plant surface. We therefore further investigated the role of MoDLD1 on appressorium penetration and invasive growth. The penetration assay conducted on barley epidermal cells showed that *⊿MoDLD1* was able to gain entry into host cells by the penetration peg as efficiently as Ku70 24 hpi, suggesting appressorium function was not compromised. However, elaboration and growth of invasive hyphae from penetration pegs were severely impaired in *⊿MoDLD1* mutants. Invasive hyphae formed by *⊿MoDLD1* inside host cells were less branched and bulbous than those of Ku70 according to observation 48 hpi (Fig. 3.16C). It was also found that only about 7% of successful penetration by *⊿MoDLD1* extended invasive hyphae from primarily infected cells to neighboring cells compared to approximately 72% of Ku70 penetration that moved into neighboring cells 48 hpi (Table 3.1). It was possible that subsequent transition from narrow primary hyphae to enlarged and bulbous invasive hyphae was blocked in *⊿MoDLD1* mutants. Taken together, *⊿MoDLD1* mutants' defects in invasive growth was directly responsible for restricted necrosis at infection sites, which resulted in a significant loss of virulence.

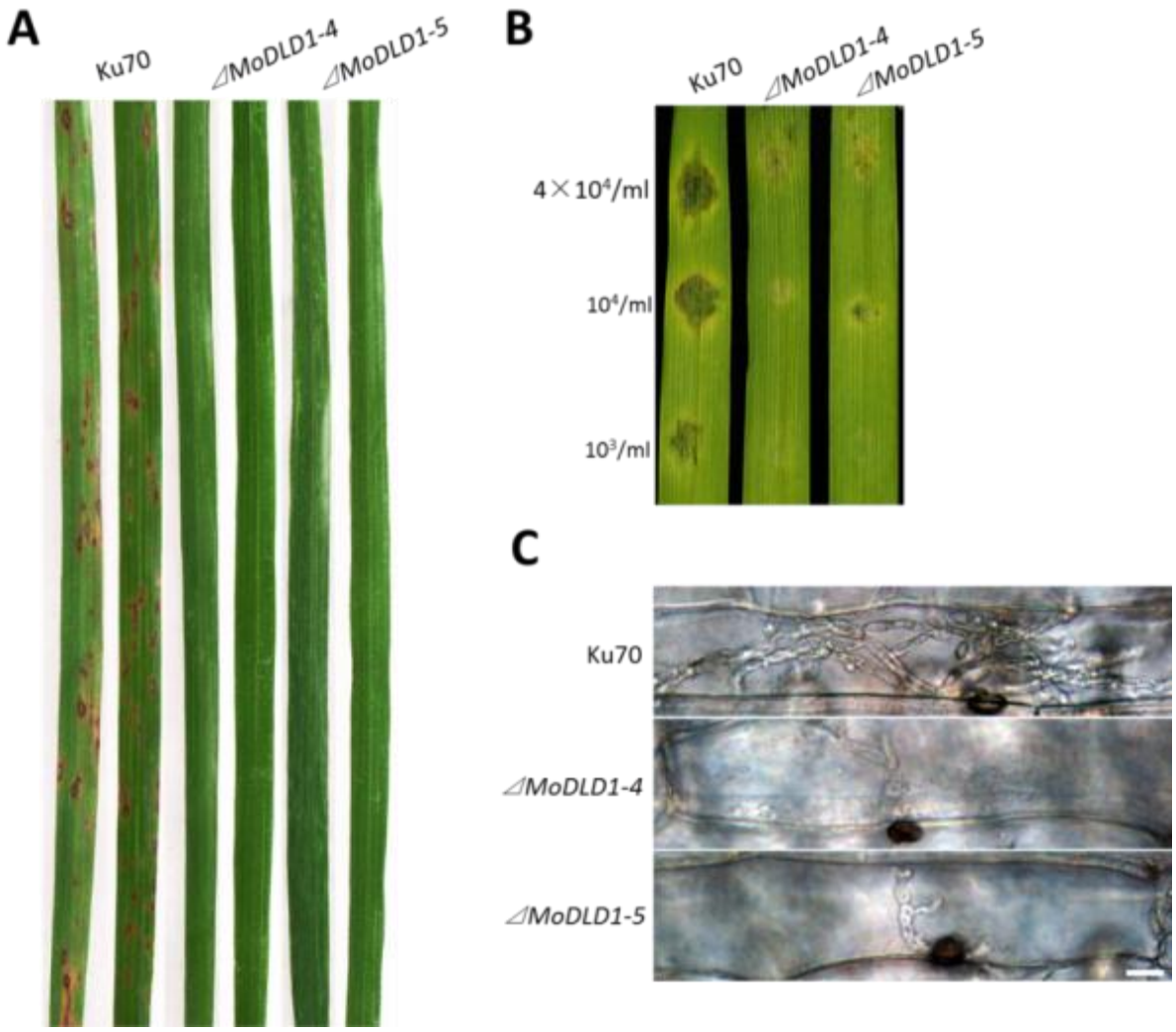

Figure 3.16 Loss of *MoDLD1* leads to significant reduction in fungal virulence. (A) 15 day-old leaves of susceptible rice cultivar C0-39 were spay-inoculated with conidial suspension (4×10^4 /ml) of Ku70 and *⊿MoDLD1* mutants. Typical leaves were photographed 7 dpi. (B) 10 day-old barley leaves of CDC silky cultivar were drop-inoculated with conidial suspension of Ku70 and *⊿MoDLD1* mutants. The concentration of conidial suspension is indicated to the left. Typical lesions were photographed 5 dpi. (C) Conidia of Ku70 and *⊿MoDLD1* mutants were drop–inoculated on barley leaves. Appressorium penetration and invasive hyphal growth were examined 48 hpi. Bar=10 μm.

3.5.7 Correct cellular localization of MoDLD1 modulates its function

To explore the importance of MoDLD1 sub-mitochondrial localization in its function, expression cassettes of *MoDLD1-eGFP* lacking a mitochondrial targeting sequence and

transmembrane domain *(MoDLD1*$^{\triangle SP+TM}$*-eGFP*) or transmembrane domain alone (*MoDLD1*$^{\triangle TM}$*-eGFP*) at the N-terminus were generated by overlap PCR and confirmed by sequencing analysis (Fig. 3.17A). Two expression cassettes under the control of the *MoDLD1* native promoter were introduced into *⊿MoDLD1* following protoplast transformation. The resulting transformants were confirmed by PCR analysis (Fig. 3.17B). Confocal microscope analysis revealed cytosolic localization of both MoDLD1$^{\triangle TM}$ and MoDLD1$^{\triangle SP+TM}$ alleles (Fig. 3.17C), indicating that the transmembrane domain alone was required for proper MoDLD1 localization in the mitochondria. Transformants expressing either MoDLD1$^{\triangle TM}$ or MoDLD1$^{\triangle SP+TM}$ alleles were as defective in vegetative growth, conidiogenesis, appressorium formation on hydrophobic surface and pathogenicity as *⊿MoDLD1* mutants (Fig. 3.17D). Therefore, it may suggest that the correct localization of MoDLD1 in the mitochondria was essential for its function.

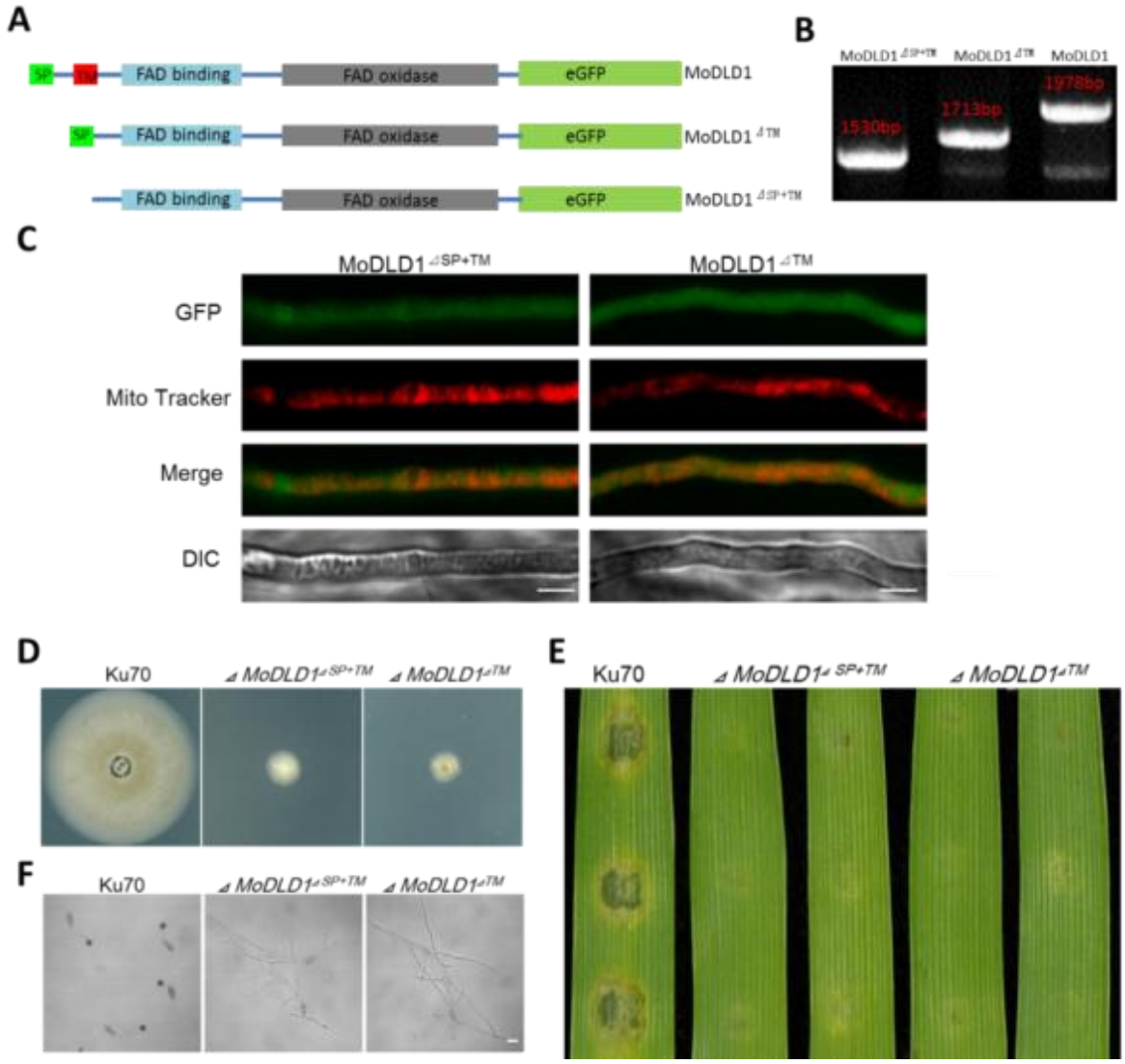

Figure 3.17 Functional characterization of the MoDLD1 transmembrane domain.

(A) Schematic drawing of different mutant alleles of MoDLD1. (B) Total genomic DNA from hyphae of transformants carrying mutant alleles MoDLD1$^{\triangle SP+TM}$ and MoDLD1$^{\triangle TM}$ were extracted and subjected to PCR analysis using MoDLD1 specific primers. The PCR products from MoDLD1$^{\triangle SP+TM}$, MoDLD1$^{\triangle TM}$ and wild type are indicated. (C) Vegetative hyphae of transformants *⊿MoDLD1*$^{\triangle SP+TM}$ and *⊿MoDLD1*$^{\triangle TM}$ were examined by confocal microscope. Bar=5 μm. (D) Colonies of Ku70, *⊿MoDLD1*$^{\triangle SP+TM}$ and *⊿MoDLD1*$^{\triangle TM}$ formed on CM medium for 7 days. (E) Conidia of Ku70, *⊿MoDLD1*$^{\triangle SP+TM}$ and *⊿MoDLD1*$^{\triangle TM}$ were incubated on hydrophobic cover slips for 24 hr. Bar=10 μm. (F) Conidia of Ku70, *⊿MoDLD1*$^{\triangle SP+TM}$ and *⊿MoDLD1*$^{\triangle TM}$ were applied to 10-day old barley leaves of susceptible cultivar CDC silky at the concentration of 4×10^4 /ml spores. Photos were taken after 5 dpi.

3.6 Functional analysis of other lactate dehydrogenases

3.6.1 MoDLD2 is involved in hyphae pigmentation and response to oxidative stress

The disruption of *MoDLD2* caused a severe defect in colony pigmentation. Both ⊿*MoDLD2-1* and ⊿*MoDLD2-3* formed colonies that were significantly less pigmented during growth on PDA medium, which was accompanied with a small reduction in the colony growth rate compared to the control strain (Fig 3.18A); (Table 3.2). Deletion of the *MoDLD2* gene had no significant change on conidiation, appressorium formation or fungal virulence, suggesting that *MoDLD2* was not necessary for fungal conidiogenesis and pathogenicity of *M. oryzae* (Table 3.2), (Fig 3.1BB-C).

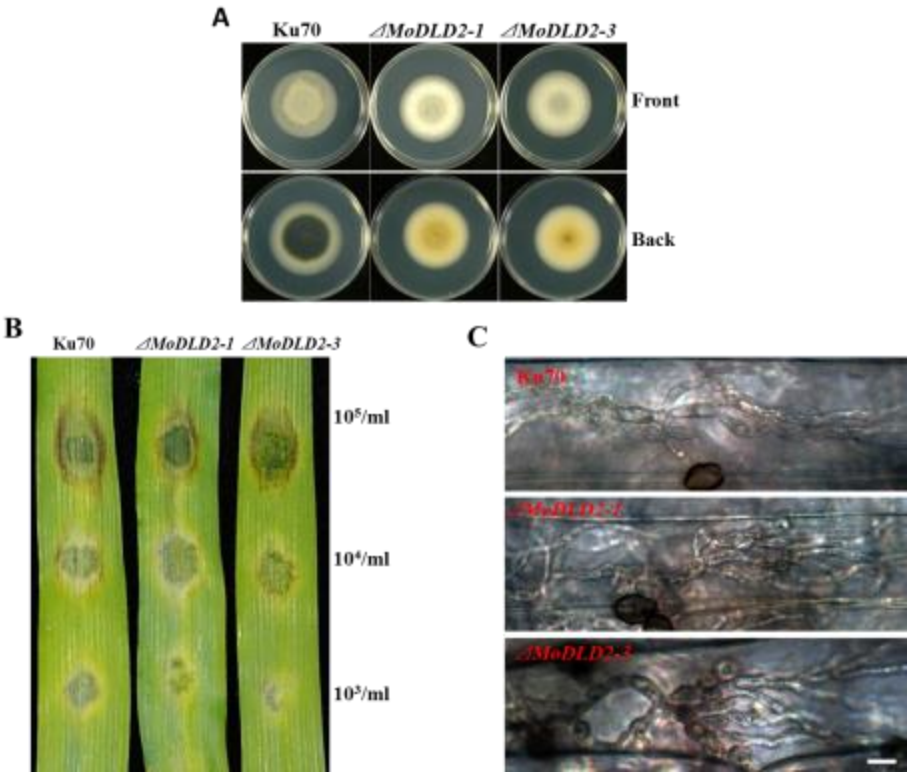

Figure 3.18 Effects of *MoDLD2* deletion on hyphal development and pathogenicity of *M. oryzae*.

(A) Ku70 strain, ⊿*MoDLD2* deletion mutants and ectopic insertion line *MoDLD2-ect* were grown on PDA medium, and growth was monitored after 7 days. (B) 10 day-old barley leaves were drop-inoculated with conidia of Ku70 and ⊿*MoDLD2* mutants at different concentrations. Typical leaves were photographed 5 dpi. (C) Conidia of Ku70 and ⊿*MoDLD2* mutants were drop-inoculated on barley leaves. Appressorium penetration and invasive hyphae growth were examined 48 hpi. Bar=10 μm.

Table 3.2 Phenotypic analysis of ⊿*MoDLD2* mutants.

Strains	Growth rate (mm/day)	Conidiation spore/cm^2 (10^3)	Appressorium formation (%)
Ku70	3.27±0.04 a	32.81±1.39 a	95.37±4.33 a
⊿*MoDLD2-1*	2.98±0.08 b	32.48±1.97 a	97.24±6.12 a
⊿*MoDLD2-3*	3.01±0.07 b	32.89±2.25 a	95.22±5.52 a
MoDLD2-Com-eGFP	3.33±0.85 a	33.24±1.13 a	95.66±7.11 a

Growth rate (daily extension in colony diameter) was measured on PDA or CM culture medium.

Number of conidia harvested from 10-day-old oatmeal agar plates at room temperature.

Percentage of appressorium formation over total number of conidia that formed germ tubes 24 h post-inoculation on hydrophobic cover slips.

Data in all columns are means and standard deviations calculated with results from three independent experiments with three replicates. Different letters were used to mark statistically significant difference (P=0.01).

In fungal hyphae, reduced pigmentation is always associated with the alteration of oxidative status (Guo et al., 2011). To determine if MoDLD2 was involved in the modulation of the oxidative stress response, *⊿MoDLD2* mutants and the wild type strain Ku70 were exposed to H_2O_2. *⊿MoDLD2* mutants were resistant to oxidative stress following the challenge by oxidative agent H_2O_2 (Fig 3.19A). Cultures on PDA medium containing 2.5 and 5 mM H_2O_2, respectively, caused an average reduction of 19% (2.5 mM) and 22% (5 mM) in the growth inhibition rate of the *⊿MoDLD2* mutants than that of Ku70 strain (Fig 3.19B).

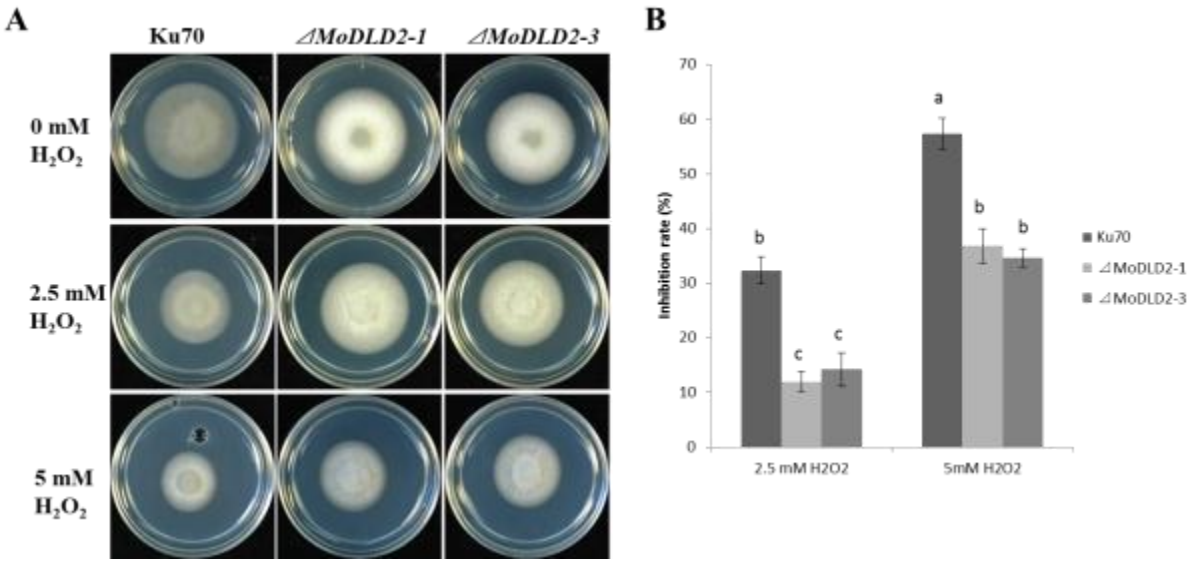

Figure 3.19 The *⊿MoDLD2-1* mutants are resistant to oxidative stress.
(A) Mycelium growth under H_2O_2. Ku70 strain and *⊿MoDLD2* mutants were cultured on PDA medium without and with 2.5 or 5 mM H_2O_2 for 5 days. (B) Colony diameters of Ku70 and *⊿MoDLD2-1* mutants grown on PDA medium without and with 2.5 or 5 mM H_2O_2 for 5 days were measured and analyzed statistically. The growth inhibition rate was used to express the effect of H_2O_2 on growth of testing strains. Inhibition rate= [(the diameter of untreated strain-the diameter of treated strain)/ (the diameter of untreated strain) ×100%]. Three independent experiments with three replicates were performed. Error bars indicate deviations. Different letters are used to demonstrate significant difference for each data column. (P= 0.01).

3.6.2 The Subcellular localization of MoDLD2

To determine the expression and subcellular localization of MoDLD2 in *M. oryzae*, the

MoDLD2 open reading frame under its native promoter was fused with GFP in the pKNTG plasmid harboring the neomycin-resistance gene, and then was introduced into the ⊿*MoDLD2* mutant (Fig 3.20A). Nine independent transformants were screened on neomycin plates, two of which were identified with the expression of the fusion construct by PCR and confocal microscopy. The transformant line *MoDLD2-Com-eGFP-8* was selected for further analysis. Growth tests on PDA medium indicated that the hyphal pigmentation defect was rescued in *MoDLD2-Com-eGFP-8* (Fig 3.20B), suggesting that it was a true transformant expressing the *MoDLD2*-eGFP fusion construct. MoDLD2 had a mitochondrial targeting signal at the N-terminal and showed 60% sequence similarity with yeast ScDLD2 that was already demonstrated to encode a mitochondrial matrix D-lactate dehydrogenase. Staining by a mitochondria-specific dye MitoTracker Red on mycelia collected from CM medium and appressoria of *MoDLD2-Com-eGFP-8* induced on an hydrophobic surfaces revealed co-localization of the dye-labeled mitochondrial signals and the GFP signals (Fig 3.20C). The analysis of amino acid sequences indicated that no transmembrane domain was predicted on MoDLD2. Therefore, MoDLD2 is a putative D-lactate dehydrogenase localizing to the mitochondrial matrix.

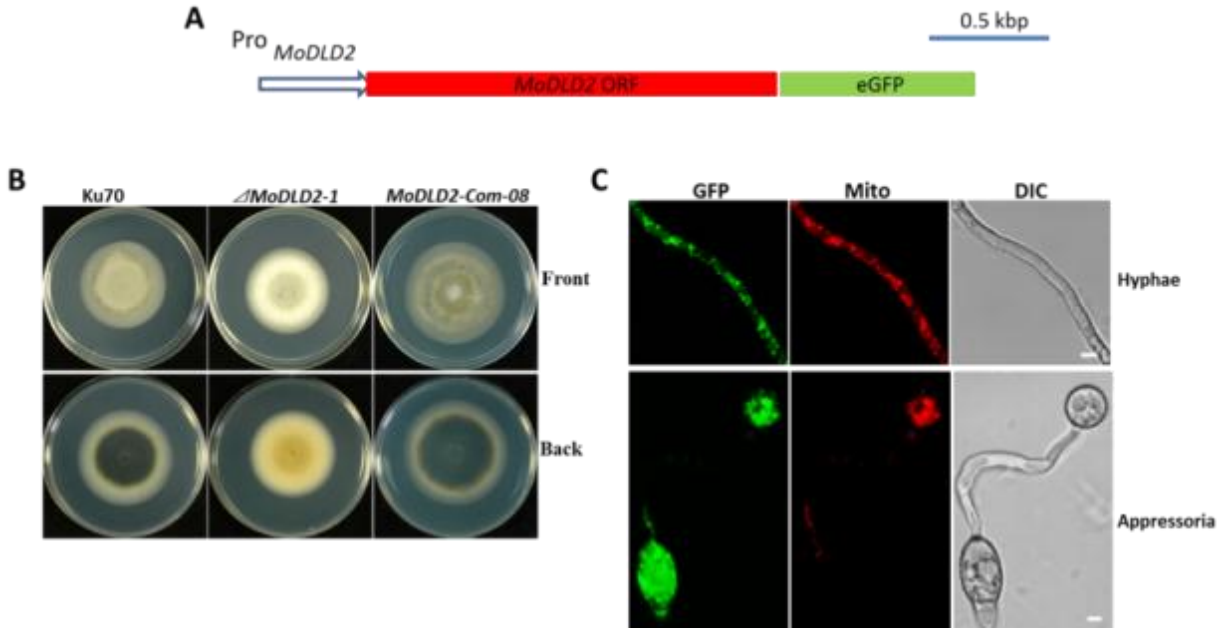

Figure 3.20 Subcellular localization of the MoDLD2-eGFP fusion protein.
(A) The schematic representation of complementation and cellular localization construct. (B) Colonies of Ku70 and *MoDLD2-Com-eGFP-8* formed on PDA medium for 7 days. (C) Confocal microscopy analysis of MoDLD2-eGFP localization during vegetative and appressorium development in *M. oryzae.* The *MoDLD2-Com-eGFP-8* was stained by Mito-Tracker Red CMXRos to facilitate visualization of mitochondria at indicated stages. Bar=5 μm.

3.6.3 The expression of *MoDLD2* does not respond to lactate and is independent of MoDLD1

To determine if the expression of *MoDLD2* responded to the presence of lactate, *MoDLD2-Com-eGFP-8* strain was cultured in CM medium, and then mycelia were recovered and transferred to minimal medium with either glucose or lactate as the sole carbon source for 3 days. Signals detected by confocal microscopy of mycelia collected from CM and MM with glucose or lactate showed no significant variation of signal intensity (Fig 3.21A). This result indicated that the expression of *MoDLD2* was not subject to regulation by exogenous lactate.

Previous studies in mammals indicated that lactate or pyruvate was transported into the mitochondrial matrix to participate in cellular respiration, indicating that lactate dehydrogenase

in the mitochondrial matrix is involved in the transportation of reducing equivalents for the respiratory chain (Brooks et al., 1999). To investigate if MoDLD2 is involved in the MoDLD1-mediated cellular metabolite flow, the *MoDLD2-eGFP* construct was introduced into the ⊿*MoDLD1* mutant to examine its expression and accumulation pattern. Mycelia collected from CM medium observed by confocal microscopy under the same conditions indicated that the expression of *MoDLD2* was not altered in the ⊿*MoDLD1* mutant compared to that in the Ku70 strain (Fig 3.21B). This result was consistent with the observation of eGFP signals of MoDLD2-eGFP detected in conidia from the ⊿*MoDLD1* mutant and the control strain (Fig 3.21B). Both MoDLD1 and MoDLD2 were shown to localize in the mitochondria and displayed a peripheral pattern associated with the plasma membrane in conidia. The mitochondrial distribution in conidia was revealed by TEM. TEM analysis confirmed that the majority of mitochondria accumulate at the vicinity of the plasma membrane, which suggested a spatial regulated pattern of ATP production (Fig 3.21C). The signal pattern of MoDLD2-eGFP in conidia of the ⊿*MoDLD1* mutant was consistent with that observed in conidia of the control strain by either confocal microscopy or TEM analysis (Fig 3.21B). During appressorium development (6 and 20 hr post inoculation) in the control strain, conidia experienced autophagy to recycle cellular components and nutrients to fuel the differentiation of infectious structures; therefore, the MoDLD2-eGFP signal dissolved in the conidium of the control strain but was expressed again in the appressorium (Fig 3.21B). In contrast, in association with the inability to develop the appressorium, the MoDLD2-eGFP remained the original pattern in the conidium of the ⊿*MoDLD1* mutant during appressorium development (Fig 3.21B). This may imply that the autophagy machinery was blocked due to the disruption of MoDLD1, but cannot be taken as evidence that the expression and accumulation of MoDLD2 was subject to the regulation by MoDLD1.

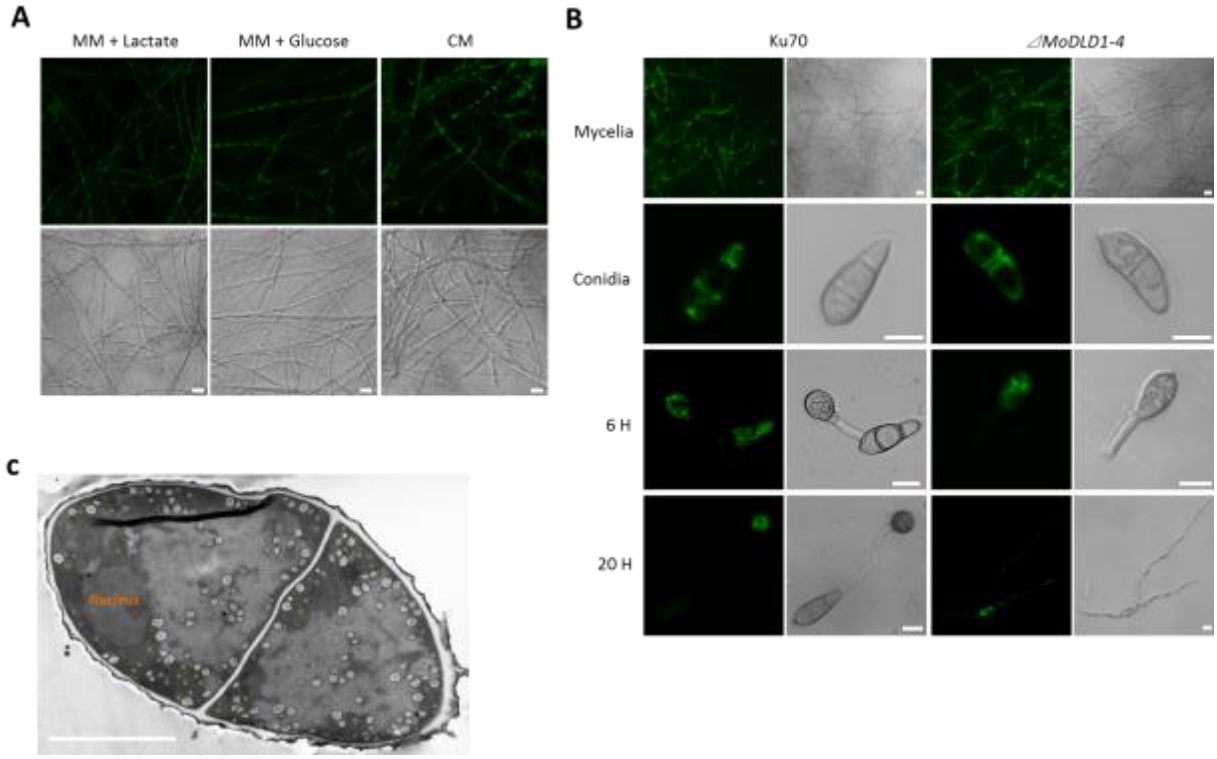

Figure 3.21 Confocal microscopy observations on the expression of *MoDLD2-Com-eGFP.* (A) Spatial analysis of *MoDLD2* expression in the presence of lactate, glucose or rich nutrient of CM. (B) Expression of *MoDLD2* in the control strain Ku70 and ⊿*MoDLD1* during stages of vegetative growth, conidial and appressorium development. Bar=10 μm. (C) Transmission electron micrograph of the conidium of the wild type strain, showing the distribution pattern of mitochondria. Bar=5 μm.

3.6.4 MoDLD3 is not necessary for fungal development and pathogenicity of *M. oryzae*

In spite of the higher similarity that MoDLD3 shared with MoDLD1 than other lactate dehydrogenase members, the ⊿*MoDLD3* mutants displayed no obvious effects on vegetative growth, conidiation, conidial morphology, appressorium formation and disease development on plants (Table 3.3) (Fig 3.22A-B). The distinction between MoDLD1 and MoDLD3 in the regulation of fungal development and pathogenicity of *M. oryzae* remains unknown.

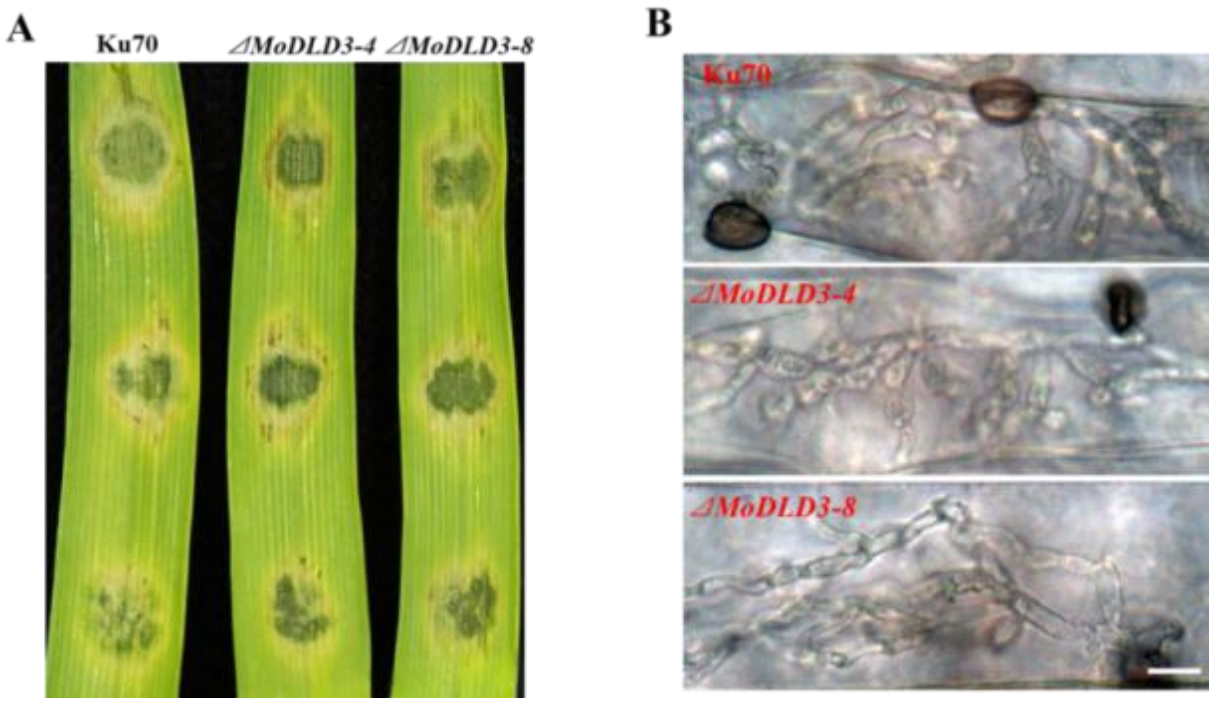

Figure 3.22 The effect of *MoDLD3* deletion on pathogenicity of *M. oryzae*.
(A) 10 day-old barley leaves were drop-inoculated with conidia of Ku70 and ⊿*MoDLD3* mutants. Typical leaves were photographed 5 dpi. (B) Conidia of Ku70 and ⊿*MoDLD3* mutants were drop-inoculated on barley leaves. Appressorium penetration and invasive hyphae growth were examined 48 hpi. Bar=10 μm.

Table 3.3 Phenotypic analysis of ⊿*MoDLD3* mutants.

Strains	Growth rate (mm/day)[a]	Conidiation spore/cm^2 (10^3)[b]	Appressorium formation (%)[c]
Ku70	3.29 ±0.13 a	33.73 ±2.61 a	93.47 ±4.23 a
⊿*MoDLD3-4*	3.25 ±0.15 a	35.60 ±4.13 a	96.04 ±6.18 a
⊿*MoDLD3-8*	3.34 ±0.08 a	33.86 ±3.03 a	95.71 ±8.05 a

Growth rate (daily extension in colony diameter) was measured on PDA or CM culture medium.

Number of conidia harvested from 10-day-old oatmeal agar plates at room temperature.

Percentage of appressorium formation over total number of conidia that formed germ tubes 24 h post-inoculation on hydrophobic cover slips.

Data in all columns are means and standard deviations calculated with results from three independent experiments with three replicates. Different letters were used to mark statistically significant difference (P=0.01).

3.6.5 Deletion of L-lactate dehydrogenase *MoLLD1* or *MoLLD2* in the peroxisomes does not affect appressorium development and pathogenicity of *M. oryzae*

Based on the hypothesis, the peroxisomal members of lactate dehydrogenase that are supposed to oxidize NADH when converting pyruvate to lactate represent another key point in operating the lactate shuttle. Two putative L-lactate dehydrogenases with peroxisomal targeting signal 1 (PTS1) MoLLD1 and MoLLD2 were identified in the *M. oryzae* genome (Dean et al., 2005). Deletion of either *MoLLD1* or *MoLLD2* did not result in any significant alterations in hyphal development, conidiation, appressorium development and fungal invasion compared to the wild type strain. Both gene deletion mutants consequently remained fully pathogenic on host plants (Table 3.4) (Fig 3.23). These results suggested that no single L-lactate dehydrogenase in the peroxisomes was essential for fungal development and virulence. We concluded that the re-oxidation of reducing equivalents and the generation of lactate from pyruvate in the peroxisomes involved either unidentified lactate dehydrogenases or the combined action of several members of lactate dehydrogenase.

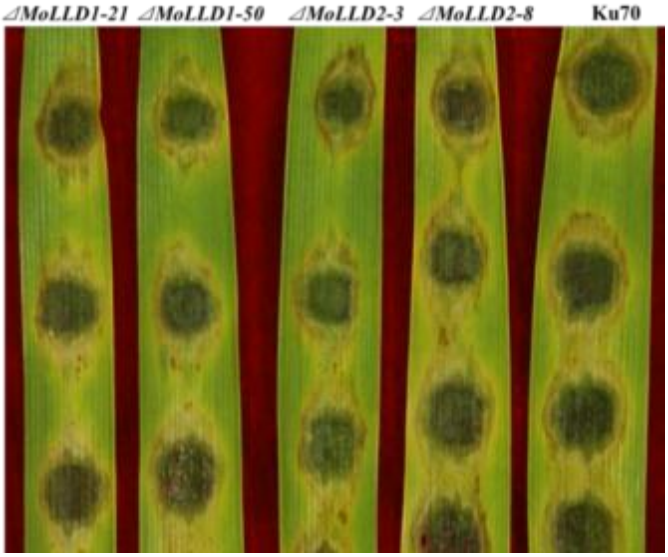

Figure 3.23 Effects of *MoLLD1* and *MoLLD2* deletion on pathogenicity of *M. oryzae*.
10 day-old barley leaves were drop-inoculated with conidia of Ku70, ⊿*MoLLD1* mutants and ⊿*MoLLD2* mutants. Typical leaves were photographed 5 dpi.

Table 3.4 Phenotypic analysis of ⊿*MoLLD1* and ⊿*MoLLD2* mutants.

Strains	Growth rate (mm/day) [a]	Conidiation spore/cm^2 (10^3) [b]	Appressorium formation (%)[c]
Ku70	3.32 ±0.08 a	35.53 ±6.63 a	92.65 ±5.09 a
⊿*MoLLD1-21*	3.59 ±0.36 a	36.66 ±5.69 a	95.62 ±5.06 a
⊿*MoDLD1-50*	3.50 ±0.30 a	34.65 ±5.66 a	96.42 ±6.55 a
⊿*MoLLD2-3*	3.36 ±0.56 a	33.85 ±4.21 a	95.56 ±3.22 a
⊿*MoLLD2-8*	3.33 ±0.69 a	37.63 ±5.43 a	94.24 ±4.68 a

Growth rate (daily extension in colony diameter) was measured on PDA or CM culture medium.

Number of conidia harvested from 10-day-old oatmeal agar plates at room temperature.

Percentage of appressorium formation over total number of conidia that formed germ tubes 24 h post-inoculation on hydrophobic cover slips.

Data in all columns are means and standard deviations calculated with results from three independent experiments with three replicates. Different letters were used to mark statistically significant difference (P=0.01).

3.6.6 Disruption of *MoLLD5* results in mycelial autolysis and reduced conidiation

Growth of the ⊿*MoLLD5* mutants was indistinguishable from that of the wild type P131 strain on PDA medium or on oat meal medium. However, ⊿*MoLLD5* mutants underwent progressive autolysis of mycelia on oat meal plates during early growth. Mycelial autolysis began at the center of the plate and progressed outward for at least 7 days. The autolytic phenotype was rescued when the mutant strains were grown in a longer period for 14 days on oat meal plates (Fig 3.24A).

The ability of the ⊿*MoLLD5* mutants to produce conidia was significantly impaired. Conidiation of ⊿*MoLLD5* mutants only accounted for approximately 20% of the P131 strain (Table 3.5). To explore the difference, conidiophore development and conidial formation were compared between ⊿*MoLLD5* mutants and the P131 strain. Both ⊿*MoLLD5* mutants and the P131 strain developed identical density of conidiophore after 48 hr of light exposure. However, a relatively lower amount of conidia were differentiated from conidiophores of ⊿*MoLLD5* mutants compared to that from conidiophores of the P131 strain, in which three to five conidia were usually formed from a single conidiophore in the sympodial pattern (Fig 3.24B). Reduced conidiation of ⊿*MoLLD5* mutants was confirmed by SEM microscopy examination

of the culture surface of both ⊿*MoLLD5* mutants and the P131 strain (Fig 3.24C). Thus, the reduced conidiation of the ⊿*MoLLD5* mutants was caused by the defect in formation of conidia at the ends of conidiophores but not by the time course-dependent autolysis of aerial structures.

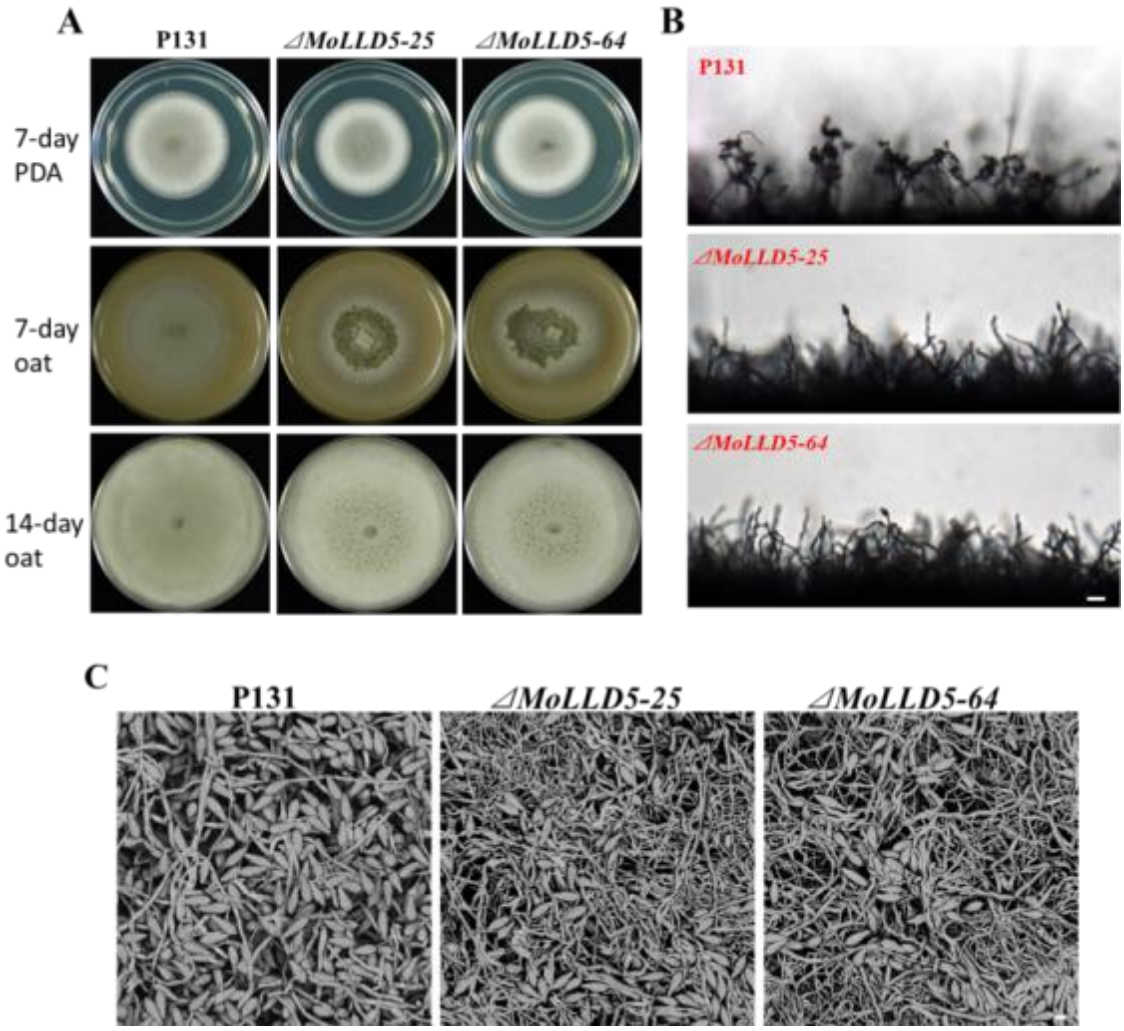

Figure 3.24 Effects of *MoLLD5* on hyphal development and conidiogenesis of *M. oryzae*. (A) Vegetative growth of P131 and ⊿*MoLLD1* mutants grown on PDA medium and oat meal medium for indicated days. (B) Development of conidia on conidiophores. Light microscopic observation was performed on strains grown on oat medium under constant light exposure. Bar=50 μm. (C) Arial structure observation by scanned electron microscope. Bar=10 μm.

3.6.7 Disruption of *MoLLD5* does not affect infection-related development and fungal virulence of *M. oryzae*

To examine the effect of MoLLD5 on appressorium development in *M. oryzae*, the appressorium formation assay was conducted on plastic cover slips. Melanized appressoria were induced after overnight incubation on a hydrophobic surface. No obvious difference was observed between ⊿*MoLLD5* mutants and the P131 strain in conidial germination, appressorium formation and penetration (Table 3.5). Inoculation on barley leaves showed that ⊿*MoLLD5* mutants were as pathogenic as the P131 strain 5-day post inoculation (Fig 3.25A-B).

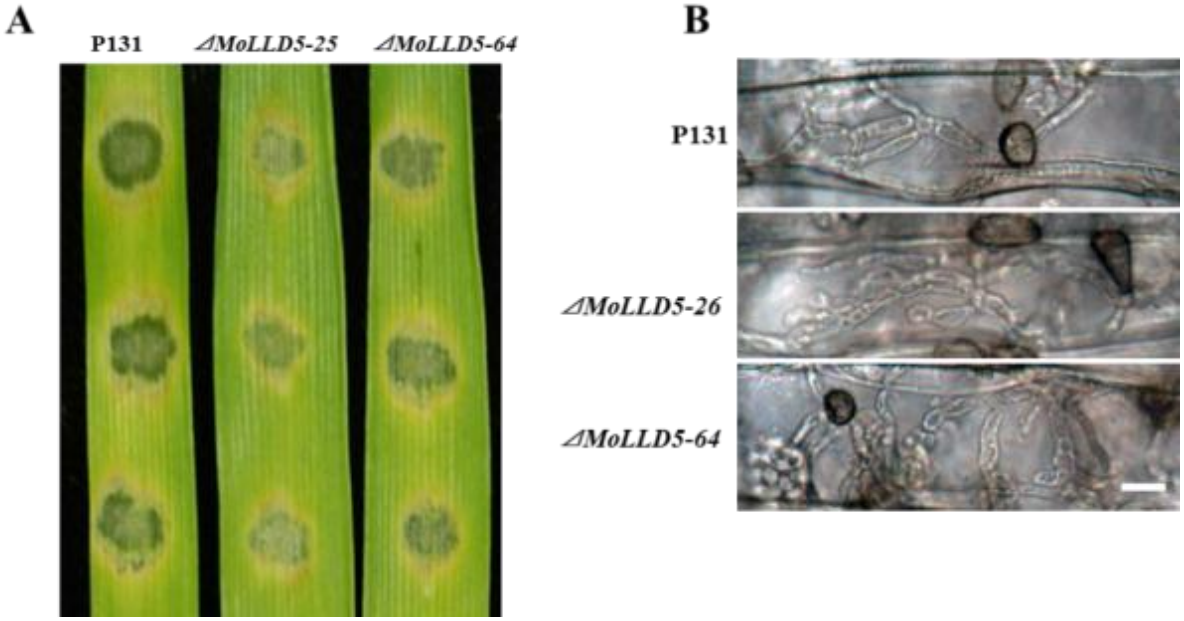

Figure 3.25 The effect of *MoLLD5* deletion on pathogenicity of *M. oryzae*.
(A) 10 day-old barley leaves were drop-inoculated with 4×10^4/ml conidia of indicated strains. Typical leaves were photographed 5 dpi. (B) Conidia from the same set of strains were drop-inoculated on barley leaves. Appressorium penetration and invasive hyphal growth were examined 48 hpi. Bar=10 μm.

Table 3.5 Phenotypic analysis of ⊿*MoLLD5* mutants.

Strains	Growth rate (mm/day) [a]	Conidiation spore/cm^2 (10^3)[b]	Appressorium formation (%)[c]
P131	3.36 ±0.16 a	114.51 ±7.51 a	94.50 ±5.13 a
⊿*MoLLD5-25*	3.44 ±0.26 a	24.14 ±1.10 b	96.26 ±5.86 a
⊿*MoLLD5-64*	3.49 ±0.19 a	25.41 ±2.00 b	93.25 ±6.65 a
MoLLD5-Com-eGFP	3.57 ±0.34 a	115.6 ±8.70 a	96.71 ±1.66 a

Growth rate (daily extension in colony diameter) was measured on PDA or CM culture medium.

Number of conidia harvested from 10-day-old oatmeal agar plates at room temperature.

Percentage of appressorium formation over total number of conidia that formed germ tubes 24 h post-inoculation on hydrophobic cover slips.

Data in all columns are means and standard deviations calculated with results from three independent experiments with three replicates. Different letters were used to mark statistically significant difference (P=0.01).

3.6.8 Subcellular localization of MoLLD5

To determine the subcellular localization of MoLLD5, the *MoLLD5* gene with its native promoter was fused with e*GFP* at the C-terminus (Fig 3.26A). The *MoLLD5-eGFP* fusion construct was introduced into the ⊿*MoLLD5* mutant**.** The transformants were screened on neomycin plates and confirmed by PCR analysis. The transformant *MoLLD5-Com-eGFP-23* was chosen for further analysis. A growth test of *MoLLD5-Com-eGFP-23* on oatmeal medium indicated that the autolytic defect in aerial mycelia was rescued. The conidiation-deficient phenotype was also recovered to the level of the P131 strain in the *MoLLD5-Com-eGFP-23* by statistical analysis (Table 3.5), indicating that the fusion construct exerted the correct function. Examination by confocal microscopy of mycelia and conidia of *MoLLD5-Com-eGFP-23* suggested that MoLLD5 localized in the cytoplasm (Fig 3.26B).

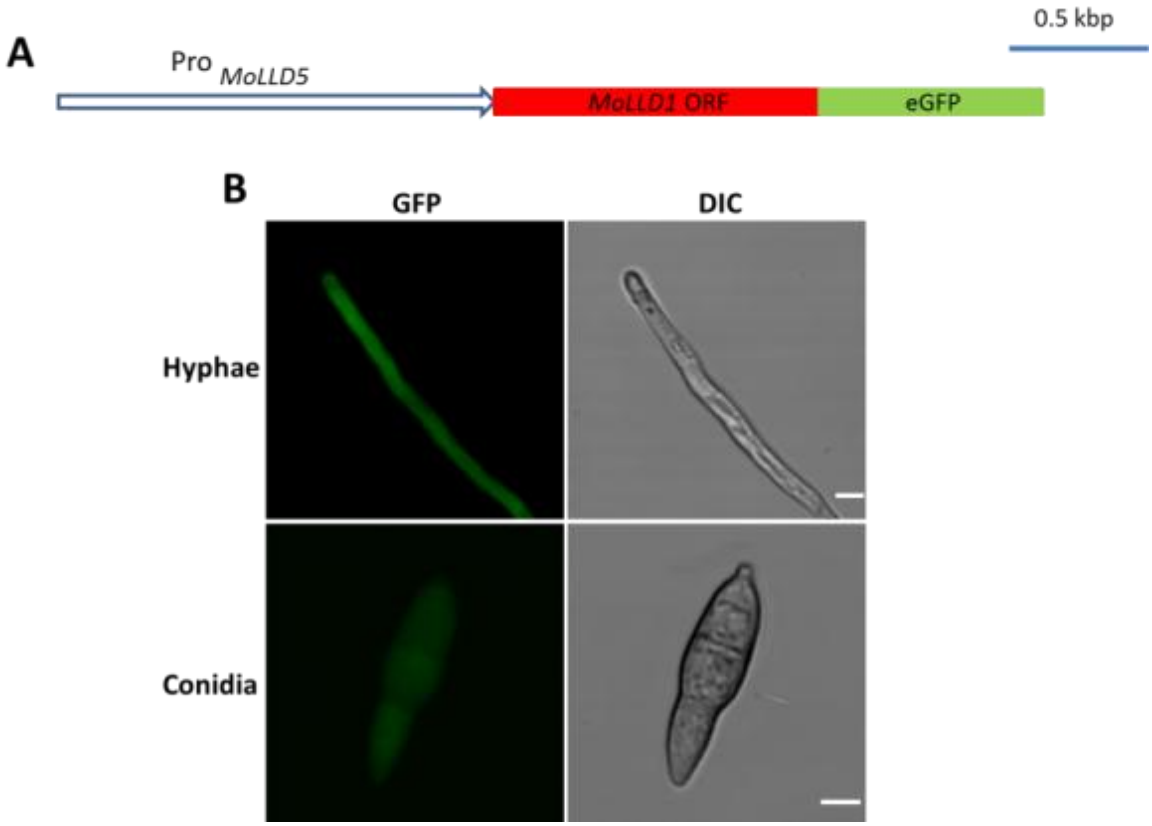

Figure 3.26 Subcellular localization of the MoLLD5-eGFP fusion protein.
(A) The schematic representation of complementation and cellular localization construct. (B) Confocal microscopy analysis of MoLLD5-eGFP localization during mycelial and conidial stages in *M. oryzae*. Bar=5 μm.

3.7 Characterization of the G-3-P shuttle in *M. oryzae*

3.7.1 Identification and transcriptional analysis of the mitochondrial component of the G-3-P shuttle in *M. oryzae*

To reveal the role of the G-3-P shuttle in fungal development and pathogenicity of *M. oryzae*, the mitochondrial glycerol-3-phosphate dehydrogenase, whose yeast homolog ScGUT2 was shown to localize to the mitochondrial inner membrane and participate in the mitochondrial G-3-P shuttle, was identified and r functionally characterized in *M. oryzae*. The yeast ScGUT2 was used to perform a BLAST search in the *M. oryzae* genome and identify Mo_03147 (MoGUT2) as the single homolog of ScGUT2 (Dean et al., 2005). Alignment of the MoGUT2

protein sequence with members of the mitochondrial glycerol-3-phosphate dehydrogenase displayed 39% identity to ScGUT2 in *S. cerevisiae* and 74% identity to a hypothetical mitochondrial glycerol-3-phosphate dehydrogenase NcGUT2 in *Neurospora crassa* (Fig 3.27A). The gene expression pattern of MoGUT2 during *in vivo* and *in planta* stages was also tested by RT-PCR. Similar to the expression pattern of *MoDLD1*, transcriptional profiling of the *MoGUT2* gene showed that it was also transcriptionally induced during the conidial stage and the early stage of infection-related development compared to that in mycelial stage (Fig 3.27B).

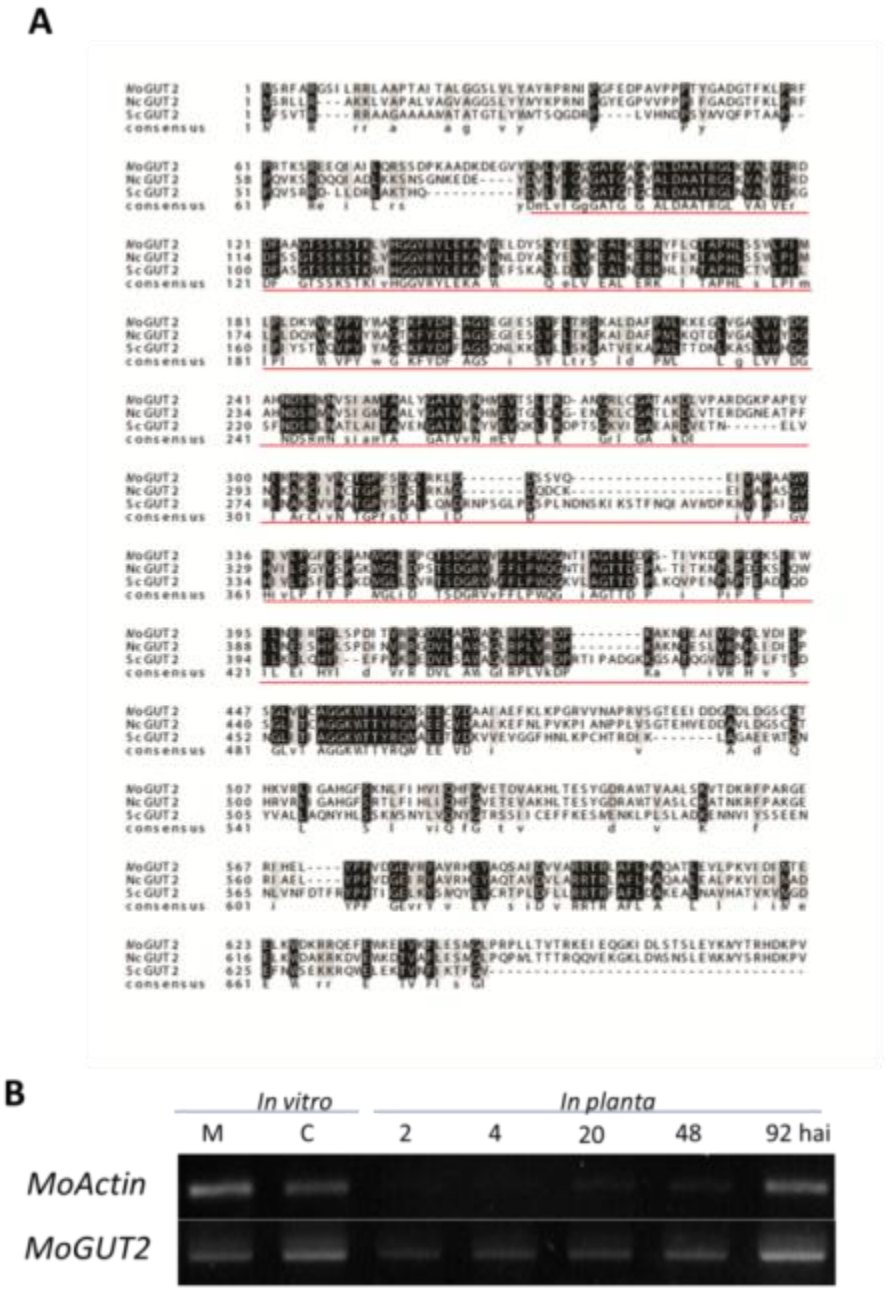

Figure 3.27 Alignment of the *M. oryzae* GUT2 and its gene transcriptional profiling.
(A) The predicted MoGUT2 sequence was aligned with identified GUT2 in *Saccharomyces cerevisiae and* putative GUT2 protein in *Neurospora crassa.* Identical sequences are highlighted in black shado*w*. Conserved amino acid residues are indicated in gray shadow. The conservative catalytic FAD-dependent oxidoreductase domain is underlined by a red line. Dashes were used to indicate gaps in the alignments. The ClustalX1.83 program is used to align sequences. (B) Transcript abundance dynamics analysis of *MoGUT2*. Expression profiling was conducted by semi-quantitative RT-PCR in mycelial, conidial states and *in planta* stages. M, mycelia; C, conidia; Hai, hours after inoculation on barley leaves.

3.10.2 Deletion of *MoGUT2* resulted in defects in aerial growth and conidiogenesis of *M. oryzae*

To understand the role of the G-3-P shuttle in fungal development and pathogenicity, here the mitochondrial glycerol-3-phosphate dehydrogenase GUT2 in *M. oryzae* was functionally characterized. The gene deletion mutant of MoGUT2 was created by replacing the open reading frame with the selection marker for hygromycin resistance (*Hph*) in the Ku70 strain. PCR screening and DNA blot analysis were performed to confirm the gene deletion mutants (Fig 3.28). The growth assay showed growth deficiency of ⊿*MoGUT2* mutants on oat meal and V8 medium (Fig 3.29A). On oat meal and V8 medium for 7 days at room temperature, ⊿*MoGUT2* mutants had a flat colony caused by reduced growth of aerial hyphae, although the radial growth was normal compared to the Ku70 strain. Given that ⊿*MoGUT2* mutants displayed reduced aerial growth, we next tested its effect on conidiogensis. Conidiation of ⊿*MoGUT2* mutants and the Ku70 strain were determined in 10-day old oat meal medium. The assessment showed over a 90% reduction in conidiation of ⊿*MoGUT2* mutants compared to the Ku70 strain (Table 3.6). The microscopic observation of the conidial production structure showed that development of conidia on conidiophores were severely affected in ⊿*MoGUT2* mutants (Fig 3.29B). This result was confirmed by SEM examination on the surface of sporulation cultures. In comparison with the Ku70 strain that produced conidia from the conidiophore in a sympodial pattern, conidiophores of ⊿*MoGUT2* mutants, in many cases, only differentiated a single conidium (Fig 3.29C). However, conidia produced by ⊿*MoGUT2* mutants remained as morphologically normal as that of the Ku70 strain. Considering this alongside the expression pattern of the *MoGUT2* gene that showed higher-level expression in the conidial stage, it could be concluded that MoGUT2 played an important role in the conidiogenesis of *M. oryzae*.

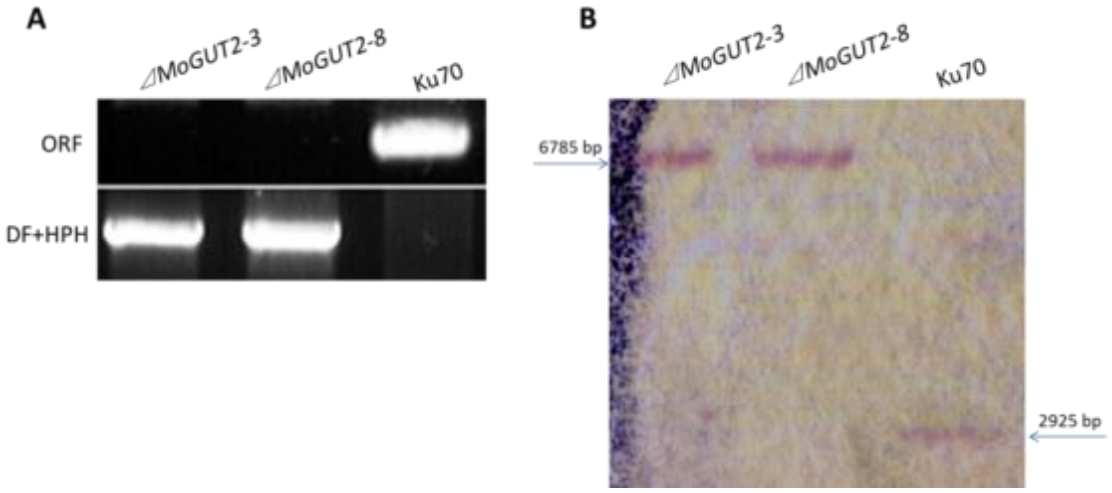

Figure 3.28 Generation and confirmation of the *MoGUT2* gene deletion mutants.

(A) Total genomic DNA isolated from mycelia of ⊿*MoGUT2* mutants and the Ku70 strain were subjected to PCR analysis using gene-specific primers (ORF) and primers (DF+HPH) spanning on the insertion hygromycin-resistant gene and the upstream flanking sequence of replaced fragments. (B) Total genomic DNA (5 μg per lane) isolated from Ku70 and ⊿*MoGUT2* mutants were digested with *SmaI* and subjected to Southern blot analysis. The probe, a 710 bp DNA fragment at the upstream of *MoGUT2* start codon, was used to hybridize *SmaI*-digested DNA from ⊿*MoGUT2-3*, ⊿*MoGUT2-8* and the Ku70 strain. This probe detected different length of fragments from ⊿*MoGUT2* mutants and the Ku70 strain as predicted.

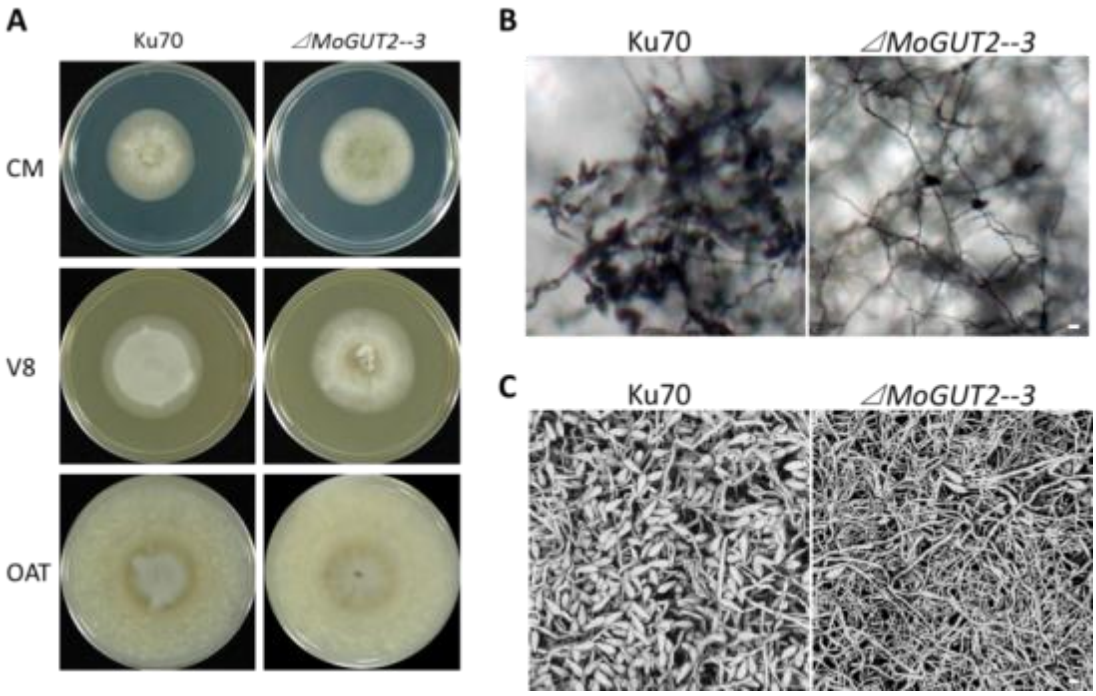

Figure 3.29 Roles of MoGUT2 in hyphal development and conidiogenesis.
(A) Growth assay on PDA, V8, and oat medium. ⊿*MoGUT2* mutant displayed reduced aeria hyphae growth in V8 and oat medium. (B) Conidiation of Ku70 and ⊿*MoGUT2* were examined under the microscope on oat medium for 2-day light illumination. ⊿*MoGUT2* showed dramatic reduction in conidiation. Bar=10 μm. (C) Arial structure observation by scanned electron microscope. Bar=10 μm.

3.10.3 MoGUT2 is not required for pathogenicity in *M. oryzae*

Although *MoGUT2* was transcriptionally induced during the early stage of infection-related development, phenotypic analysis of ⊿*MoGUT2* mutants indicated no significant difference in conidial germination, appressorium formation, and pathogenicity in comparison with the Ku70 strain (Table 3.6). Although ⊿*MoGUT2* mutants showed equal aggression on host plants compared to the Ku70 strain, blast lesions induced by ⊿*MoGUT2* mutants appeared paler than the typical brown-gray lesions on the Ku70-infected barley leaves (Fig 3.30A). This difference was caused by the inability of ⊿*MoGUT2* mutants to efficiently produce conidiophores and conidia at infection sites. The microscopic observation showed that profuse conidiophores and conidia were detected in lesions induced by the Ku70 strain for 7

days compared to those by the ⊿*MoGUT2* mutant, indicating that MoGUT2 was also important for conidiation on host plants (Fig 3.30B). Secondary infection arising from the successful reproduction of phytopathogens during primary infection is critical for plant disease epidemics. MoGUT2, therefore, regulates a critical step in the disease cycle, although it is dispensable for the plant infection under laboratory conditions.

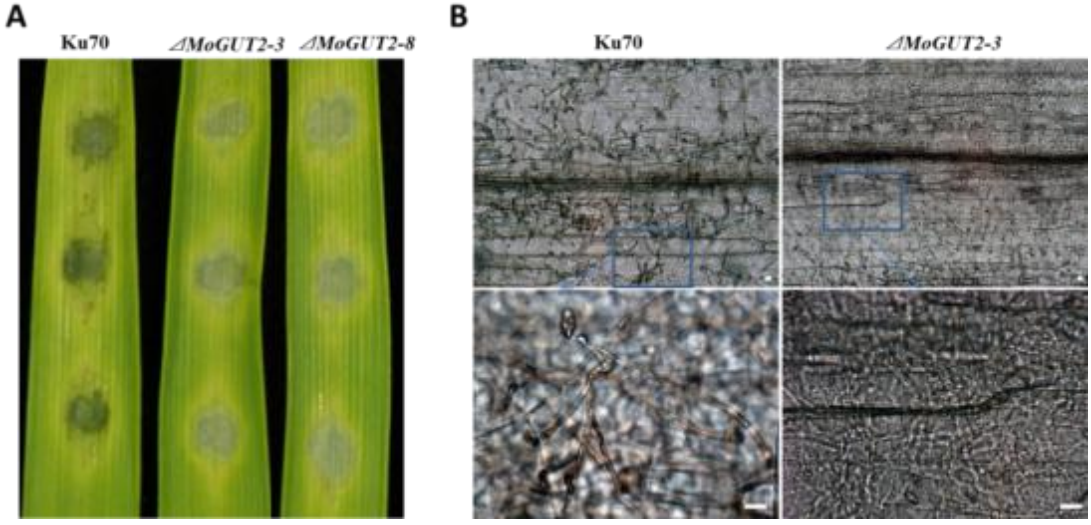

Figure 3.30 Penetration and plant infection assay with conidia of ⊿*MoGUT2* mutants.
(A). Spores harvested from 10-day-old cultures of Ku70 and ⊿*MoGUT2* were sprayed on 10-day-old barley leaves. Photos were taken after 7 days inoculation at 26℃ with high humidity. There was no obvious difference in pathogenicity between Ku70 and ⊿*MoGUT2*. (B). Lesions caused by Ku70 and ⊿*MoGUT2* were observed by microscope to examine the conidiophore and conidial development. Enlarged pictures are shown in the panel below. Bar= 20 μm.

Table 3.6 Phenotypic analysis of ⊿*MoGUT2* mutants.

Strains	Growth rate (mm/day)	Conidiation spore/cm^2 (10^3)	Appressorium formation (%)
Ku70	3.53±0.26 a	37.07±3.59 a	95±6.53 a
⊿*MoGUT2-3*	3.29±0.05 a	2.55±0.56 b	94±5.66 a
⊿*MoGUT2-8*	3.39±0.16 a	3.02±0.78 b	95±3.21 a

Growth rate (daily extension in colony diameter) was measured on PDA or CM culture medium.

Number of conidia harvested from 10-day-old oatmeal agar plates at room temperature.

Percentage of appressorium formation over total number of conidia that formed germ tubes 24 h post-inoculation on hydrophobic cover slips.

Data in all columns are means and standard deviations calculated with results from three independent experiments with three replicates. Different letters were used to mark statistically significant difference (P=0.01).

3.10.4 The Subcellular localization of MoGUT2

To investigate the subcellular localization of MoGUT2, the full *MoGUT2* ORF sequence was fused with *eGFP* at the C-terminus in the RP27-pKNTG vector, which uses the promoter of the ribosomal protein-27 gene to ensure the constitutive expression of the targeted gene (Fig 3.31A). The sequence analysis of MoGUT2 indicated that it has a mitochondrial targeting signal (MTS) and a transmembrane domain (TM) at the N-terminus. To test the role of the MTS and TM domains in the protein localization, the DNA sequence deleted for both MTS and TM-encoding regions was also cloned into the RP27-pKNTG vector and named *pRP27-MoGUT2*$^{\triangle SP+TM}$*-eGFP,* to determine the localization as well (Fig 3.31A). Both GFP expression cassettes directed by the PR27 promoter were introduced into the wild type strain Guy11 through PEG-mediated transformation of fungal protoplasts. Transformants containing the *pRP27-MoGUT2-eGFP* were screened on neomycin-resistant plates, among which *RP27-MoGUT2-eGFP-2* was selected for further localization analysis. To confirm its mitochondrial localization, MitoTracker Red was used to stain *RP27-MoGUT2-eGFP-2* mycelia collected from CM medium, showing co-localization between the dye-labeled mitochondrial signal and the GFP signal (Fig 3.31B). This result indicated that MoGUT2 is a mitochondrial protein with potential localization in the inner membrane. Transformants expressing the *pRP27-MoGUT*$^{\triangle SP+TM}$*-eGFP* were identified and subjected to the microscopic analysis. Confocal microscopic observation revealed cytosolic localization of the MoGUT2$^{\triangle SP+TM}$-eGFP allele in transformants (Fig. 3.31B), indicating that the N-terminal MTS and TM domain were required for MoGUT2 mitochondrial localization.

To investigate the expression pattern and promoter activity of *MoGUT2*, a 1.3-kb fragment of the *MoGUT2* promoter was cloned into the vector pKNTG (Fig. 3.31A). The resulting construct *pMoGUT2-eGFP* was transformed into the Guy11 strain. Transformants with neomycin resistance were screened on the plates and confirmed by confocal microscopy for GFP signals. During conidiogenesis, stronger GFP signals were gradually detected in junior and matured conidia compared to that in the incipient conidium (Fig. 3.31C), suggesting that

MoGUT2 was induced at the later stage of conidiogenesis and may be important for the conidial maturation. GFP signals were also detected in the cytoplasm of germ tubes, young and matured appressoria (Fig. 3.31D). This data is consistent with the *MoGUT2* transcriptional determination showing it was induced at the early stage of plant infection.

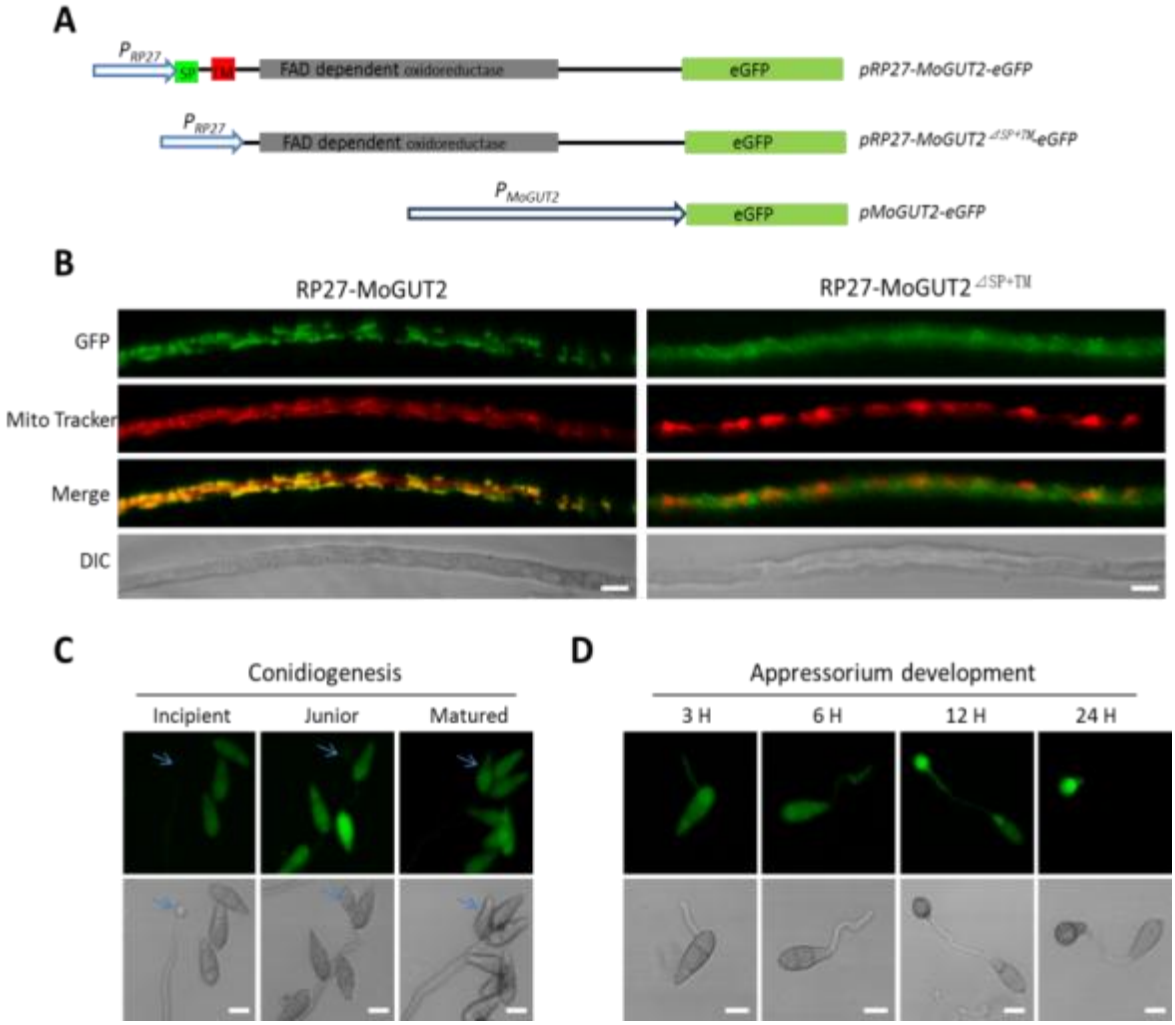

Figure 3.31 Subcellular localization of *MoGUT2* gene product and its promoter activity evaluation.

(A) Schematic diagrams of *MoGUT2* gene product cellular localization constructs and transcriptional reporter construct. (B) Confocal microscopy analysis of RP27-MoGUT2-eGFP and RP27-MoGUT2$^{\triangle SP+TM}$-eGFP localization in mycelia of *M. oryzae*. The mycelia were stained with Mito-Tracker Red CMXRos to facilitate visualization of mitochondria. Bar=5 μm. (C-D) Confocal microscopy analysis of *pMoGUT2-eGFP* product during conidiogenesis and appressorium development. Arrows indicate conidia attached on the conidiophore for different stages. Bar=10 μm.

CHAPTER 4 DISCUSSION

4.1 Pyruvate as a key metabolite involved in appressorium development of *M. oryzae*

The utilization of nutrient reserves in conidia represents a key step for appressorium development in the absence of a nutrient source on the plant surface. Metabolic pathways that break down storage compounds result in continuous production of reducing equivalents, in the form of the NADH and FADH2, which are carried by coenzymes in cellular compartments. To maintain the metabolic circuit, coenzymes then need to be re-oxidized to be used again. Under aerobic conditions, the overall process by which reducing equivalents are oxidized in a cell is via oxidative phosphorylation within mitochondria. Since reducing equivalents are prevented from traversing across cellular membranes (Tobin et al., 1980; Van Roermund et al., 1995), several redox shuttles are designated to facilitate transportation between cellular compartments.

In *M. oryzae* the mature appressorium generates enormous turgor pressure due to the accumulation of glycerol, which is partly liberated by fatty acids through lipolysis of lipid bodies stored in the conidium (Wang et al., 2007). Fatty acids freed from lipolysis are further metabolized through β-oxidation in the peroxisomes, resulting in production of reducing equivalents ($FADH_2$ and NADH) and the intermediate metabolite acetyl-CoA, which is then channeled through the glyoxylate cycle (Wang et al., 2003). Production of pyruvate in the peroxisomes by the activity of aminotransferases has been demonstrated to be an important consequence of the glyoxylate cycle in *M. oryzae* (Bhadauria et al., 2012). This is confirmed by our pharmacological evidence in which the appressorium development is prevented with the treatment of an aminotransferase-specific inhibitor, but is again rescued when excess pyruvate is provided. Pyruvate sits at the intersection of branching primary metabolic pathways and holds a pivotal position in the supply of precursor metabolites for a series of biochemical reactions within a cell (Cox and Nelson, 2004; Pronk et al., 1996). This may indicate that through the subsequent gluconeogenesis pyruvate production resulting from the lipid bodies' oxidation in the peroxisomes can contribute to synthesis of glucan, chitin, or osmolyte

generation, which are necessary for appressorium maturation in *M. oryzae* (Wilson and Talbot, 2009). Hence, pyruvate has a central role in the coordination of key pathways of energy metabolism during infection-related development in *M. oryzae.*

Accumulating evidence in mammalian systems suggests that pyruvate participates in the control of cellular redox state through the exchange with lactate across cellular membranes between two compartments (Brooks, 2009). Lactate dehydrogenases that catalyze the lactate/pyruvate interconversion and lactate/pyruvate-specific monocarboxylate transporters have been identified in various cellular compartments of animal cells (Brooks et al., 1999; Draoui and Feron, 2011; McClelland et al., 2003). On the basis of previous studies indicating pyruvate production in the peroxisomes of *M. oryzae* (Bhadauria et al., 2012), we speculate that the lactate shuttle is likely to exist intracellularly in transporting reducing equivalents out of the peroxisomes and providing re-oxidized co-enzymes back to maintain the β-oxidation function. In this study, we set out to investigate roles of lactate dehydrogenases, a group of enzymes that operate the lactate shuttle, in fungal development and pathogenicity of the model phytopathogenic fungus *M. oryzae*. Several putative lactate dehydrogenases with potential cellular localizations in the mitochondria, peroxisomes and the cytosol were identified in the *M. oryzae* genome (Dean et al., 2005). The MoDLD1 is homologous to *S. cerevisiae* ScDLD1 that functions in the mitochondrial intermembrane space and oxidizes D-lactate to pyruvate (Rojo et al., 1998). MoDLD1 is highly induced during germination and appressorium formation compared to the mycelial stage. The expression pattern of the mitochondrial G-3-P dehydrogenase MoGUT2 is similar to that of MoDLD1, whose homologs in yeast are both transcriptionally depressed by non-fermentable carbon sources (Lodi et al., 1999). The induction of mitochondrial membrane-associated dehydrogenases during germination and appressorium formation suggests the accumulation of reduced non-fermentable carbon sources such as lactate and glycerol possibly are converted from pyruvate in *M. oryzae*.

4.2 Role of MoDLD1 in fungal development by potentially acting on the cellular respiration machinery

Expression of the full ORF sequence of *MoDLD1* rescued the growth defect of yeast ScDLD1 mutants on D-lactate and thereby confirmed the enzymatic function of MoDLD1. The D-lactate auxotrophic phenotype is the only recorded defect of yeast ScDLD1 mutants, while the disruption of MoDLD1 caused a significant reduction on vegetative growth and asexual sporulation. The functional variation of the mitochondrial D-lactate dehydrogenase 1 between yeast and *M. oryzae* may result from different lifestyles that are adapted by each. Since this is the first study of the mitochondrial D-lactate dehydrogenase 1 of filamentous fungi, more studies of its homologs across the fungal kingdom are needed to test this hypothesis. It will be interesting to know whether the role of D-lactate dehydrogenase 1 is specific for phytopathogenic fungi that experience rapid physiological and morphological transitions during infection under nutrient-free conditions (Fernandez and Wilson, 2014). We also showed that ⊿*MoDLD1* mutants failed to regulate conidial morphology and development, suggesting MoDLD1 is involved in cytoskeletal organization and cellular polarized growth. Since a continuous availability of energy is required for establishment and maintenance of cell polarity, cellular respiration in the mitochondrial inner membrane could be severely affected in ⊿*MoDLD1* mutants, resulting in unmatched energy status for proper cellular development. It was reported in *Schizosaccharomyces pombe* that defects in mitochondrial integrity and cellular respiration caused by deletion of a mitochondrial ribosomal protein led to a disrupted actin cytoskeleton and alteration of cell shape (Wiley et al., 2008). Therefore, MoDLD1 may participate in the regulation of cell morphology and the cell cycle by acting on the mitochondrial cellular respiration machinery.

4.3 Involvement of MoDLD1 in appressorium-mediated infection via adjustment of redox state and nutrient metabolism

Branching and aberrant germ tubes of ⊿*MoDLD1* mutants were observed on a hydrophobic surface. The germ tube continued elongating instead of to differentiation into the appressorium in the wild type strain. ⊿*MoDLD1* mutants' conidia collapsed in response to the excess NAD^+ during germination while remaining insensitive to NADH treatment, indicating that *MoDLD1* is hyper-sensitive to the decrease of NADH/NAD^+ ratio. A balance between oxidization and reduction of pyridine nucleotides preconditions the succession of catabolism and anabolism. In *Arabidopsis*, blockage of the G-3-P shuttle by targeted disruption of either cytosolic or mitochondrial G-3-P dehydrogenase was associated with content changes of intermediate metabolites in primary metabolic pathways (Quettier et al., 2008; Shen et al., 2006). The inability of ⊿*MoDLD1* mutants to initiate appressorium formation was coupled with the failure to utilize nutrient reserves such as lipid bodies and glycogen within the conidium. It seems that *MoDLD1* has a critical role in stabilizing intracellular redox state to mediate energy metabolism essential for the appressorium differentiation in *M. oryzae*. Nonetheless, the appressorium induction on host and non-host plant surfaces may suggest that transferred metabolites from plants can partially re-adjust the redox state in favor of appressorium formation in ⊿*MoDLD1* mutants. It remains elusive how pathogenic fungi metabolically respond to the nutrient status associated with the plant surface during the appressorium development. An early study in *Colletotrichum gloeosporioides* showed that glycerol up-take by the pathogen during the early stage of infection can relieve the metabolic defect due to the targeted deletion of cytosolic G-3-P dehydrogenase (Wei et al., 2004). Besides functioning as chemical signals responsible for appressorium formation, molecules on the plant surface could be incorporated into the metabolic network of *M. oryzae* to facilitate appressorium development.

Although appressoria were induced on the host plant surfaces and successfully penetrated into host cells, disease assays indicated that ⊿*MoDLD1* mutants were significantly

attenuated in virulence on rice and barley leaves. This was mainly caused by defects in invasive growth, as lesions induced on host leaves failed to extend to large-scale necrosis. This is the first report that relates the role of a redox shuttle to the virulence of a fungal pathogen. *M. oryzae* has been widely regarded as a model organism to study the infection of hemibiotrophic pathogens on host plants, during which the switch from biotrophic to necrotrophic phases occupies a critical node (Mosquera et al., 2009). Until now, little was known about the physiological basis of the hemibiotrophic switch in *M. oryzae*, which is correlated by alterations of metabolic status (Pellier et al., 2003; Thomazella et al., 2012). The redox shuttle controlled by MoDLD1 may have a role in the mediation of this shift.

4.4 MoDLD1 as a mitochondrial component of the lactate shuttle

Deletion of the transmembrane domain in MoDLD1 led to its sorting to the cytoplasm, which also resulted from deletion of both the mitochondrial targeting signal (MTS) and the transmembrane domain (TM). These results suggested that mitochondrial sorting of MoDLD1 was mediated by the cooperative effect of the N-terminal MTS and TM domains. The association of the MTS with the membrane binding domains to determine mitochondrial localization was also observed in an autophagy related protein Atg24 of *M. oryzae* (He et al., 2013). Along with the mis-sorting of the cellular localization, deletion of the transmembrane domain completely abolished the function of MoDLD1. Moreover, the expression of the truncated allele pTEF1-MoDLD1$^{\triangle SP+TM}$ did not display enzyme activity to rescue the growth defect of yeast *ScDLD1* mutants on D-lactate. In *S. cerevisiae*, ScDLD1 only folded into its correct conformation in the intermembrane space when it was imported across the inner mitochondrial membrane (Rojo et al., 1998). The anchoring of MoDLD1 at the inner mitochondrial membrane may serve as the prerequisite of proper folding for its enzymatic function. To date, there is a growing body of literature describing the significance of peroxisomal lipid metabolism in pathogenicity of *M. oryzae*, however, relatively rare evidence

integrated these pathways to mitochondrial metabolism contributing to energy synthesis (Hooks, 2002; Ramos-Pamplona and Naqvi, 2006).

This study suggests the potential involvement of lactate as a mediator in bridging metabolite flow and redox balance between the peroxisomes/ cytosol and the mitochondria in *M. oryzae* (Fig 4.1). As the main source of energy, the lipolysis of lipid bodies and subsequent catabolism of fatty acids in the peroxisomes lead to the accumulation of pyruvate and reducing equivalents. The lactate shuttle in this situation, through which reducing equivalents in the peroxisomes are re-oxidized and reducing power stored in lactate are finally delivered for cellular respiration, plays a major role in the adjustment of the intracellular redox state accordingly. Meanwhile, pyruvate produced in the peroxisomes is transferred to the mitochondrial intermembrane space. Recently, a pyruvate carrier composed of two subunits MPC1 and MPC2 was identified in the inner mitochondrial membrane of yeast, drosophila and human (Bricker et al., 2012; Herzig et al., 2012), which facilitates the transportation of pyruvate across the mitochondrial inner membrane to the mitochondrial matrix for further utilization and assimilation to the tricarboxylic acid (TCA) cycle. Although homologs of MPC1 and MPC2 in *M. oryzae* are yet to be identified, a linkage through the lactate transportation between lipid oxidation in the peroxisomes and the TCA cycle in the mitochondria is more likely. The catabolism of another stored nutrient, glycogen, in the conidial cytosol also lead to the production of pyruvate through glycolysis, which could potentially participate in the lactate-mediated metabolite flow toward the mitochondria through the cytosolic lactate dehydrogenases. Here, as one of the control points in the lactate shuttle, MoDLD1 had comprehensive functions in fungal development and pathogenicity of *M. oryzae*. Moreover, future research should focus on identification and characterization of other participants in the lactate shuttle, including other peroxisomal/cytosolic members of lactate dehydrogenases and lactate-specific monocarboxylate transporters.

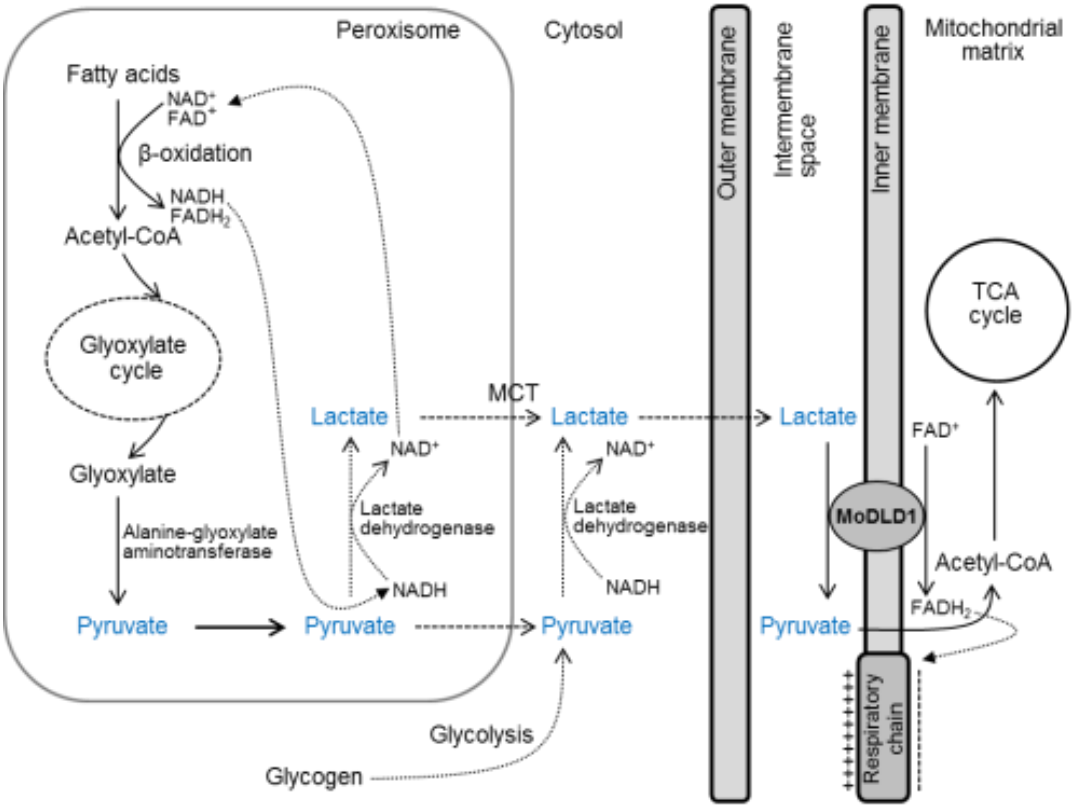

Figure 4.1 Description of the lactate shuttle for cellular metabolite flow into the mitochondria in *M. oryzae*.

Pyruvate is produced by activity of alanine-glyoxylate aminotransferase (AGT) following fatty acids oxidation and glyoxylate cycle mediation. Conversion of pyruvate to lactate by the activity of lactate dehydrogenases is coupled to the re-oxidation of NADH to NAD^+ essential for proper functioning of β-oxidation in the peroxisomes. Meanwhile, the breakdown of glycogen via glycolysis also results in cytosolic production of pyruvate, which is then reduced to lactate. Translocation of lactate from the peroxisome/cytosol to the mitochondrion is facilitated by putative specific monocarboxylate transporters (MCTs). Lactate is oxidized back to pyruvate via MoDLD1 in accompany with the production of $FADH_2$ that subsequently contributes to the respiratory chain.

4.5 Involvement of MoDLD2 in mitochondrial redox state and copper metabolism

In this study, a D-lactate dehydrogenase showing a 60% homology to the yeast D-lactate dehydrogenase 2 was identified and functionally characterized in *M. oryzae*. The D-lactate dehydrogenase 2 (ScDLD2) was firstly identified as an actin interacting protein in a yeast

two-hybrid screen for searching proteins that physically interacted with actin in yeast (Hachiya et al., 2004). Through the enzymatic assay, this protein was found to be responsible for the conversion of D-lactate to pyruvate, the characteristic of D-lactate dehydrogenase (Chelstowska et al., 1999). However, ScDLD2 appeared not to be involved in lactate metabolism but may have other preferred substrates and exerted functions unrelated to nutrient metabolism. Disruption of ScDLD2 resulted in clustered F-actin filaments and abnormal morphology of the yeast cell, which further led to the hypersensitivity of yeast cells to osmotic stress (Hachiya et al., 2004). It is unlikely that MoDLD2 in *M. oryzae* is involved in the regulation of the actin cytoskeleton, since ⊿*MoDLD2* mutants did not show any abnormal phenotypes associated with actin dysfunction. In *M. oryzae*, disorganization or dysfunction of the actin cytoskeleton always resulted in the morphological alteration of aerial hyphae and conidia, or defects on infection-related development such as deformed appressorium differentiation and invasive growth. In contrast, MoDLD2 played a role in the regulation of response to oxidative stress, which could logically lead to the assumption that MoDLD2 was related to the mitochondrial redox state.

Evidence suggested that MoDLD2 was a mitochondrial protein that localized to the matrix but not to the membrane of the mitochondrion. In addition, the expression of *MoDLD2* was independent of the regulation of *MoDLD1*. These facts suggested that MoDLD2 was not involved in the MoDLD1-operated adjustment of the redox state but was affiliated with other regulatory mechanisms in response to oxidative stress. Metallothioneins (MTs) are a group of small and metal binding proteins existing in eukaryotes and some prokaryotes. One of functions of MTs is to act as cellular redox sensors to trigger metal-dependent biochemical and cellular responses upon oxidative challenges (Fabisiak et al., 2001). In *M. oryzae*, a metallothionein MMT1 was found to have an affinity for zinc and was involved in cell wall differentiation through its function as a cellular redox sensor. Deletion of the *mmt1* gene resulted in a weaker cell wall that consequently caused the accelerated hyphal growth even under the oxidative stress and inability of the appressorium to elaborate penetration hyphae (Tucker et al., 2004).

Studies have indicated that the expression and activity of lactate dehydrogenase was modulated by its property of interacting with various metals including zinc and copper (Koiri et al., 2008; Morpeth and Massey, 1982). The mitochondrial proteome plays a critical role in the regulation of cellular copper homeostasis. For example, genes showing altered regulation associated with changed copper levels in the environment were clustered in the mitochondria, of which the *ScDLD2* was transcriptionally induced when yeast cells were exposed to elevated copper levels (van Bakel et al., 2005). This may suggested that MoDLD2 was able to detoxify the excess copper through direct binding to copper. While the treatment of excess of oxidative stress such as H_2O_2 on the wild type strain may affect the binding nature of MoDLD2 to copper, leading the release of bound copper that exhibited higher toxicity to the Ku70 strain than to *⊿MoDLD2* mutants. However, this assumption needs more experimental data for support, for example the gene expression of *MoDLD2* and growth change of the *⊿MoDLD2* mutants under the conditions of copper exposure should be determined.

4.6 Functionally redundant lactate dehydrogenases in the peroxisome

In this study, in addition to identification and characterization of mitochondrial members of lactate dehydrogenases that present a key point in the operation of the hypothetical lactate shuttle in *M. oryzae*, efforts were also made to uncover the cytosolic and peroxisomal members of lactate dehydrogenases and reveal their roles in fungal development and pathogenesis. Based on our assumption, reduction of pyruvate to lactate, coupled with the reoxidation of NADH, is critical for the continuous functioning of β-oxidation, which also acts to harness reducing power generated due to the lipid metabolism in the peroxisomes. However, disruption of either member of lactate dehydrogenases in the peroxisome did not cause any significant difference in fungal development and virulence of *M. oryzae*. Both *⊿MoLLD1* and *⊿MoLLD2* mutants developed functionally normal appressoria with the ability to penetrate barley leaves and enable invasive growth similar to that of the control strain. These results suggested that peroxisomal

lactate dehydrogenases might function redundantly in a complex manner that cannot be tested by individual gene functional analysis. The double knock-out or gene silencing of *MoLLD1* and *MoLLD2* by RNA interference, which has been used to determine the function of gene family in *M. oryzae* (Kadotani et al., 2004), may provide appealing strategies to characterize the function of peroxisomal lactate dehydrogenases during infection-related development in the rice blast fungus.

4.7 Potential roles of MoLLD5 in *M. oryzae*

Three cytosolic putative lactate dehydrogenases were identified through the overall search of the *M. oryzae* genome (Dean et al., 2005), of which MoLLD5 shared a distant similarity to the remaining members of L-lactate dehydrogenases but showed an infection-specific expression pattern; therefore, it was picked for functional analysis. MoLLD5 was demonstrated to be a cytoplasmic protein, while its enzymatic activity and substrate preference were yet to be characterized. Deletion of the *MoLLD5* caused unexpected defects in fungal conidiogenesis during which *MoLLD5* was not transcriptionally induced. During growth on oat meal medium, ⊿*MoLLD5* mutants showed the age dependent autolysis of aerial structures, which occurred in 5 to 7-day-old cultures and recovered in older cultures. Therefore, the possibility that autolysis decreased conidiation was ruled out because conidiation was assayed in 10-day-old cultures, which showed no defect in conidiophore development. The protrusion and swelling of the apex of the conidiophore resulted in the production of conidia in a sympodial pattern (Lau and Hamer, 1998). The microscopic observation revealed that, in most cases, only a single conidium was differentiated from the end of the conidiophore in ⊿ *MoLLD5* mutants. As mycelial autolysis is related to defects in cell wall integrity, it is tempting to assume that MoLLD5 is important to sustain the cell wall structure for mycelial development and conidial differentiation. A second possibility is that MoLLD5 is involved in the regulation of redox status, a functional commonality of most dehydrogenases. Loss of the *MoLLD5* gene

may cause the intracellular redox imbalance, which consequently affects mycelial development and conidiation of *M. oryzae*. However, more evidence lines, including assays to test the cell wall integrity and intracellular redox status, are required to test both assumptions of the cytoplasmic function of MoLLD5 in *M. oryzae*.

4.8 The G-3-P shuttle plays a minor role in the appressorium-mediated infection by *M. oryzae*

Functional analysis of lactate dehydrogenases in *M. oryzae* revealed a critical role of MoDLD1 in regulating fungal development and virulence, potentially suggesting the existence of the lactate shuttle, partly operated by MoDLD1, in phytopathogenic fungi. This appears to be the first evidence of the importance of a lactate dehydrogenase in lower eukaryotes, which by definition acts as a pivot for metabolite flow and redox rebalance. To explore whether the lactate shuttle is uniquely vital in the regulation of cellular metabolism, the role of the G-3-P shuttle was investigated in *M. oryzae*. The mitochondrial component G-3-P dehydrogenase MoGUT2 of the G-3-P shuttle in *M. oryzae* was identified and functionally characterized. Although *MoGUT2* showed a similar expression pattern to *MoDLD1*, it was not functionally homologous to MoDLD1 apart from commonality in regulating fungal conidiation. This was consistent with the study on the cytosolic member of G-3-P dehydrogenase (GPDH) in *Colletotrichum gloeosporioides*, which showed that CgGPDH was required for glycerol utilization and initiation of conidiation (Wei et al., 2004).

In *S. cerevisiae*, ScDLD1 and ScGUT2 are included in a supermolecular structure composed of five mitochondrial intermembrane space-facing dehydrogenases to form a complex (Grandier-Vazeille et al., 2001), which couples the electron transfer from the cytosolic matrix to the inner mitochondrial membrane for further oxidative phosphorylation. Along with ScDLD1 and ScGUT2, the supermolecular complex also includes two external NADH dehydrogenases, Nde1p and Nde2p, that oxidize cytosolic NADH, and L-lactate

dehydrogenases Cyb2p. Subcellular localization analysis showed that MoDLD1 anchored in the inner mitochondria membrane with hydrophobic domains in the intermembrane space. ScGUT2 was also suggested to span the inner mitochondrial membrane and to fulfill its function in the intermembrane space. The lactate shuttle and G-3-P shuttle were made up of by the mitochondrial members of lactate dehydrogenase and G-3-P dehydrogenase, respectively, in association with their isozymes in other cellular compartments to deliver electrons to the respiratory chain via FAD^+ (Gladden, 2004; Larsson et al., 1998). Using eGFP fusion, MoGUT2 was shown to be a mitochondrial protein potentially locating to the inner membrane; however, deletion of MoGUT2 did not affect the appressorium development and pathogenicity, suggesting a minor role of the G-3-P shuttle in energy metabolism during fungal infection in *M. oryzae*.

4.9 Conclusion and future respective

Previous studies of *M. oryzae* have indicated the importance of lipid metabolism in fungal virulence, as mobilization of lipid droplets from the conidium to the appressorium and subsequent degradation and utilization are required for appressorium development and penetration (Thines et al., 2000; Wang et al., 2007). Following the degradation of lipid bodies by intracellular triacylglycerol lipases, the utilization of fatty acids through several metabolic pathways in the peroxisome including β-oxidation, the glyoxylate cycle, and the alanine-glyoxylate transaminase-mediated production of pyruvate has been shown to be essential for the development of infectious structures and fungal virulence in *M. oryzae* (Bhadauria et al., 2012; Bhambra et al., 2006; Wang et al., 2003). On this basis, we propose that the reducing power produced by lipid oxidation is delivered to the respiratory chain in the mitochondrial inner membrane through the lactate shuttle in *M. oryzae*. In this thesis, I set out to investigate the possible existence of the lactate shuttle, and decipher its role in primary nutrient metabolism and redox state regulation during infection-related development of the

phytopathogenic fungus *M. oryzae*. Using a combination of bioinformatics, molecular genetics, cell biology and biochemical techniques, I identified and studied lactate dehydrogenases, one of the key control points in the lactate shuttle, particularly in the mitochondria and peroxisomes of *M. oryzae*. For the first time, genetic evidence is provided to demonstrate the presence of the lactate shuttle in lower eukaryotes, as well as its importance in bridging primary metabolic pathways in the peroxisomes and mitochondria.

In total, six genes including five D, L-lactate dehydrogenase-coding genes and one G-3-P dehydrogenase-coding gene were functionally characterized in this study. MoDLD1, showing high sequence similarity to the yeast mitochondrial D-lactate dehydrogenase 1, was suggested to have a comprehensive role in regulating fungal development regarding hyphal development, conidiogenesis, infection-related development and virulence in *M. oryzae*. MoDLD1 was localized in the mitochondrial inner membrane and observed to be involved in modulating the $NADH/NAD^+$ ratio and lipid metabolism. These results suggest that the lactate shuttle-operated by MoDLD1 presents a pivot in the mediation of lipid metabolism as the main nutrient source for fungal development in *M. oryzae*. The importance of the lactate shuttle was further highlighted through functional comparison with the G-3-P shuttle, which was involved in hyphal development and conididation but dispensable for infection-related development and pathogenicity in *M. oryzae*. In addition, two peroxisomal lactate dehydrogenases, which stored reducing equivalents generated from the fatty acid oxidation, were functionally analyzed, but were shown not to be required for fungal development and virulence in *M. oryzae*. These results come as a surprise; double knockout or RNA silencing of both genes should be carried out to analyze the function of lactate dehydrogenases in the peroxisome.

When considered together, the results reported in this thesis led to the revelation of the lactate shuttle that mediates the metabolite flow entry into the mitochondria and redox rebalance during fungal infection of *M. oryzae*. It is also apparent that evidence presented in this thesis is distinct from elaborating the proposed model of the lactate shuttle in cellular metabolism. In the future, more lines of evidence arerequired to support this hypothesis. Firstly,

the intracellular NADH/NAD^+ ratio and redox level should be measured in ⊿*MoDLD1* mutants to confirm the role of MoDLD1 in cellular redox adjustment. Meanwhile, the role of lactate as a potential mobile fuel during appressorium development in *M. oryzae* is yet to be investigated. The cellular content of lactate in lipid metabolism-deficient mutants will be determined compared to the wild type strain in germination and appressorium development stages. Secondly, to reveal the function of lactate dehydrogenases in the peroxisome, the double knockout mutant of *MoLLD1* and *MoLLD2* or the RNA interference-mediated silencing line will be generated, followed by analysis using biochemical and cell biology approaches. In this study, the involvement of MoDLD1 in glycogen utilization, which proceeded to occur in the cytosol during appressorium development, suggested that the lactate shuttle might facilitate the translocation of reducing equivalents from the cytosol to the mitochondria. Although functional analysis of MoLLD5 showed that it was dispensable for the appressorium development and pathogenicity, the functions of other two lactate dehydrogenases MoLLD3 and MoLLD4, which shared similar characteristics of domain structures to typical L-lactate dehydrogenases, remain unknown. Finally, functional analysis will be conducted on MoLLD3 and MoLLD4. The study will focus on revealing how cytosolic lactate dehydrogenases connect glycogen metabolism to cellular respiration in the mitochondria.

REFERENCES

Adachi, K., and Hamer, J.E. (1998). Divergent cAMP signaling pathways regulate growth and pathogenesis in the rice blast fungus Magnaporthe grisea. The Plant Cell Online *10*, 1361-1373.

Ainsworth, G.C. (2008). Ainsworth & Bisby's dictionary of the fungi (Cabi).

Albertyn, J., Hohmann, S., Thevelein, J.M., and Prior, B.A. (1994). GPD1, which encodes glycerol-3-phosphate dehydrogenase, is essential for growth under osmotic stress in Saccharomyces cerevisiae, and its expression is regulated by the high-osmolarity glycerol response pathway. Molecular and Cellular Biology *14*, 4135-4144.

Argüelles, J.C. (2000). Physiological roles of trehalose in bacteria and yeasts: a comparative analysis. Archives of Microbiology *174*, 217-224.

Badaruddin, M., Holcombe, L.J., Wilson, R.A., Wang, Z.Y., Kershaw, M.J., and Talbot, N.J. (2013). Glycogen metabolic genes are involved in trehalose-6-phosphate synthase-mediated regulation of pathogenicity by the rice blast fungus Magnaporthe oryzae. PLoS pathogens *9*, e1003604.

Baumgart, E., Fahimi, H.D., Stich, A., and Völkl, A. (1996). L-Lactate Dehydrogenase A-and AB Isoforms Are Bona Fide Peroxisomal Enzymes in Rat Liver EVIDENCE FOR INVOLVEMENT IN INTRAPEROXISOMAL NADH REOXIDATION. Journal of Biological Chemistry *271*, 3846-3855.

Bhadauria, V., Banniza, S., Vandenberg, A., Selvaraj, G., and Wei, Y. (2012). Peroxisomal alanine: glyoxylate aminotransferase AGT1 is indispensable for appressorium function of the rice blast pathogen, Magnaporthe oryzae. PloS one *7*, e36266.

Bhambra, G.K., Wang, Z.Y., Soanes, D.M., Wakley, G.E., and Talbot, N.J. (2006). Peroxisomal carnitine acetyl transferase is required for elaboration of penetration hyphae during plant infection by Magnaporthe grisea. Mol Microbiol *61*, 46-60.

Bozzola, J.J., and Russell, L.D. (1999). Electron microscopy: principles and techniques for biologists (Jones & Bartlett Learning).

Bremer, J., and Davis, E.J. (1975). Studies on the active transfer of reducing equivalents into mitochondria via the malate-aspartate shuttle. Biochimica et Biophysica Acta (BBA)-Bioenergetics *376*, 387-397.

Bricker, D.K., Taylor, E.B., Schell, J.C., Orsak, T., Boutron, A., Chen, Y.-C., Cox, J.E., Cardon, C.M., Van Vranken, J.G., and Dephoure, N. (2012). A mitochondrial pyruvate carrier required for pyruvate uptake in yeast, Drosophila, and humans. Science *337*, 96-100.

Brooks, G. (2002). Lactate shuttles in nature. Biochemical Society Transactions *30*, 258.

Brooks, G.A. (2007). Lactate. Sports Medicine *37*, 341-343.

Brooks, G.A. (2009). Cell–cell and intracellular lactate shuttles. The Journal of physiology *587*, 5591-5600.

Brooks, G.A., Dubouchaud, H., Brown, M., Sicurello, J.P., and Butz, C.E. (1999). Role of mitochondrial lactate dehydrogenase and lactate oxidation in the intracellular lactate shuttle. Proceedings of the National Academy of Sciences *96*, 1129-1134.

Cao, Y., Cheong, H., Song, H., and Klionsky, D.J. (2008). In vivo reconstitution of autophagy in

Saccharomyces cerevisiae. The Journal of cell biology *182*, 703-713.

Cheeseman, A.J., and Clark, J.B. (1988). Influence of the Malate‐Aspartate Shuttle on Oxidative Metabolism in Synaptosomes. Journal of neurochemistry *50*, 1559-1565.

Chelstowska, A., Liu, Z., Jia, Y., Amberg, D., and Butow, R.A. (1999). Signalling between mitochondria and the nucleus regulates the expression of a new d‐lactate dehydrogenase activity in yeast. Yeast *15*, 1377-1391.

Chen, Y.-T., He, J.-K., Ding, J.-H., and Brown, B.I. (1987). Glycogen debranching enzyme: purification, antibody characterization, and immunoblot analyses of type III glycogen storage disease. American journal of human genetics *41*, 1002.

Chi, M.H., and Lee, Y.H. (2009). A quick and safe method for fungal DNA extraction. The Plant Pathology Journal *25*, 108-111.

Choi, W., and Dean, R.A. (1997). The adenylate cyclase gene MAC1 of Magnaporthe grisea controls appressorium formation and other aspects of growth and development. The Plant Cell Online *9*, 1973-1983.

Chumley, F.G., and Valent, B. (1990). Genetic analysis of melanin-deficient, nonpathogenic mutants of Magnaporthe grisea. Mol Plant-Microbe Interact *3*, 135-143.

Couch, B.C., Fudal, I., Lebrun, M.-H., Tharreau, D., Valent, B., van Kim, P., Nottéghem, J.-L., and Kohn, L.M. (2005). Origins of host-specific populations of the blast pathogen Magnaporthe oryzae in crop domestication with subsequent expansion of pandemic clones on rice and weeds of rice. Genetics *170*, 613-630.

Cox, M., and Nelson, D. (2004). Lehninger principles of biochemistry (Freeman).

Cristescu, M.E., Innes, D.J., Stillman, J.H., and Crease, T.J. (2008). D-and L-lactate dehydrogenases during invertebrate evolution. BMC Evolutionary Biology *8*, 268.

Danpure, C.J., Guttridge, K.M., Fryer, P., Jennings, P.R., Allsop, J., and Purdue, P.E. (1990). Subcellular distribution of hepatic alanine: glyoxylate aminotransferase in various mammalian species. Journal of cell science *97*, 669-678.

de Jong, J.C., McCormack, B.J., Smirnoff, N., and Talbot, N.J. (1997). Glycerol generates turgor in rice blast. Nature *389*, 244-244.

de Vries, S., and Marres, C.A. (1987). The mitochondrial respiratory chain of yeast. Structure and biosynthesis and the role in cellular metabolism. Biochimica et Biophysica Acta (BBA)-Reviews on Bioenergetics *895*, 205-239.

Dean, R.A., Talbot, N.J., Ebbole, D.J., Farman, M.L., Mitchell, T.K., Orbach, M.J., Thon, M., Kulkarni, R., Xu, J.-R., and Pan, H. (2005). The genome sequence of the rice blast fungus Magnaporthe grisea. Nature *434*, 980-986.

DeZwaan, T.M., Carroll, A.M., Valent, B., and Sweigard, J.A. (1999). Magnaporthe grisea pth11p is a novel plasma membrane protein that mediates appressorium differentiation in response to inductive substrate cues. The Plant Cell Online *11*, 2013-2030.

Dixon, K.P., Xu, J.-R., Smirnoff, N., and Talbot, N.J. (1999). Independent signaling pathways regulate cellular turgor during hyperosmotic stress and appressorium-mediated plant infection by Magnaporthe grisea. The Plant Cell Online *11*, 2045-2058.

Dohlman, H.G., and Thorner, J. (2001). Regulation of G protein-initiated signal transduction in

yeast: paradigms and principles. Annual review of biochemistry *70*, 703-754.

Draoui, N., and Feron, O. (2011). Lactate shuttles at a glance: from physiological paradigms to anti-cancer treatments. Disease models & mechanisms *4*, 727-732.

Eastmond, P.J., Van Dijken, A.J., Spielman, M., Kerr, A., Tissier, A.F., Dickinson, H.G., Jones, J.D., Smeekens, S.C., and Graham, I.A. (2002). Trehalose‐6‐phosphate synthase 1, which catalyses the first step in trehalose synthesis, is essential for Arabidopsis embryo maturation. The Plant Journal *29*, 225-235.

Ebbole, D.J. (2007). Magnaporthe as a model for understanding host-pathogen interactions. Annu Rev Phytopathol *45*, 437-456.

Elion, E.A., Brill, J.A., and Fink, G.R. (1991). FUS3 represses CLN1 and CLN2 and in concert with KSS1 promotes signal transduction. Proceedings of the National Academy of Sciences *88*, 9392-9396.

Fabisiak, J.P., Borisenko, G.G., Liu, S.-X., Tyurin, V.A., Pitt, B.R., and Kagan, V.E. (2001). Redox sensor function of metallothioneins. Methods in enzymology *353*, 268-281.

Farkas, I., Hardy, T.A., Goebl, M., and Roach, P.J. (1991). Two glycogen synthase isoforms in Saccharomyces cerevisiae are coded by distinct genes that are differentially controlled. Journal of Biological Chemistry *266*, 15602-15607.

Fernandez, J., and Wilson, R.A. (2011). The sugar sensor, trehalose-6-phosphate synthase (Tps1), regulates primary and secondary metabolism during infection by the rice blast fungus: Will Magnaporthe oryzae's “sweet tooth” become its “Achilles’ heel”? Mycology *2*, 46-53.

Fernandez, J., and Wilson, R.A. (2014). Cells in cells: morphogenetic and metabolic strategies conditioning rice infection by the blast fungus Magnaporthe oryzae. Protoplasma *251*, 37-47.

Fimia, G.M., and Sassone-Corsi, P. (2001). Cyclic AMP signalling. Journal of cell science *114*, 1971-1972.

Finn, R.D., Bateman, A., Clements, J., Coggill, P., Eberhardt, R.Y., Eddy, S.R., Heger, A., Hetherington, K., Holm, L., and Mistry, J. (2013). Pfam: the protein families database. Nucleic acids research, gkt1223.

Foster, A.J., Jenkinson, J.M., and Talbot, N.J. (2003). Trehalose synthesis and metabolism are required at different stages of plant infection by Magnaporthe grisea. The EMBO journal *22*, 225-235.

Gómez, L.D., Baud, S., Gilday, A., Li, Y., and Graham, I.A. (2006). Delayed embryo development in the ARABIDOPSIS TREHALOSE‐6‐PHOSPHATE SYNTHASE 1 mutant is associated with altered cell wall structure, decreased cell division and starch accumulation. The Plant Journal *46*, 69-84.

Gietz, R.D., Schiestl, R.H., Willems, A.R., and Woods, R.A. (1995). Studies on the transformation of intact yeast cells by the LiAc/SS‐DNA/PEG procedure. Yeast *11*, 355-360.

Gladden, L.B. (2004). Lactate metabolism: a new paradigm for the third millennium. The Journal of physiology *558*, 5-30.

Goepfert, S., Vidoudez, C., Rezzonico, E., Hiltunen, J.K., and Poirier, Y. (2005). Molecular identification and characterization of the Arabidopsis Δ3, 5, Δ2, 4-dienoyl-coenzyme A isomerase, a peroxisomal enzyme participating in the β-oxidation cycle of unsaturated fatty acids. Plant physiology *138*, 1947-1956.

Goff, S.A. (1999). Rice as a model for cereal genomics. Current opinion in plant biology *2*, 86-89.

Grandier-Vazeille, X., Bathany, K., Chaignepain, S., Camougrand, N., Manon, S., and Schmitter, J.-M. (2001). Yeast mitochondrial dehydrogenases are associated in a supramolecular complex. Biochemistry *40*, 9758-9769.

Green, M.R., and Sambrook, J. (2012). Molecular cloning: a laboratory manual (Cold Spring Harbor Laboratory Press Cold Spring Harbor, New York:).

Guo, M., Chen, Y., Du, Y., Dong, Y., Guo, W., Zhai, S., Zhang, H., Dong, S., Zhang, Z., and Wang, Y. (2011). The bZIP transcription factor MoAP1 mediates the oxidative stress response and is critical for pathogenicity of the rice blast fungus Magnaporthe oryzae. PLoS pathogens *7*, e1001302.

Hachiya, N.S., Sakasegawa, Y., Jozuka, A., Tsukita, S., and Kaneko, K. (2004). Interaction of d-lactate dehydrogenase protein 2 (Dld2p) with F-actin: implication for an alternative function of Dld2p. Biochemical and biophysical research communications *319*, 78-82.

Hall, M.D., Levitt, D.G., and Banaszak, L.J. (1992). Crystal structure of Escherichia coli malate dehydrogenase. A complex of the apoenzyme and citrate at 1.87 A resolution. Journal of molecular biology *226*, 867-882.

Hamer, J.E., Howard, R.J., Chumley, F.G., and Valent, B. (1988). A mechanism for surface attachment in spores of a plant pathogenic fungus. Science *239*, 288-290.

Hardy, T.A., Huang, D., and Roach, P.J. (1994). Interactions between cAMP-dependent and SNF1 protein kinases in the control of glycogen accumulation in Saccharomyces cerevisiae. Journal of Biological Chemistry *269*, 27907-27913.

He, Y., Deng, Y.Z., and Naqvi, N.I. (2013). Atg24-assisted mitophagy in the foot cells is necessary for proper asexual differentiation in Magnaporthe oryzae. Autophagy *9*, 1818-1827.

Herzig, S., Raemy, E., Montessuit, S., Veuthey, J.L., Zamboni, N., Westermann, B., Kunji, E.R., and Martinou, J.C. (2012). Identification and functional expression of the mitochondrial pyruvate carrier. Science *337*, 93-96.

Hiltunen, J., Wenzel, B., Beyer, A., Erdmann, R., Fosså, A., and Kunau, W. (1992). Peroxisomal multifunctional beta-oxidation protein of Saccharomyces cerevisiae. Molecular analysis of the fox2 gene and gene product. Journal of Biological Chemistry *267*, 6646-6653.

Hiltunen, J.K., Mursula, A.M., Rottensteiner, H., Wierenga, R.K., Kastaniotis, A.J., and Gurvitz, A. (2003). The biochemistry of peroxisomal β-oxidation in the yeast Saccharomyces cerevisiae. FEMS microbiology reviews *27*, 35-64.

Honka, E., Fabry, S., Niermann, T., Palm, P., and Hensel, R. (1990). Properties and primary structure of the L-malate dehydrogenase from the extremely thermophilic archaebacterium Methanothermus fervidus. European journal of biochemistry / FEBS *188*, 623-632.

Hooks, M.A. (2002). Molecular biology, enzymology, and physiology of β-oxidation. In Plant Peroxisomes (Springer), pp. 19-55.

Huser, A., Takahara, H., Schmalenbach, W., and O'Connell, R. (2009). Discovery of pathogenicity genes in the crucifer anthracnose fungus Colletotrichum higginsianum, using random insertional mutagenesis. Molecular plant-microbe interactions *22*, 143-156.

Hynes, M.J., Murray, S.L., Duncan, A., Khew, G.S., and Davis, M.A. (2006). Regulatory genes controlling fatty acid catabolism and peroxisomal functions in the filamentous fungus Aspergillus nidulans. Eukaryotic cell *5*, 794-805.

Igarashi, D., Tsuchida, H., Miyao, M., and Ohsumi, C. (2006). Glutamate: glyoxylate aminotransferase modulates amino acid content during photorespiration. Plant physiology *142*, 901-910.

Jendrossek, D., Kratzin, H.D., and Steinbuchel, A. (1993). The Alcaligenes eutrophus ldh structural gene encodes a novel type of lactate dehydrogenase. FEMS Microbiol Lett *112*, 229-235.

Jeon, J., Goh, J., Yoo, S., Chi, M.-H., Choi, J., Rho, H.-S., Park, J., Han, S.-S., Kim, B.R., and Park, S.-Y. (2008). A putative MAP kinase kinase kinase, MCK1, is required for cell wall integrity and pathogenicity of the rice blast fungus, Magnaporthe oryzae. Molecular plant-microbe interactions *21*, 525-534.

Kadotani, N., Nakayashiki, H., Tosa, Y., and Mayama, S. (2004). One of the two Dicer-like proteins in the filamentous fungi Magnaporthe oryzae genome is responsible for hairpin RNA-triggered RNA silencing and related small interfering RNA accumulation. Journal of Biological Chemistry *279*, 44467-44474.

Kang, S., Chumley, F.G., and Valent, B. (1994). Isolation of the mating-type genes of the phytopathogenic fungus Magnaporthe grisea using genomic subtraction. Genetics *138*, 289-296.

Kershaw, M.J., and Talbot, N.J. (2009). Genome-wide functional analysis reveals that infection-associated fungal autophagy is necessary for rice blast disease. Proceedings of the National Academy of Sciences *106*, 15967-15972.

Kersten, S. (2001). Mechanisms of nutritional and hormonal regulation of lipogenesis. EMBO reports *2*, 282-286.

Khang, C.H., Berruyer, R., Giraldo, M.C., Kankanala, P., Park, S.-Y., Czymmek, K., Kang, S., and Valent, B. (2010). Translocation of Magnaporthe oryzae effectors into rice cells and their subsequent cell-to-cell movement. The Plant Cell Online *22*, 1388-1403.

Kobayashi, T., Kanda, E., Kitada, K., Ishiguro, K., and Torigoe, Y. (2001). Detection of rice panicle blast with multispectral radiometer and the potential of using airborne multispectral scanners. Phytopathology *91*, 316-323.

Kohli, M., Mehta, Y., Guzman, E., Viedma, L., and Cubilla, L. (2011). Pyricularia blast-a threat to wheat cultivation. Paper presented at: Czech Journal of Genetics and Plant Breeding (Institute of Agricultural Economics and Information for the Czech Academy of Agricultural Sciences).

Koiri, R.K., Trigun, S.K., Dubey, S.K., Singh, S., and Mishra, L. (2008). Metal Cu (II) and Zn

(II) bipyridyls as inhibitors of lactate dehydrogenase. Biometals *21*, 117-126.
Kraemer, F.B., and Shen, W.-J. (2002). Hormone-sensitive lipase control of intracellular tri-(di-) acylglycerol and cholesteryl ester hydrolysis. Journal of lipid research *43*, 1585-1594.
Lane, M., and Gardner, D.K. (2005). Mitochondrial malate-aspartate shuttle regulates mouse embryo nutrient consumption. Journal of Biological Chemistry *280*, 18361-18367.
Larsson, C., Påhlman, I.L., Ansell, R., Rigoulet, M., Adler, L., and Gustafsson, L. (1998). The importance of the glycerol 3‐phosphate shuttle during aerobic growth of Saccharomyces cerevisiae. Yeast *14*, 347-357.
Lau, G.W., and Hamer, J.E. (1998). Acropetal: A Genetic Locus Required for Conidiophore Architecture and Pathogenicity in the Rice Blast Fungus. Fungal Genetics and Biology *24*, 228-239.
Lee, Y.-H., and Dean, R.A. (1993). cAMP regulates infection structure formation in the plant pathogenic fungus Magnaporthe grisea. The Plant Cell Online *5*, 693-700.
Leung, H., Borromeo, E.S., Bernardo, M.A., and Notteghem, J.L. (1988). Genetic analysis of virulence in the rice blast fungus Magnaporthe grisea. Phytopathology *78*, 1227-1233.
Liepman, A.H., and Olsen, L.J. (2001). Peroxisomal alanine: glyoxylate aminotransferase (AGT1) is a photorespiratory enzyme with multiple substrates in Arabidopsis thaliana. The Plant Journal *25*, 487-498.
Liu, S., and Dean, R.A. (1997). G protein α subunit genes control growth, development, and pathogenicity of Magnaporthe grisea. Molecular Plant-Microbe Interactions *10*, 1075-1086.
Liu, W., Zhou, X., Li, G., Li, L., Kong, L., Wang, C., Zhang, H., and Xu, J.-R. (2011). Multiple plant surface signals are sensed by different mechanisms in the rice blast fungus for appressorium formation. PLoS pathogens *7*, e1001261.
Lodi, T., Alberti, A., Guiard, B., and Ferrero, I. (1999). Regulation of the Saccharomyces cerevisiae DLD1 gene encoding the mitochondrial protein D-lactate ferricytochrome c oxidoreductase by HAP1 and HAP2/3/4/5. Molecular and General Genetics MGG *262*, 623-632.
Lodi, T., and Ferrero, I. (1993). Isolation of the DLD gene of Saccharomyces cerevisiae encoding the mitochondrial enzyme D-lactate ferricytochrome c oxidoreductase. Molecular and General Genetics MGG *238*, 315-324.
Lodi, T., and Guiard, B. (1991). Complex transcriptional regulation of the Saccharomyces cerevisiae CYB2 gene encoding cytochrome b2: CYP1 (HAP1) activator binds to the CYB2 upstream activation site UAS1-B2. Molecular and cellular biology *11*, 3762-3772.
Lorenz, M.C., and Fink, G.R. (2001). The glyoxylate cycle is required for fungal virulence. Nature *412*, 83-86.
Lu, M., Banerjee, S., Saidel, G.M., and Yu, X. (2011). Regulation of cytosolic and mitochondrial oxidation via malate-aspartate shuttle: an observation using dynamic (1)(3)C NMR spectroscopy. Advances in experimental medicine and biology *701*, 185-192.
Müller, J., Aeschbacher, R.A., Wingler, A., Boller, T., and Wiemken, A. (2001). Trehalose and trehalase in Arabidopsis. Plant physiology *125*, 1086-1093.
Maggio‐Hall, L.A., and Keller, N.P. (2004). Mitochondrial β‐oxidation in Aspergillus

nidulans. Molecular microbiology *54*, 1173-1185.

Marcel, S., Sawers, R., Oakeley, E., Angliker, H., and Paszkowski, U. (2010). Tissue-adapted invasion strategies of the rice blast fungus Magnaporthe oryzae. The Plant Cell Online *22*, 3177-3187.

Mather, B., and Donahue, M. (1998). Simultaneous measurement of cell cycle and apoptotic cell death. Methods Cell Biol *57*, 265.

McAlister-Henn, L., and Thompson, L.M. (1987). Isolation and expression of the gene encoding yeast mitochondrial malate dehydrogenase. Journal of bacteriology *169*, 5157-5166.

McClelland, G.B., Khanna, S., González, G.F., Eric Butz, C., and Brooks, G.A. (2003). Peroxisomal membrane monocarboxylate transporters: evidence for a redox shuttle system? Biochemical and biophysical research communications *304*, 130-135.

McKinney, J.D., zu Bentrup, K.H., Muñoz-Elías, E.J., Miczak, A., Chen, B., Chan, W.-T., Swenson, D., Sacchettini, J.C., Jacobs, W.R., and Russell, D.G. (2000). Persistence of Mycobacterium tuberculosis in macrophages and mice requires the glyoxylate shunt enzyme isocitrate lyase. Nature *406*, 735-738.

Mettler, I.J., and Beevers, H. (1980). Oxidation of NADH in glyoxysomes by a malate-aspartate shuttle. Plant physiology *66*, 555-560.

Minard, K.I., and McAlister-Henn, L. (1991). Isolation, nucleotide sequence analysis, and disruption of the MDH2 gene from Saccharomyces cerevisiae: evidence for three isozymes of yeast malate dehydrogenase. Mol Cell Biol *11*, 370-380.

Mizushima, N. (2007). Autophagy: process and function. Genes & development *21*, 2861-2873.

Morpeth, F.F., and Massey, V. (1982). Metal binding to D-lactate dehydrogenase. Biochemistry *21*, 1318-1323.

Mosquera, G., Giraldo, M.C., Khang, C.H., Coughlan, S., and Valent, B. (2009). Interaction transcriptome analysis identifies Magnaporthe oryzae BAS1-4 as biotrophy-associated secreted proteins in rice blast disease. The Plant Cell Online *21*, 1273-1290.

Motley, A., Lumb, M.J., Oatey, P.B., Jennings, P.R., De Zoysa, P.A., Wanders, R., Tabak, H.F., and Danpure, C.J. (1995). Mammalian alanine/glyoxylate aminotransferase 1 is imported into peroxisomes via the PTS1 translocation pathway. Increased degeneracy and context specificity of the mammalian PTS1 motif and implications for the peroxisome-to-mitochondrion mistargeting of AGT in primary hyperoxaluria type 1. The Journal of cell biology *131*, 95-109.

Nevoigt, E., Kohnke, J., Fischer, C.R., Alper, H., Stahl, U., and Stephanopoulos, G. (2006). Engineering of promoter replacement cassettes for fine-tuning of gene expression in Saccharomyces cerevisiae. Applied and environmental microbiology *72*, 5266-5273.

Nishimura, M., Park, G., and Xu, J.R. (2003). The G‐beta subunit MGB1 is involved in regulating multiple steps of infection‐related morphogenesis in Magnaporthe grisea. Molecular microbiology *50*, 231-243.

Novoa, W.B., Winer, A.D., Glaid, A.J., and Schwert, G.W. (1959). Lactic dehydrogenase. V. Inhibition by oxamate and by oxalate. The Journal of biological chemistry *234*, 1143-1148.

Ou, S.H. (1985). Rice diseases (IRRI).

Park, G., Xue, C., Zhao, X., Kim, Y., Orbach, M., and Xu, J.-R. (2006). Multiple upstream signals converge on the adaptor protein Mst50 in Magnaporthe grisea. The Plant Cell Online *18*, 2822-2835.

Parrou, J.L., Teste, M.-A., and François, J. (1997). Effects of various types of stress on the metabolism of reserve carbohydrates in Saccharomyces cerevisiae: genetic evidence for a stress-induced recycling of glycogen and trehalose. Microbiology *143*, 1891-1900.

Patkar, R.N., Ramos‐Pamplona, M., Gupta, A.P., Fan, Y., and Naqvi, N.I. (2012). Mitochondrial β‐oxidation regulates organellar integrity and is necessary for conidial germination and invasive growth in Magnaporthe oryzae. Molecular microbiology *86*, 1345-1363.

Pellier, A.L., Laugé, R., Veneault‐Fourrey, C., and Langin, T. (2003). CLNR1, the AREA/NIT2‐like global nitrogen regulator of the plant fungal pathogen Colletotrichum lindemuthianum is required for the infection cycle. Molecular microbiology *48*, 639-655.

Peng, Y.-L., and Shishiyama, J. (1988). Temporal sequence of cytological events in rice leaves infected with Pyricularia oryzae. Canadian journal of botany *66*, 730-735.

Piekarska, K., Hardy, G., Mol, E., van den Burg, J., Strijbis, K., van Roermund, C., van den Berg, M., and Distel, B. (2008). The activity of the glyoxylate cycle in peroxisomes of Candida albicans depends on a functional beta-oxidation pathway: evidence for reduced metabolite transport across the peroxisomal membrane. Microbiology *154*, 3061-3072.

Pitoniak, A., Birkaya, B., Dionne, H.M., Vadaie, N., and Cullen, P.J. (2009). The signaling mucins Msb2 and Hkr1 differentially regulate the filamentation mitogen-activated protein kinase pathway and contribute to a multimodal response. Molecular biology of the cell *20*, 3101-3114.

Poso, A.R. (2002). Monocarboxylate transporters and lactate metabolism in equine athletes: a review. Acta veterinaria Scandinavica *43*, 63-74.

Pronk, J.T., Steensma, H.Y., and Van Dijken, J.P. (1996). Pyruvate metabolism in Saccharomyces cerevisiae. Yeast *12*, 1607-1633.

Quettier, A.L., Shaw, E., and Eastmond, P.J. (2008). SUGAR-DEPENDENT6 encodes a mitochondrial flavin adenine dinucleotide-dependent glycerol-3-p dehydrogenase, which is required for glycerol catabolism and post germinative seedling growth in Arabidopsis. Plant physiology *148*, 519-528.

Rønnow, B., and Kielland‐Brandt, M.C. (1993). GUT2, a gene for mitochondrial glycerol 3‐phosphate dehydrogenase of Saccharomyces cerevisiae. Yeast *9*, 1121-1130.

Ramos-Pamplona, M., and Naqvi, N.I. (2006). Host invasion during rice-blast disease requires carnitine-dependent transport of peroxisomal acetyl-CoA. Mol Microbiol *61*, 61-75.

Regev-Rudzki, N., Karniely, S., Ben-Haim, N.N., and Pines, O. (2005). Yeast aconitase in two locations and two metabolic pathways: seeing small amounts is believing. Molecular biology of the cell *16*, 4163-4171.

Resh, M.D. (2013). Covalent lipid modifications of proteins. Current Biology *23*, R431-R435.

Rojo, E.E., Guiard, B., Neupert, W., and Stuart, R.A. (1998). Sorting of d-Lactate

Dehydrogenase to the Inner Membrane of Mitochondria ANALYSIS OF TOPOGENIC SIGNAL AND ENERGETIC REQUIREMENTS. Journal of Biological Chemistry *273*, 8040-8047.

Rowen, D.W., Meinke, M., and LaPorte, D.C. (1992). GLC3 and GHA1 of Saccharomyces cerevisiae are allelic and encode the glycogen branching enzyme. Molecular and cellular biology *12*, 22-29.

Samson, R.A., Stalpers, J.A., and Verkerke, W. (1979). A simplified technique to prepare fungal specimens for scanning electron. Cytobios *24*, 7-11.

Saunders, D.G., Aves, S.J., and Talbot, N.J. (2010). Cell Cycle–Mediated Regulation of Plant Infection by the Rice Blast Fungus. The Plant Cell Online *22*, 497-507.

Schlösser, T., Gätgens, C., Weber, U., and Stahmann, K. (2004). Alanine: glyoxylate aminotransferase of Saccharomyces cerevisiae–encoding gene AGX1 and metabolic significance. Yeast *21*, 63-73.

Schluepmann, H., Pellny, T., van Dijken, A., Smeekens, S., and Paul, M. (2003). Trehalose 6-phosphate is indispensable for carbohydrate utilization and growth in Arabidopsis thaliana. Proceedings of the National Academy of Sciences *100*, 6849-6854.

Sesma, A., and Osbourn, A.E. (2004). The rice leaf blast pathogen undergoes developmental processes typical of root-infecting fungi. Nature *431*, 582-586.

Shen, W., Wei, Y., Dauk, M., Tan, Y., Taylor, D.C., Selvaraj, G., and Zou, J. (2006). Involvement of a glycerol-3-phosphate dehydrogenase in modulating the NADH/NAD+ ratio provides evidence of a mitochondrial glycerol-3-phosphate shuttle in Arabidopsis. The Plant cell *18*, 422-441.

Silva‐Udawatta, D., Mihiri, N., and Cannon, J.F. (2001). Roles of trehalose phosphate synthase in yeast glycogen metabolism and sporulation. Molecular microbiology *40*, 1345-1356.

Sinha, S., and Cossins, E. (1965). The importance of glyoxylate in amino acid biosynthesis in plants. Biochemical journal *96*, 254-261.

Sirerol-Piquer, M.S., Cebrián-Silla, A., Alfaro-Cervelló, C., Gomez-Pinedo, U., Soriano-Navarro, M., and Verdugo, J.-M.G. (2012). GFP immunogold staining, from light to electron microscopy, in mammalian cells. Micron *43*, 589-599.

Smith, J.J., Brown, T.W., Eitzen, G.A., and Rachubinski, R.A. (2000). Regulation of peroxisome size and number by fatty acid β-oxidation in the yeast Yarrowia lipolytica. Journal of Biological Chemistry *275*, 20168-20178.

Steffan, J.S., and McAlister-Henn, L. (1992). Isolation and characterization of the yeast gene encoding the MDH3 isozyme of malate dehydrogenase. The Journal of biological chemistry *267*, 24708-24715.

TABATA, S., and HIZUKURI, S. (1992). Properties of yeast debranching enzyme and its specificity toward branched cyclodextrins. European Journal of Biochemistry *206*, 345-348.

Takan, J. (2004). Finger millet blast pathogen diversity and management in East Africa: A summary of project activities and outputs. International sorghum and millets newsletter *45*, 66-69.

Talbot, N.J. (2003). On the trail of a cereal killer: exploring the biology of Magnaporthe grisea. Annual Reviews in Microbiology *57*, 177-202.

TeBeest, D.O., Guerber, C., and Ditmore, M. (2007). Symptoms and Signs.

Teste, M.A., Enjalbert, B., Parrou, J.L., and Fran ̧ois, J.M. (2000). The Saccharomyces cerevisiaeYPR184w gene encodes the glycogen debranching enzyme. FEMS microbiology letters *193*, 105-110.

Thevelein, J.M., and Hohmann, S. (1995). Trehalose synthase: guard to the gate of glycolysis in yeast? Trends in biochemical sciences *20*, 3-10.

Thiam, A.R., Farese Jr, R.V., and Walther, T.C. (2013). The biophysics and cell biology of lipid droplets. Nature Reviews Molecular Cell Biology *14*, 775-786.

Thines, E., Weber, R.W., and Talbot, N.J. (2000). MAP kinase and protein kinase A–dependent mobilization of triacylglycerol and glycogen during appressorium turgor generation by Magnaporthe grisea. The Plant Cell Online *12*, 1703-1718.

Thomazella, D., Teixeira, P.J.P., Oliveira, H.C., Saviani, E.E., Rincones, J., Toni, I.M., Reis, O., Garcia, O., Meinhardt, L.W., and Salgado, I. (2012). The hemibiotrophic cacao pathogen Moniliophthora perniciosa depends on a mitochondrial alternative oxidase for biotrophic development. New Phytologist *194*, 1025-1034.

Tobin, A., Djerdjour, B., Journet, E., Neuburger, M., and Douce, R. (1980). Effect of NAD+ on malate oxidation in intact plant mitochondria. Plant physiology *66*, 225-229.

Torres, L., Martin, H., Garcí a‐Saez, M., Arroyo, J., Molina, M., Sanchez, M., and Nombela, C. (1991). A protein kinase gene complements the lytic phenotype of Saccharomyces cerevisiae lyt2 mutants. Molecular microbiology *5*, 2845-2854.

Tucker, S.L., and Talbot, N.J. (2001). Surface attachment and pre-penetration stage development by plant pathogenic fungi. Annual review of phytopathology *39*, 385-417.

Tucker, S.L., Thornton, C.R., Tasker, K., Jacob, C., Giles, G., Egan, M., and Talbot, N.J. (2004). A fungal metallothionein is required for pathogenicity of Magnaporthe grisea. The Plant Cell Online *16*, 1575-1588.

Valent, B., Farrall, L., and Chumley, F.G. (1991). Magnaporthe grisea genes for pathogenicity and virulence identified through a series of backcrosses. Genetics *127*, 87-101.

van Bakel, H., Strengman, E., Wijmenga, C., and Holstege, F.C. (2005). Gene expression profiling and phenotype analyses of S. cerevisiae in response to changing copper reveals six genes with new roles in copper and iron metabolism. Physiological genomics *22*, 346.

Van Roermund, C., Elgersma, Y., Singh, N., Wanders, R., and Tabak, H. (1995). The membrane of peroxisomes in Saccharomyces cerevisiae is impermeable to NAD (H) and acetyl-CoA under in vivo conditions. The EMBO journal *14*, 3480.

Veneault-Fourrey, C., Barooah, M., Egan, M., Wakley, G., and Talbot, N.J. (2006). Autophagic fungal cell death is necessary for infection by the rice blast fungus. Science *312*, 580-583.

Walker, J.E. (1992). The NADH: ubiquinone oxidoreductase (complex I) of respiratory chains. Quarterly reviews of biophysics *25*, 253-324.

Wallach, D. (1961). Studies on the GABA pathway—I: The inhibition of γ-aminobutyric acid-α-ketoglutaric acid transaminase in vitro and in vivo by U-7524 (Amino-oxyacetic

acid). Biochemical pharmacology *5*, 323-331.
Walther, T.C., and Farese Jr, R.V. (2012). Lipid droplets and cellular lipid metabolism. Annual review of biochemistry *81*, 687.
Wang, Z.-Y., Soanes, D.M., Kershaw, M.J., and Talbot, N.J. (2007). Functional analysis of lipid metabolism in Magnaporthe grisea reveals a requirement for peroxisomal fatty acid β-oxidation during appressorium-mediated plant infection. Molecular plant-microbe interactions *20*, 475-491.
Wang, Z.Y., Thornton, C.R., Kershaw, M.J., Debao, L., and Talbot, N.J. (2003). The glyoxylate cycle is required for temporal regulation of virulence by the plant pathogenic fungus Magnaporthe grisea. Molecular microbiology *47*, 1601-1612.
Wei, Y., Shen, W., Dauk, M., Wang, F., Selvaraj, G., and Zou, J. (2004). Targeted gene disruption of glycerol-3-phosphate dehydrogenase in Colletotrichum gloeosporioides reveals evidence that glycerol is a significant transferred nutrient from host plant to fungal pathogen. Journal of Biological Chemistry *279*, 429-435.
Weiss, H., Friedrich, T., Hofhaus, G., and Preis, D. (1992). The respiratory-chain NADH dehydrogenase (complex I) of mitochondria. In EJB Reviews 1991 (Springer), pp. 55-68.
Wiley, D.J., Catanuto, P., Fontanesi, F., Rios, C., Sanchez, N., Barrientos, A., and Verde, F. (2008). Bot1p is required for mitochondrial translation, respiratory function, and normal cell morphology in the fission yeast Schizosaccharomyces pombe. Eukaryotic cell *7*, 619-629.
Wilson, R.A., Gibson, R.P., Quispe, C.F., Littlechild, J.A., and Talbot, N.J. (2010). An NADPH-dependent genetic switch regulates plant infection by the rice blast fungus. Proceedings of the National Academy of Sciences *107*, 21902-21907.
Wilson, R.A., Jenkinson, J.M., Gibson, R.P., Littlechild, J.A., Wang, Z.Y., and Talbot, N.J. (2007). Tps1 regulates the pentose phosphate pathway, nitrogen metabolism and fungal virulence. The EMBO journal *26*, 3673-3685.
Wilson, R.A., and Talbot, N.J. (2009). Under pressure: investigating the biology of plant infection by Magnaporthe oryzae. Nature Reviews Microbiology *7*, 185-195.
Xiaohong, W., Mingjie, X., Jian, J., Baoling, Y., Yanlong, S., Wei, H., Li, L., and Yi, Z. (2013). Advances in Research on Control Method of Rice Blast. Chinese Agricultural Science Bulletin *3*, 038.
Xu, J.-R., and Hamer, J.E. (1996). MAP kinase and cAMP signaling regulate infection structure formation and pathogenic growth in the rice blast fungus Magnaporthe grisea. Genes & development *10*, 2696-2706.
Xu, J.-R., Staiger, C.J., and Hamer, J.E. (1998). Inactivation of the mitogen-activated protein kinase Mps1 from the rice blast fungus prevents penetration of host cells but allows activation of plant defense responses. Proceedings of the National Academy of Sciences *95*, 12713-12718.
Xu, J.-R., Urban, M., Sweigard, J.A., and Hamer, J.E. (1997). The CPKA gene of Magnaporthe grisea is essential for appressorial penetration. Molecular plant-microbe interactions *10*, 187-194.
Yu, J.-H., Hamari, Z., Han, K.-H., Seo, J.-A., Reyes-Dom ńguez, Y., and Scazzocchio, C.

(2004). Double-joint PCR: a PCR-based molecular tool for gene manipulations in filamentous fungi. Fungal Genetics and Biology *41*, 973-981.

Yu, L., Strandberg, L., and Lenardo, M.J. (2008). The selectivity of autophagy and its role in cell death and survival. Autophagy *4*, 567.

Zhu, Y., Chen, H., Fan, J., Wang, Y., Li, Y., Chen, J., Fan, J., Yang, S., Hu, L., and Leung, H. (2000). Genetic diversity and disease control in rice. Nature *406*, 718-722.

APPENDIX TABLE

List of primers

Primer name	Sequence (5' -3')	Application
MoDLD1CF	CAGAAGGCACCCTGGGTTTG	RT-PCR analysis
MoDLD1CR	GGCGAGGTAGTCCCGTTTGA	RT-PCR analysis
MoDLD2CF	CCCATTCTACTGCCTGATT	RT-PCR analysis
MoDLD2CR	GTAAGGGTTCATGATACCGT	RT-PCR analysis
MoDLD3CF	GACCACGACATCATCTCCAC G	RT-PCR analysis
MoDLD3CR	TCAGGTTTACCACCCGCATC	RT-PCR analysis
MoLLD1CF	AAAACGGCTCTTCCCTTCTA C	RT-PCR analysis
MoLLD1CR	TGAGGCTCTTGGTGTCAACC	RT-PCR analysis
MoLLD2CF	TTGAAGAGGTCGCCAAGCA	RT-PCR analysis
MoLLD2CR	AGGGTCGTGGTCCAGGTCAG	RT-PCR analysis
MoLLD5CF	TGGTTGCCTCGGGTCTCA	RT-PCR analysis
MoLLD5CR	GGGATTCCGCTCTTGGTTC	RT-PCR analysis
MoGUT2CF	ACAACGACTCCCGTATGAAT G	RT-PCR analysis
MoGUT2CR	GGCGAAATATCTACAAGGTG G	RT-PCR analysis
MoActinF	GTTCGGGTATGTGCAAGGC	RT-PCR analysis
MoActinR	TTCATCAGGTAGTCGGTCAAGT	RT-PCR analysis
HYG/F	GCTGGAGCTAGTGGAGGTC	Targeted gene deletion
HY/R	GAAATCACGCCATGTAGTGT A	Targeted gene deletion
YG/F	GGCGAAGAATCTCGTGCTTT CA	Targeted gene deletion
HYG/F	GCTGGAGCTAGTGGAGGTCA ACACATC	Targeted gene deletion
MoDLD1AF	AGACGCACCGAAGAAGAGG	Targeted gene deletion
MoDLD1AR	GATGTGTTGACCTCCACTAG CTCCAGCATGGCAGCAAGCT GAAGAC	Targeted gene deletion
MoDLD1BF	GCAAAGGAATAGAGTAGATG CCGACCGAAGACAGCAGGT TCCCAGTG	Targeted gene deletion
MoDLD1BR	ACGATTCGGACACCACCA	Targeted gene deletion
MoDLD1ORF-F	CAGTGACGGGCTACAGTGGT G	Mutant verification
MoDLD1ORF-R	GCTTCATGTCCGCCTTGGT	Mutant verification

MoDLD1TEST-F	ACTGGAGCGAGGCGATGT	Mutant verification
MoDLD1TEST-R	GAACGGGATGACGCAAGG	Mutant verification
MoDLD2AF	GCCGAGTAGATGCCTGAAG	Targeted gene deletion
MoDLD2AR	GATGTGTTGACCTCCACTAG CTCCAGCCAAAACCAAAAG GGGTGTAG	Targeted gene deletion
MoDLD2BF	GCAAAGGAATAGAGTAGATG CCGACCGACCCTCCATTATAC CACTATCC	Targeted gene deletion
MoDLD2BR	GCCCTTCCATTCATTACGC	Targeted gene deletion
MoDLD2ORF-F	AGTCAGCAAGATCCTCAGGT	Mutant verification
MoDLD2ORF-R	TCAATCAGGCAGTAGAATGG	Mutant verification
MoDLD2TEST-F	CCTCCCTCGTCAAGATAGC	Mutant verification
MoDLD2TEST-R	AAGTGCCGATAAACATAACG	Mutant verification
MoDLD3AF	CAATCAATGTTCCTATCTATC GG	Targeted gene deletion
MoDLD3AR	GATGTGTTGACCTCCACTAG CTCCAGCGCAAGCAGAATAC ACGCAGA	Targeted gene deletion
MoDLD3BF	GCAAAGGAATAGAGTAGATG CCGACCGACAACCACCCACA GGAATC	Targeted gene deletion
MoDLD3BR	AAGAACTTGGAAGTCTAATA GCC	Targeted gene deletion
MoDLD3ORF-F	CGTGAAGATACTCCCATAATA CA	Mutant verification
MoDLD3ORF-R	GGACCCGACAAACAATACC	Mutant verification
MoDLD3TEST-F	GAGACTTGTTCACTGATTTTC C	Mutant verification
MoDLD3TEST-R	CAGTTCGGTTTCAGGCAG	Mutant verification
MoLLD1AF	GGATGTTTCTCCAGGTTTGC	Targeted gene deletion
MoLLD1AR	GATGTGTTGACCTCCACTAG CTCCAGCGTCCTTGGGATAG GCGATT	Targeted gene deletion
MoLLD1BF	GCAAAGGAATAGAGTAGATG CCGACCGGGTCCTGCTTATC AGTTCGG	Targeted gene deletion
MoLLD1BR	GGAGTTTATTATTGTTTGTGG TGC	Targeted gene deletion
MoLLD1ORF-F	AAAACGGCTCTTCCCTTCTA C	Mutant verification

MoLLD1ORF-R	TGAGGCTCTTGGTGTCAACC	Mutant verification
MoLLD1TEST-F	ATGCAACCCTCATTCACAATT	Mutant verification
MoLLD1TEST-R	CCGCTCGTCTGGCTAAGAT	Mutant verification
MoLLD2AF	AGTTGTTGGTGGACCTTGATG	Targeted gene deletion
MoLLD2AR	GATGTGTTGACCTCCACTAGCTCCAGCCGGGTGGATTCCGATGTA	Targeted gene deletion
MoLLD2BF	GCAAAGGAATAGAGTAGATGCCGACCGGGATACTGTGGGATTACTCAACT	Targeted gene deletion
MoLLD2BR	ATTTATACCCTCCTTCCTCTTCT	Targeted gene deletion
MoLLD2ORF-F	TTGAAGAGGTCGCCAAGCA	Mutant verification
MoLLD2ORF-R	AGGGTCGTGGTCCAGGTCAG	Mutant verification
MoLLD1TEST-F	GCGTTACAAGGAACAGGAAA	Mutant verification
MoLLD1TEST-R	GCGGGAGATGCAATAGGT	Mutant verification
MoLLD5AF	GACCCTGTTGCGTCCTCT	Targeted gene deletion
MoLLD5AR	GATGTGTTGACCTCCACTAGCTCCAGCCTAAATCCAAGTGCCGAAGT	Targeted gene deletion
MoLLD5BF	GCAAAGGAATAGAGTAGATGCCGACCGGGCTAGAGCGTCGGACTT	Targeted gene deletion
MoLLD5BR	CACCACGGACCGATAGAAT	Targeted gene deletion
MoLLD5ORF-F	TGGTTGCCTCGGGTCTCA	Mutant verification
MoLLD5ORF-R	GGGATTCCGCTCTTGGTTC	Mutant verification
MoLLD5TEST-F	GGCTCCAACAATGTCCTG	Mutant verification
MoLLD5TEST-R	TCTCCTGCTCCGACAACC	Mutant verification
MoGUT2AF	AATGGTGAATCGTGGCAAAC	Targeted gene deletion
MoGUT2AR	GATGTGTTGACCTCCACTAGCTCCAGCCCTCCCTTAGAAGCGAGATGA	Targeted gene deletion
MoGUT2BF	GCAAAGGAATAGAGTAGATGCCGACCGACCTTCCCTTCACTCACCAA	Targeted gene deletion
MoGUT2BR	GTCGCCTTTCACGCTGTC	Targeted gene deletion
MoGUT2ORF-F	ACAACGACTCCCGTATGAATG	Mutant verification
MoGUT2ORF-R	GGCGAAATATCTACAAGGTG	Mutant verification

	G	
MoGUT2TEST-F	ATTGGACTCTACAGGGAGGTAA	Mutant verification
MoGUT2TEST-R	GTTCGGTTTCAGGCAGGT	Mutant verification
MoDLD1eGFP-F	GGGGTACCGGTAGGGAACGGCCAAAG	Cellular localization
MoDLD1eGFP-R	CCCAAGCTTCCACTCATCGACCTCACCC	Cellular localization
MoDLD2eGFP-F	GCGGGCCCGAACTTTGTTGTTATGCGATCT	Cellular localization
MoDLD2eGFP-R	CCATCGATTATGTATTTGTAAGGGTTCATG	Cellular localization
MoLLD5eGFP-F	CCATCGATGTTGGTGGTGGCGAGGTA	Cellular localization
MoLLD5eGFP-R	CCCAAGCTTCCTAGCAACAATCTCTTGGATC	Cellular localization
MoDLD1Del-Mem-R	AAGCCTTGACTTCCTTGAGAGGTTGTGTTAGACGCTGCTGGATGCTC	Domain deletion
MoDLD1Del-MTS-Mem-R	AAGCCTTGACTTCCTTGAGAGGTTGTGTCATAGGTTTTCAGTTCGTATGTTG	Domain deletion
MoDLD1Del–F	ACACAACCTCTCAAGGAAGTCAAGGCTT	Domain deletion
Mgg03147CDNCF	CCATCGATATGTCCAGGTTCGCTCGCGGGA	MoGUT2 localization
Mgg03147CDNCR	CCCAAGCTTCAGCTCCTCCACCGGCTTA	MoGUT2 localization
03147promoter-R	CCATCGATCATGGTAGATTGTTCTCAAGG	MoGUT2 Promoter
03147promoter-F	GCGGGCCCGATGTCGAGATGGAGCTTTC	MoGUT2 Promoter
03147-Del-MM-F	CCATCGATGGGCGCGGATGGCACATTT	MoGUT2 cytosolic domain localization
03147-Del-MM-R	CCCAAGCTTCAGCTCCTCCACCGGCTTA	MoGUT2 cytosolic domain localization
pYESDLD1BOP-F	CGGGATCCATGTCGCACCTGGGTGCGAAG	Yeast complementation
pYESDLD1BOP-F1	CGGGATCCATGACACAACCTCTCAAGGAAGTC	Yeast complementation
pYESDLD1BOP-R	CCCAAGCTTCTACCACTCATC	Yeast complementation

	GACCTCACCC	
pTEF1-R	CGGGATCCCTTAGATTAGATT GCTATG	TEF1 promoter cloning
pTEF1-F	GGACTAGTGATCCCCCACAC ACCATAG	TEF1 promoter cloning